

AWARD NUMBER: **W81XWH-14-1-0358 (BC134025)**

TITLE: **Musculoskeletal Complications and Bone Metastases in Breast Cancer Patients Undergoing Estrogen Deprivation Therapy**

PRINCIPAL INVESTIGATOR: **Laura E. Wright, Ph.D.**

CONTRACTING ORGANIZATION: **Indiana University School of Medicine,  
Indianapolis, IN 46202**

REPORT DATE: **October 2016**

TYPE OF REPORT: **Annual**

PREPARED FOR: **U.S. Army Medical Research and Materiel Command  
Fort Detrick, Maryland 21702-5012**

DISTRIBUTION STATEMENT: **Approved for Public Release;  
Distribution Unlimited**

The views, opinions and/or findings contained in this report are those of the author(s) and should not be construed as an official Department of the Army position, policy or decision unless so designated by other documentation.

<b>REPORT DOCUMENTATION PAGE</b>				<i>Form Approved</i> <i>OMB No. 0704-0188</i>	
Public reporting burden for this collection of information is estimated to average 1 hour per response, including the time for reviewing instructions, searching existing data sources, gathering and maintaining the data needed, and completing and reviewing this collection of information. Send comments regarding this burden estimate or any other aspect of this collection of information, including suggestions for reducing this burden to Department of Defense, Washington Headquarters Services, Directorate for Information Operations and Reports (0704-0188), 1215 Jefferson Davis Highway, Suite 1204, Arlington, VA 22202-4302. Respondents should be aware that notwithstanding any other provision of law, no person shall be subject to any penalty for failing to comply with a collection of information if it does not display a currently valid OMB control number. <b>PLEASE DO NOT RETURN YOUR FORM TO THE ABOVE ADDRESS.</b>					
<b>1. REPORT DATE</b> October 2016		<b>2. REPORT TYPE</b> Annual		<b>3. DATES COVERED</b> 30Sep2015 - 29Sep2016	
<b>4. TITLE AND SUBTITLE</b>  Musculoskeletal Complications and Bone Metastases in Breast Cancer Patients Undergoing Estrogen Deprivation Therapy				<b>5a. CONTRACT NUMBER</b>	
				<b>5b. GRANT NUMBER</b> W81XWH-14-1-0358	
				<b>5c. PROGRAM ELEMENT NUMBER</b>	
<b>6. AUTHOR(S)</b>  Laura E. Wright, Ph.D.  E-Mail: laewrig@iu.edu				<b>5d. PROJECT NUMBER</b>	
				<b>5e. TASK NUMBER</b>	
				<b>5f. WORK UNIT NUMBER</b>	
<b>7. PERFORMING ORGANIZATION NAME(S) AND ADDRESS(ES)</b>  Indiana University School of Medicine 980 West Walnut Street R3 Room C132 Indianapolis, IN 46202				<b>8. PERFORMING ORGANIZATION REPORT NUMBER</b>	
<b>9. SPONSORING / MONITORING AGENCY NAME(S) AND ADDRESS(ES)</b>  U.S. Army Medical Research and Materiel Command Fort Detrick, Maryland 21702-5012				<b>10. SPONSOR/MONITOR'S ACRONYM(S)</b>	
				<b>11. SPONSOR/MONITOR'S REPORT NUMBER(S)</b>	
<b>12. DISTRIBUTION / AVAILABILITY STATEMENT</b>  Approved for Public Release; Distribution Unlimited					
<b>13. SUPPLEMENTARY NOTES</b>					
<b>14. ABSTRACT</b> Aromatase inhibitors (AIs) cause muscle weakness, bone loss, and joint pain in up to half of cancer patients. Preclinical studies have demonstrated that increased osteoclastic bone resorption can impair muscle contractility and prime the bone microenvironment to accelerate metastatic growth. I hypothesized that AI-induced bone loss could increase breast cancer progression in bone and exacerbate muscle weakness associated with bone metastases. Female athymic nude mice underwent ovariectomy (OVX) or sham surgery and were treated with vehicle or AI (letrozole; Let). An OVX+Let group was then further treated with bisphosphonate (zoledronic acid; Zol). At week three, trabecular bone volume was measured and mice were inoculated with MDA-MB-231 cells into the cardiac ventricle and followed for progression of bone metastases. Five weeks after tumor cell inoculation, tumor-induced osteolytic lesion area was increased in OVX-Let mice and reduced in OVX-Let-Zol mice compared to sham-vehicle. Tumor burden in bone was increased in OVX-Let mice relative to sham-vehicle and OVX-Let-Zol mice. At the termination of the study, muscle-specific force of the extensor digitorum longus muscle was reduced in OVX-Let mice compared to sham-vehicle mice, however, the addition of Zol improved muscle function. In summary, AI treatment induced bone loss and skeletal muscle weakness, recapitulating effects observed in cancer patients. Prevention of AI-induced osteoclastic bone resorption using a bisphosphonate attenuated the development of breast cancer bone metastases and improved muscle function in mice. These findings highlight the bone microenvironment as a modulator of tumor growth locally and muscle function systemically. Ongoing studies during the next project period will evaluate how AIs and the selective estrogen receptor modulator tamoxifen impact skeletal muscle in the absence of bone metastases, and the role that bone loss plays in AI-induced muscle weakness using in vivo and in vitro models.					
<b>15. SUBJECT TERMS</b> Breast cancer; bone metastases; estrogen; endocrine therapy; aromatase inhibitors; letrozole; selective estrogen receptor modulators; tamoxifen; bone loss; TGF $\beta$ ; skeletal muscle; ryanodine receptor; myocyte.					
<b>16. SECURITY CLASSIFICATION OF:</b>			<b>17. LIMITATION OF ABSTRACT</b>  Unclassified	<b>18. NUMBER OF PAGES</b>  64	<b>19a. NAME OF RESPONSIBLE PERSON</b> USAMRMC
<b>a. REPORT</b> Unclassified	<b>b. ABSTRACT</b> Unclassified	<b>c. THIS PAGE</b> Unclassified			<b>19b. TELEPHONE NUMBER</b> (include area code)

## TABLE OF CONTENTS

	<u>Page</u>
1. Introduction.....	4
2. Keywords.....	4
3. Accomplishments.....	4
4. Impact.....	8
5. Changes/Problems.....	9
6. Products.....	10
7. Participants & Other Collaborating Organizations.....	10
8. Special Reporting Requirements.....	10
9. Appendices.....	10

## 1. INTRODUCTION

Adjuvant endocrine therapy using an aromatase inhibitor (AI), which drastically depletes peripheral 17 $\beta$ -estradiol (E2) concentrations, is a standard treatment for postmenopausal women with estrogen receptor (ER)-positive breast cancer. Unlike selective estrogen receptor modulators (SERMs), which spare bone, AI treatment leads to severe bone loss and musculoskeletal complications that result in low patient compliance for life-prolonging AI therapy. The mechanism(s) of AI-induced muscular dysfunction have not been identified, however, E2-deprivation is characterized by inflammation and release of systemic factors during bone resorption, which together have been demonstrated in other disease models to cause skeletal muscle weakness through oxidation and nitrosylation of RyR1 and SERCA1, critical calcium channels required for skeletal muscle contraction. What is more, a state of high bone turnover resulting from AI-induced E2 depletion could alter the bone microenvironment by releasing matrix-derived growth factors (e.g., TGF- $\beta$ ) that prime the pre-metastatic niche and increase breast cancer progression in bone. This proposal was therefore designed to evaluate the effects of AI therapy on the musculoskeletal system in the context of breast cancer by determining 1) how AI-induced E2 depletion impairs muscle function, 2) whether AI-induced E2 depletion increases breast cancer bone metastases and 3) the relative contribution of bone loss in each case. Data obtained during this project period support the postulate that AI-induced bone loss can increase breast cancer bone metastases and contributes to muscle dysfunction.

## 2. KEYWORDS

**Breast cancer; bone metastases; estrogen; endocrine therapy; aromatase inhibitors; letrozole; selective estrogen receptor modulators; tamoxifen; endoxifen; bone loss; skeletal muscle; ryanodine receptor; myocyte; bone marrow adipose tissue.**

## 3. ACCOMPLISHMENTS

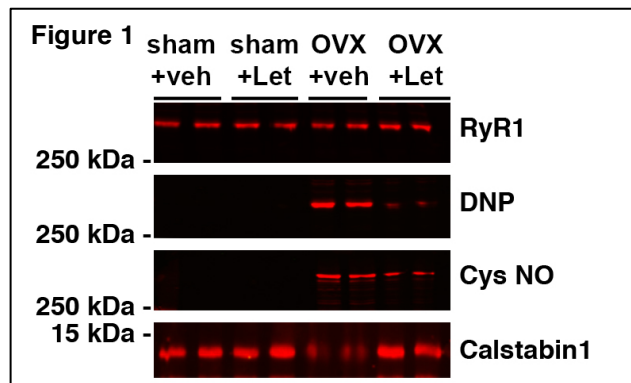
### A. Major scientific goals

**Task 1. Determine effects of the aromatase inhibitor (AI) letrozole and the selective estrogen receptor modulator (SERM) tamoxifen on skeletal muscle function in vivo. [50% complete]**

- As reported in the first project period, I have confirmed that ovariectomy (OVX) is sufficient to cause skeletal muscle weakness in mice 6-weeks post-surgery. I am currently examining whether estrogen deprivation-induced skeletal muscle weakness is *further* exacerbated by the addition of an AI (10 $\mu$ g/day) or SERM (endoxifen; 10mg/kg/d) in non-tumor bearing C57Bl/6 mice. This eight-week *in vivo* study is underway and scheduled to be completed on December 14<sup>th</sup> 2016. Results from this study (BMD, body composition, muscle contractility, grip strength, and bone volume by  $\mu$ CT) will be reported in the final annual report and will result in the completion of Task 1.

**Task 2. Evaluate biochemical changes in skeletal muscle resulting from estrogen (E2) deprivation therapy. [70% complete]**

- In order to determine how AI (letrozole) therapy impacts calcium handling at the molecular level, skeletal muscle lysates were obtained from sham-vehicle, sham-letrozole, OVX-vehicle, and OVX-letrozole-treated mice. RyR1-calstabin1 co-immunoprecipitation, oxidation of RyR1 and nitrosylation of RyR1 were analyzed by immunoblot (**Figure 1**). RyR1 channels appeared oxidized (DNP) and nitrosylated (Cys NO) in OVX mice regardless of drug treatment. Co-expression of RyR1 with its stabilizing



subunit calstabin1 was *not* altered by treatment with the AI letrozole, and therefore our initial hypothesis was not supported. Surprisingly, RyR1-calstabin dissociation was observed in OVX-vehicle treated muscle lysates, indicating that ovarian estrogen depletion alone may alter calcium handling at the myocyte level. These results indicate that AI-induced muscle weakness is likely not attributed to changes in RyR1 stability. I therefore plan to pursue a new mechanistic basis for AI-induced muscle weakness using *in vitro* culture experiments proposed in Task 4.

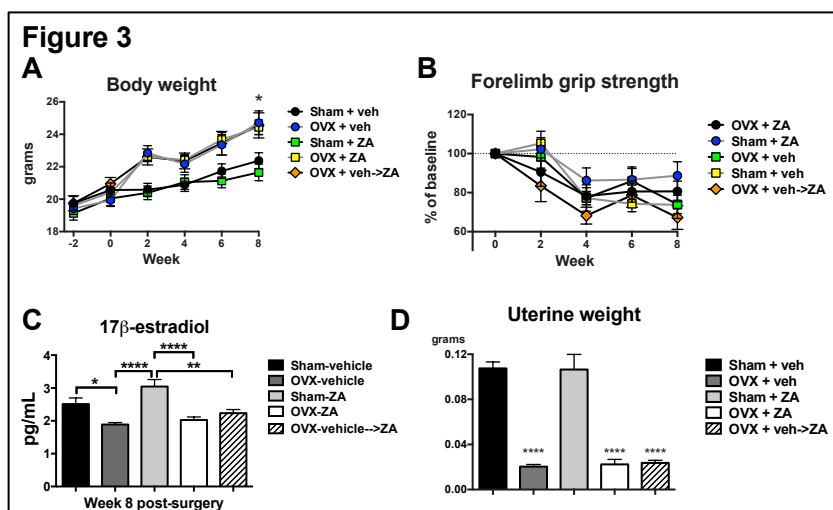
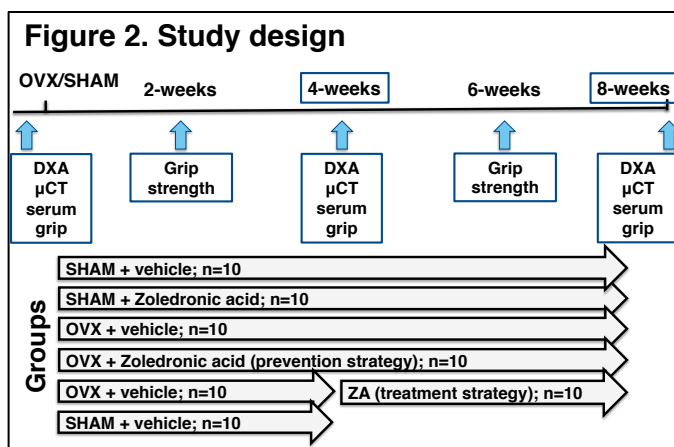
- In order to confirm that maladaptive modifications to RyR1 are not mechanistically responsible for muscle weakness in estrogen deprived mice, muscle lysates collected at the termination of the final study described in Task 1 will be analyzed for nitrosylation and oxidation of RyR1, as well as for co-expression of RyR1 and calstabin1. These data will be presented in the final annual report and will result in the completion of Task 2.

**Task 3. Evaluate whether the degree of AI- and SERM-induced muscle weakness correlates with treatment-induced bone loss. [70% complete]**

- As described in Task 1, the current study that I have initiated this fall (to be completed on December 14<sup>th</sup>, 2016) will evaluate changes in skeletal muscle function in non-tumor-bearing AI and SERM-treated mice. Mice are being followed prospectively for changes in body composition and bone-specific parameters by DXA (for BMD) and bone  $\mu$ CT (for bone volume). The complete data set will then be analyzed using regression analyses in order to determine the relationship between bone loss and muscle weakness in mice treated with estrogen deprivation therapies. Representative  $\mu$ CT reconstructions of all groups will be compiled and included in the final report.

**Task 4. Determine whether prevention of osteoclastic bone resorption can ameliorate muscle weakness associated with E2 deprivation *in vivo*. [80% complete]**

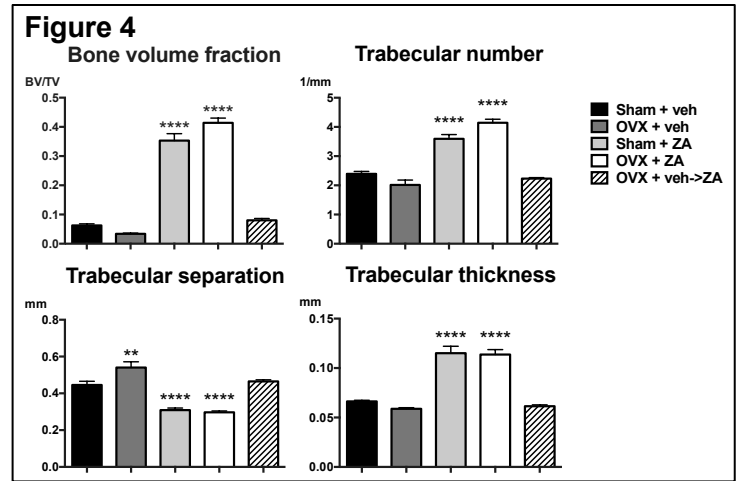
- Female C57Bl/6 mice were sham-operated or ovariectomized (OVX) and treated with or without the anti-bone resorptive zoledronic acid (ZA) using both prevention and treatment strategies for eight weeks (**Figure 2**). OVX mice gained weight relative to sham mice regardless of treatment (**Figure 3A**). Forelimb



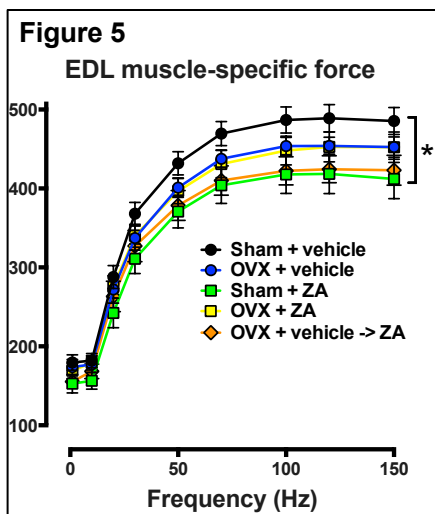
grip strength was not altered between any groups (**Figure 3B**), despite the fact that serum estradiol levels were reduced in OVX mice (**Figure 3C**). Effects of surgery and loss of estrogenic activity were confirmed by a significant reduction in uterine weight at the termination of the study (**Figure 3D**).

- Changes in trabecular bone volume were analyzed by  $\mu$ CT in order to assess the effects of

estrogen deprivation on bone loss. OVX mice lost approximately half of their trabecular bone volume fraction relative to sham-vehicle control mice and trabecular microarchitecture was compromised in OVX mice (**Figure 4**). The addition of the anti-resorptive zoledronic acid (ZA) reversed these effects and resulted in drastic increases in bone volume fraction, trabecular number and trabecular thickness, and a favorable reduction in trabecular spacing (**Figure 4**).



- After confirming bone loss in OVX mice and increased bone in OVX-ZA mice (**Figure 4**), whole muscle contractility of the extensor digitalis longus (EDL) muscle was evaluated *ex vivo*. OVX mice had a reduction in muscle contractility relative to sham-vehicle mice; however, this trend did not reach statistical significance (**Figure 5**). Addition of ZA to OVX mice did not result in increased muscle contractility, and interestingly, ZA treatment in sham mice resulted in a significant reduction in muscle-specific force production relative to sham-vehicle mice (**Figure 5**). These data indicate that zoledronic acid may have direct deleterious effects on muscle function, a postulate I have begun to pursue in task 5.



- In order to further examine the effects of estrogen deprivation-induced bone loss on muscle weakness *in vivo*, I am currently conducting a study comparing changes in bone and muscle in OVX-vehicle, OVX-AI, and OVX-AI-Zol-treated mice. We hypothesize that depletion of both ovarian and peripheral estrogen levels through the combination of OVX and AI therapy is necessary to induce significant muscle weakness in our model. Results from the ongoing study will be reported in the final project period and will result in the completion of Task 4.

**Task 5. Test the direct effects of E2 deprivation therapies letrozole (AI), tamoxifen (SERM), and the anti-resorptive therapy bisphosphonate (zoledronic acid) on skeletal muscle *in vitro*. [15% complete]**

- C2C12 cell cultures were differentiated into myotubes and treated with the bisphosphonate zoledronic acid (0.001-10 $\mu$ g/mL) and the aromatase inhibitor letrozole (0.001-10 $\mu$ g/mL) in a dose-response study. Cells were then scraped and stored with protease inhibitors at -20°C for full characterization of drug treatment-induced changes in skeletal muscle. I am now beginning to examine changes in myotube oxidation, nitrosylation, and protein levels of ubiquitin ligases relative to vehicle-treated control cell cultures. These studies will be completed and reported in the final project period.

**Task 6. Determine whether estrogen deprivation therapy and breast cancer bone metastases are associated with maladaptive modifications to RyR1 in human tissue samples. [0% complete]**

- Due to a lack of evidence that RyR1 is involved in AI-induced muscle weakness (**Figure 1**), I will not be collecting human muscle biopsies to assess biochemical modifications to the RyR1 channel complex. Please see “*Changes in approach and reasoning*” (pp. 9) for the justification of a new scientific goal to replace Task 6.

**Task 7. Prepare manuscript containing novel findings from Tasks 1-6. [0% complete]**

**Task 8. Determine whether the E2 deprivation therapy accelerates the progression of breast cancer bone metastases *in vivo*. [100% complete]**

- Please see completed manuscript in the appendix.

**Task 9. Determine whether prevention of E2 deprivation-induced bone loss can reduce the progression of breast cancer bone metastases *in vivo*. [100% complete]**

- Please see completed manuscript in the appendix .

**Task 10. Prepare manuscript containing novel findings from Tasks 8-9. [100% complete]**

- During this project period, I completed tasks 7-10 and have submitted my work for publication in the high-impact peer-reviewed cancer research journal *Oncotarget*. This manuscript is currently under review (see appendix).

**B. Training & professional development accomplishments**

A major component to this postdoctoral grant involves professional training in order for me to reach my primary career objective of becoming an independent cancer investigator.

- During this award period (January 2016), I was promoted from postdoctoral fellow to Assistant Research Professor within the Department of Medicine at Indiana University School of Medicine (see appendix).
- In March of 2016, I received the John G. Haddad Young Investigator Award from the American Society for Bone and Mineral Research (ASBMR) for outstanding research in the field of bone (see appendix).
- As part of my development as primary investigator, I mentored a second year medical student named Michael Campbell through the Indiana University Student Research Program in Academic Medicine (SRPinAM). During his three months under my wing, I developed a project for him related to his interests in radiation therapy, trained him in the necessary laboratory techniques, and monitored his progress throughout the study. Upon successful completion of the project, he presented his work to peers and researchers associated with the SRPinAM program at Indiana University.
- In March of 2016, I became a member of the Indiana University Simon Cancer Center (IUSCC) where I will be able to make meaningful contributions to research and outreach activities in collaboration with other members. Through the IUSCC, I now have access to its research programs and resources that will support and augment the aims of this grant proposal (see appendix).

**C. Dissemination of results to communities of interest**

- Results for these studies were presented by invitation to peers and thought-leaders in the fields of oncology and bone biology at 1) the Advances in Mineral and Metabolism (AIMM) conference in Breckenridge CO March 2016, 2) the European Calcified Tissue Society (ECTS) annual meeting in Rome, Italy May of 2016, and 3) the IUSCC Tumor Microenvironment and Metastasis (TMM) working group annual retreat in Indianapolis, IN August of 2016.

- Investigators rely on mouse models to better understand the pathogenesis of skeletal complications of malignancy in order to identify therapeutic targets that may ultimately prevent and treat tumor metastasis to bone. In the process of working on this project, I have learned about the many experimental models of breast cancer bone metastases in use today, each with its own caveats. In collaboration with cancer researchers from around the world, I spearheaded the publication of a methods review article (see appendix) where we described and reported methods for optimizing tumor-take in murine models of bone metastasis. We then provided working protocols for four of the most common xenograft and syngeneic inoculation routes for modeling breast cancer metastasis to the skeleton in mice, including the intra-cardiac method of tumor cell injection utilized in my studies. Recommendations for *in vivo* and *ex vivo* assessment of tumor progression and bone destruction were also provided, followed by discussion of the strengths and limitations of the available tools and translational models that aid investigators in the study of breast cancer metastasis to bone.

#### **D. Anticipated activities for the next reporting period (09/2016 – 09/2017)**

##### **Scientific goals:**

In brief, the next reporting period will be focused on completing the final analyses of data obtained from *in vivo* studies currently underway examining the effects of AI and SERM on skeletal muscle function in non-cancer bearing mice, as described in Tasks 1-4. In addition to this work and the subsequent drafting of a second manuscript related to the funded project, I plan to look at the potential direct effects of AI, SERM, and bisphosphonates on myocyte cultures (Task 5).

##### **Professional development goals**

As I begin the final year of the award, my primary professional goal is to develop and prepare a new grant proposal for submission in the year 2017 so that I am able to carry my work forward with continuous funding. I will also be attending the Cancer and Bone Society (CABS) meeting in May of 2017 in Indianapolis IN and presenting my work to peers and colleagues in the oncology field.

## **4. IMPACT**

### **Impact of accomplishments on breast cancer field**

Results obtained during this reporting period were significant for the field of breast cancer metastasis in that they support the concept that a state of high bone turnover can alter the bone microenvironment to increase the progression of tumor growth at this site. The greater implications for the field are that any treatment or environmental factor that leads to bone loss (e.g., glucocorticoids, GnRH inhibitors, radiation, fracture, osteoporosis, etc.) could increase the homing of dormant disseminated cancer cells to the skeleton. Clinicians thus need to be mindful of bone health in breast cancer patients and survivors.

### **Impact of accomplishments on progress of the project**

During this reporting period, I was able to characterize the effects of bisphosphonates on skeletal muscle *in vivo* in a non-tumor setting. Moreover, the completion of Tasks 8-10 resulted in a publication that will likely be accepted and disseminated in the year 2017.

### **Impact on society and public health**

Next to nothing is known about the impact that hormone therapies have on muscle function at the cellular and molecular level, despite clinical reports of muscle weakness in patients undergoing AI treatment. Work from this second reporting period investigating this common yet understudied complication of breast cancer treatment revealed that oxidation and nitrosylation of calcium channels in skeletal muscle are likely not the mechanistic basis for AI-induced muscle weakness. If this can be confirmed in future reporting periods, antioxidants may be a viable therapeutic in the prevention or treatment of muscle weakness with AI therapy.

Finally, cancer mortality is typically not caused by growth of the primary tumor, but rather is the result of complications associated with tumor cell metastasis to secondary organ sites including bone. Information obtained from my studies could help guide the selection of therapeutics for breast cancer patients and survivors, with emphasis on the importance of maintaining bone health in order to reduce patient risk of deadly breast cancer bone metastases. The studies presented here address important



unanswered clinical questions that have the potential to improve the quality and longevity of life for breast cancer patients.

## 5. CHANGES/PROBLEMS

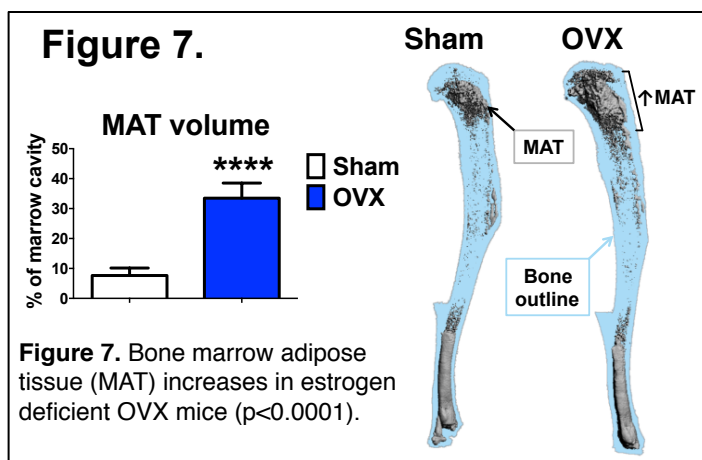
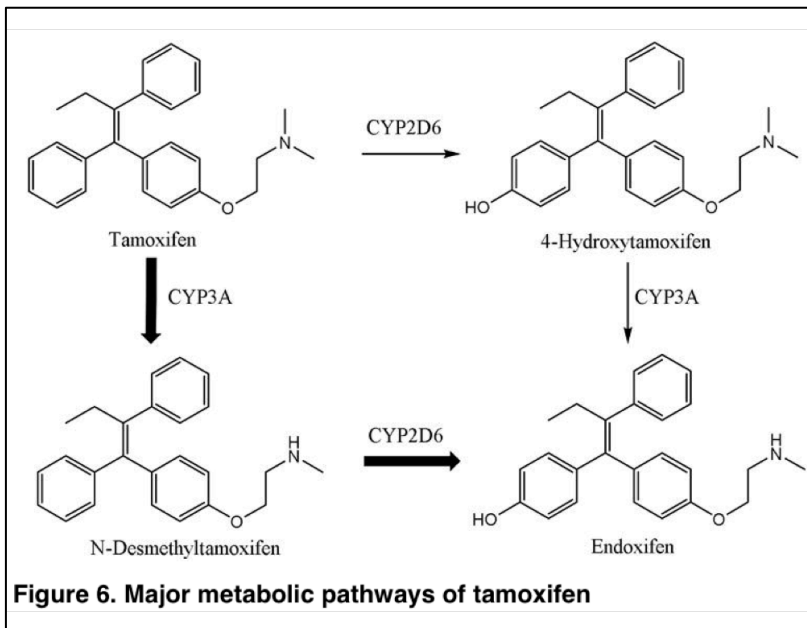
### Changes in approach and reasoning

1. After further research and literature review, I learned that mice do not possess the enzyme CYP2D6 necessary for metabolism of the drug tamoxifen into its active metabolites 4-HT and endoxifen (**Figure 6**). As endoxifen is thought to be the most active metabolite of tamoxifen, we will therefore be treating the mice directly with the endoxifen in Tasks 1,3 rather than dosing with tamoxifen.

2. Human muscle samples will not be collected due to lack of evidence of RyR1 involvement in AI-induced muscle weakness. We propose replacing Task 6 with an exciting new direction related to changes in bone marrow adipose tissue (MAT) in estrogen deficient mice.

Epidemiological studies have demonstrated a strong link between obesity and increased breast cancer recurrence and mortality. Previous cell culture and clinical studies have demonstrated that peripheral adipose (fat) tissue promotes cancer growth, yet the contribution of increased MAT on metastatic tumor growth in bone is currently unknown. MAT, which is a historically understudied fat depot, accounts for 10-15% of the body's total adipose tissue mass and can occupy up to 70% of the bone marrow compartment. MAT increases gradually with age; however, the accrual of MAT is dramatically accelerated with obesity, estrogen deprivation, glucocorticoid use, chemotherapy, and radiation therapy, putting breast cancer patients at increased risk of early and accelerated deposition of MAT.

Bone is the preferred site for breast cancer metastasis, and because fat tissue makes up such a large proportion of the marrow environment, the lack of understanding regarding the effects of MAT accrual on tumor cell invasiveness and growth represents a significant knowledge gap in the breast cancer field. I measured MAT in mice harvested in Task 4 and found that OVX mice had increased MAT compared to sham-control mice (**Figure 7**). We therefore propose measuring changes in MAT volume with OVX, AI therapy, SERM treatment, and bisphosphonate treatment in order to characterize its potential impact on the tumor microenvironment. An updated SOW is included in the appendix.



### Anticipated problems or delays

Nothing to report

### Changes that had a significant impact on expenditures

Nothing to report

### Changes in use or care of vertebrate animals

Nothing to report

## 6. PRODUCTS—see appendices for full details and documentation

### Award:

John G. Haddad Young Investigator Award from the American Society for Bone and Mineral Research (ASBMR).

### Invited seminars:

1. Advances in Mineral and Metabolism (AIMM) invited speaker March 31, 2016, Breckenridge CO.

Title: *Bone Loss Due to Complete Estrogen Deprivation Causes Muscle Weakness and Increased Progression of ER-Negative Breast Cancer in Bone*

2. European Calcified Tissue Society (ECTS) invited speaker May 3, 2016, Rome, Italy.

Title: *Bisphosphonates prevent osteolysis and muscle weakness in aromatase inhibitor-treated mice with breast cancer bone metastases*

3. Tumor Microenvironment and Metastasis (TMM) annual retreat invited speaker August 8, 2016, Indianapolis, IN.

Title: *Cancer therapy-induced changes to bone and implications for the tumor microenvironment*

### Peer-reviewed publications:

1. **Wright LE**, Ottewell PD, Rucci N, Peyruchaud O, Pagnotti GM, Chiechi A, Buijs JT, Sterling JA. Murine models of breast cancer bone metastases. *Bonekey Rep.* 2016, doi:10.1038/bonekey.2016.31.
2. **Wright LE**, Harhash AA, Kozlow WM, Waning DL, Regan JN, She Y, John SK, Murthy S, Niewolna M, Marks AR, Mohammad KS, Guise TA. Aromatase inhibitor-induced bone loss increases the progression of estrogen receptor-negative breast cancer in bone and exacerbates muscle weakness in vivo. *Oncotarget.* 2016 (under review).

## 7. PARTICIPANTS & OTHER COLLABORATING ORGANIZATIONS

Primary investigator (PI): Laura E. Wright, Ph.D. – *no change*.

## 8. SPECIAL REPORTING REQUIREMENTS

Nothing to report

## 9. APPENDICES

See attached documents

## Appendices - BC134025 - Annual Report, October 20, 2016

### **Aromatase Inhibitor-Induced Bone Loss Increases the Progression of Estrogen Receptor-Negative Breast Cancer in Bone and Exacerbates Muscle Weakness *In Vivo***

Laura E. Wright<sup>1</sup>, Ahmed A. Harhash<sup>1</sup>, Wende M. Kozlow<sup>2</sup>, David L. Waning<sup>3</sup>, Jenna N. Regan<sup>1</sup>, Yun She<sup>1</sup>, Sutha K. John<sup>1</sup>, Sreemala Murthy<sup>1</sup>, Maryla Niewolna<sup>1</sup>, Andrew R. Marks<sup>4</sup>, Khalid S. Mohammad<sup>1</sup>, Theresa A. Guise<sup>1</sup>

<sup>1</sup>*Department of Medicine, Division of Endocrinology, Indiana University, Indianapolis, IN, USA;*

<sup>2</sup>*Department of Internal Medicine, Division of Endocrinology, University of Virginia, Charlottesville, VA, USA;*

<sup>3</sup>*Department of Cellular and Molecular Physiology, The Pennsylvania State University College of Medicine, Hershey, PA, USA.*

<sup>4</sup>*Department of Physiology, Columbia University, New York, NY, USA.*

#### **To whom correspondence may be addressed:**

Laura E. Wright, Ph.D.  
Assistant Research Professor  
980 West Walnut Street  
Walther Hall R3, Room C126  
Indianapolis, IN 46202, USA

**Conflict of interest:** The authors have no conflicts to disclose.

**Keywords (5):** Breast cancer; bone; metastasis; aromatase inhibitor; skeletal muscle.

**Figures:** 7

**Word count:** 6511

## **ABSTRACT**

Aromatase inhibitors (AIs) cause muscle weakness, bone loss, and joint pain in up to half of cancer patients. Preclinical studies have demonstrated that increased osteoclastic bone resorption can impair muscle contractility and prime the bone microenvironment to accelerate metastatic growth. We hypothesized that AI-induced bone loss could increase breast cancer progression in bone and exacerbate muscle weakness associated with bone metastases. Female athymic nude mice underwent ovariectomy (OVX) or sham surgery and were treated with vehicle or AI (letrozole; Let). An OVX+Let group was then further treated with bisphosphonate (zoledronic acid; Zol). At week three, trabecular bone volume was measured and mice were inoculated with MDA-MB-231 cells into the cardiac ventricle and followed for progression of bone metastases. Five weeks after tumor cell inoculation, tumor-induced osteolytic lesion area was increased in OVX-Let mice and reduced in OVX-Let-Zol mice compared to sham-vehicle. Tumor burden in bone was increased in OVX-Let mice relative to sham-vehicle and OVX-Let-Zol mice. At the termination of the study, muscle-specific force of the extensor digitorum longus muscle was reduced in OVX-Let mice compared to sham-vehicle mice, however, the addition of Zol improved muscle function. In summary, AI treatment induced bone loss and skeletal muscle weakness, recapitulating effects observed in cancer patients. Prevention of AI-induced osteoclastic bone resorption using a bisphosphonate attenuated the development of breast cancer bone metastases and improved muscle function in mice. These findings highlight the bone microenvironment as a modulator of tumor growth locally and muscle function systemically.

## **INTRODUCTION**

Breast cancer is the most commonly diagnosed cancer in women [1] and the majority of breast tumors are hormone-responsive [2]. Adjuvant endocrine therapies that impair the action

of estrogen on breast tissue have become an important treatment strategy, reducing the risk of recurrence and death in women with estrogen receptor (ER)-positive disease [3,4]. Aromatase inhibitors, which block the rate-limiting step of estrogen biosynthesis [5], have replaced selective estrogen receptor modulators (SERMs; e.g., tamoxifen) as the standard of care in postmenopausal breast cancer patients due to improved disease-free survival [6,7]. AI treatment regimens in the adjuvant setting are typically administered for five years and the extension of AI treatment regimens to ten years is under study [8]. Between 25-50% of women treated with AIs report musculoskeletal toxicities, including joint pain, muscle weakness, and fragility, which result in diminished quality of life and poor compliance [9-18]. Relatively little is known about the molecular mechanism(s) of AI-induced arthralgia or muscle dysfunction. However, it is well established that AI treatment results in significant bone loss and increased fracture risk [16-18]. Our laboratory has had a longstanding interest in investigating how bone loss can impact tumor behavior in the bone microenvironment, a question that is of relevance to breast cancer patients undergoing prolonged AI therapy in the absence of a bone-protective intervention.

During a state of excessive bone resorption, matrix-derived growth factors have been shown to increase the growth of metastatic cancer cells in bone as well as stimulate their expression of osteolytic factors, which further perpetuate the destructive cycle of breast cancer in bone [19]. Additionally, osteoclast-derived proteolytic enzymes have been shown to promote angiogenesis, cancer cell invasiveness, and engraftment at metastatic sites [20]. In the case of estrogen deficiency, a strong systemic increase in oxidative stress and inflammatory tone [21] could further perpetuate bone loss and, ultimately, cancer progression. Effects of bone loss resulting from AI-induced depletion of peripheral estrogen levels on the breast cancer bone metastases have not yet been tested. Thus, our first aim was to assess the role of AI therapy-induced bone loss on the progression of disseminated breast cancer cells *in vivo*.

The impact of AI therapy on skeletal muscle function at the cellular and molecular level remains unknown despite clinical reports of muscle fatigue in AI-treated patients [9-12]. Because the bone matrix can be a source of growth factors, including members of the transforming growth factor (TGF)- $\beta$  superfamily that affect both bone and muscle [22-23]. A state of high bone turnover could cause release of growth factors into circulation where they act on peripheral tissues. Previous studies in our laboratory have demonstrated that bone-derived TGF $\beta$  leads to oxidative overload in neighboring skeletal muscle and impaired muscle contractility in mice with osteolytic bone metastases [24]. The second aim of this study was to evaluate the effect of AI therapy and bone loss on skeletal muscle function in mice with bone metastases.

The overarching hypothesis driving this work is that estrogen deprivation therapy results in a high bone turnover state that increases breast cancer bone metastases and potentiates muscle weakness. It is important to note that we selected a triple negative breast cancer cell line (MDA-MB-231) in order to examine microenvironment-specific effects on tumor growth in the absence of direct effects of inhibition of ER signaling. Here we report that AI treatment causes bone loss and skeletal muscle weakness in OVX mice, and that the prevention of osteoclastic bone resorption attenuates the development of ER-negative breast cancer bone metastases and improves muscle function in AI-treated estrogen deprived mice.

## RESULTS

### **Aromatase inhibitor treatment reduced serum 17 $\beta$ -estradiol and trabecular bone volume in OVX nude mice prior to tumor inoculation**

Four-week female athymic nude mice underwent ovariectomy (OVX) or sham surgery and were treated via daily subcutaneous injection with vehicle (PBS, 50 $\mu$ L), or the aromatase inhibitor letrozole (Let, 10 $\mu$ g/d) (**Figure 1**). A second OVX-Let-treated group was treated with the bisphosphonate zoledronic acid (Zol, 5 $\mu$ g/kg 3x/week) in order to determine the relative

importance of bone loss on tumor growth and muscle function in the setting of AI therapy (**Figure 1**). Prior to the inoculation of tumor cells and three weeks after surgery, serum  $17\beta$ -estradiol was reduced in OVX-Let and OVX-Let-Zol mice relative to sham groups (**Figure 2A**). A partial reduction in serum estradiol was observed in OVX-PBS-treated mice relative to sham, although this did not reach statistical significance (**Figure 2A**). As a terminal and surrogate measure of estrogenic activity [25], uterine weight was recorded at the end of the study (nine weeks post-surgery and five weeks after tumor inoculation). As anticipated, OVX resulted in significant uterine atrophy relative to sham groups regardless of drug treatment, and the addition of aromatase inhibitor to ovary intact mice (sham-Let) resulted in a moderate reduction in uterine weight relative to sham-PBS, though this did not reach statistical significance (**Figure 2B**).

In line with observed estrogenic changes, trabecular bone volume (BV/TV) assessed by bone microcomputed tomography was reduced in sham-Let and OVX-PBS mice (-29% and -52%, respectively) relative to estrogen-replete sham-PBS controls (**Figure 3A**). The combination of OVX and letrozole (OVX-Let) resulted in 67% reduction in trabecular bone volume relative to sham-PBS mice (**Figure 3A**). The anti-resorptive zoledronic acid increased trabecular bone volume in the OVX-Let-Zol mice by over three times that of sham-PBS mice and over ten times that of OVX-Let mice after three weeks of treatment (**Figure 3A**). Bone microarchitectural parameters, including connectivity density, structure model index, and trabecular number, separation and thickness, mirrored changes observed in trabecular bone volume for all treatment groups (**Figure 3B-G**). In summary, each microarchitectural property assessed was severely compromised in OVX-Let mice relative to estrogen-replete sham-PBS mice and these maladaptive modifications in trabecular bone were significantly improved by zoledronic acid treatment (**Figure 3B-G**).

**Osteolysis and tumor burden were increased in aromatase inhibitor-treated OVX mice**

Having established an estrogen deficiency-driven high bone turnover state in OVX-Let mice by week three, MDA-MB-231 human breast cancer cells were inoculated into the left cardiac ventricle to generate a model of breast cancer metastatic to bone in order to determine the importance of aromatase inhibitor-induced changes to the bone microenvironment on tumor progression in the skeleton. Weekly body weight measurements were performed as a general assessment of disease progression and overall health [26]. For the duration of the study, OVX-Let-Zol mice maintained a higher average absolute body weight, achieving statistical significance relative to sham-Let and OVX-Let animals (**Figure 4A**). Body composition analyses by dual energy X-ray absorptiometry (DXA) revealed similar patterns of change in lean mass and fat mass percentage over time between groups, with differences observed only in fat mass percentage at week nine between OVX-Let-Zol and sham-PBS-treated mice (**Figure 4B,A**). The rapid decline in total body weight, lean mass, and fat mass observed in all treatment groups at week six (three weeks post-tumor inoculation) (**Figure 4A-C**) is indicative of tumor progression in this model [26].

Changes in bone mineral density (BMD) following the inoculation of tumor cells were assessed by DXA over time. Consistent with the observed increase in trabecular bone volume three weeks after onset of Zol treatment (**Figure 3A**), BMD was significantly increased in the total skeleton, lumbar vertebrae, distal femur, and proximal tibia in OVX-Let-Zol mice relative to estrogen-replete (sham-PBS), partial estrogen-deprived (sham-Let, OVX-PBS), and total estrogen-deprived mice (OVX-Let) (**Figure 4D-G**), confirming that the drug's anti-resorptive effect persisted throughout the study. Importantly, the OVX-Let group had a significant reduction in total skeletal BMD at the nine-week time point relative to sham-PBS (**Figure 4D**), indicating that AI treatment continued to cause significant bone loss over the course of the nine-week study due to estrogen deficiency and its possible role in cancer-induced osteolysis.

In order to directly assess cancer-induced destruction of bone, radiographs were acquired three and five weeks post-tumor inoculation, and X-rays were carefully examined for



radiolucent regions indicative of cancer-mediated osteolysis. Osteolytic lesion area was increased in estrogen deprived OVX-Let mice relative to all treatment groups (**Figure 5A,B**). Lesions were detected in AI-treated OVX mice treated with bisphosphonate (OVX-Let-Zol) (**Figure 5A**); however, the anti-resorptive effects of Zol drastically reduced the total osteolytic lesion area relative to their estrogen-deprived counterparts (OVX-let) (**Figure 5A,B**). These data were corroborated at the histological level through the quantitation of multinucleated bone-resorbing osteoclasts at the bone-tumor interface in the marrow compartment [26]. Osteoclast numbers were increased in OVX-let mice relative to all groups, and Zol treatment reversed this heightened state of osteoclastogenesis (**Figure 6A**), in line with the drug's ability to induce osteoclast apoptosis [27].

Having confirmed effects on bone, a primary aim of the study was to evaluate how these AI- and Zol-induced changes to the bone microenvironment could influence tumor progression in the absence of direct inhibition of tumor growth through manipulation of ER signaling. Use of the MDA-MB-231 triple-negative human breast cancer cell line permitted this bone-centric objective. Tumor burden in OVX-Let mice was measured at sites of skeletal metastases in histological sections, and total tumor area (mm<sup>2</sup>) was significantly increased relative to all groups (**Figure 6B-E**). Trabecular bone appeared intact in OVX-Let-Zol mice despite the presence of tumor cells (**Figure 6E**). The overall reduction in tumor area in Zol-treated mice relative to OVX-Let mice (**Figure 6D**) is likely attributed to the prevention in osteoclastic bone resorption and its feed-forward effect on osteolytic cancer metastases.

### **Bisphosphonates improved muscle function in AI-treated OVX mice independent of muscle mass**

Whole muscle contractility of the extensor digitorum longus (EDL) was measured at the termination of the study to evaluate the potential role of bone loss on muscle dysfunction in a state of AI-induced estrogen deprivation. Estrogen-replete mice with bone metastases (sham-

PBS) had a reduction in muscle specific force of the EDL relative to non-tumor age-matched controls, and this reduction reached statistical significance when mice were ovariectomized (OVX-PBS) (**Figure 7A**). Addition of letrozole to OVX tumor-bearing mice (OVX-Let) led to a further reduction of muscle specific force production of the EDL, reaching statistical significance relative to both tumor and non-tumor and tumor-bearing sham-PBS mice (**Figure 7A**). This deleterious effect on muscle function in OVX-Let mice was partially reversed by the prevention of osteoclastic bone resorption through zoledronic acid treatment (OVX-Let-Zol) (**Figure 7A**). Observed changes in muscle specific force production were independent of changes in EDL muscle mass because force production measurements were corrected for size and weight of the EDL [28]. Furthermore, hind limb muscles including the EDL, tibialis anterior, gastrocnemius, and soleus collected at the termination of the study in cancer-bearing mice were similar between treatment groups (**Figure 7B-E**), indicating that deficits in muscle specific force production in this study can likely be attributed to functional defects as opposed to muscle atrophy.

## DISCUSSION

The estrogen-replete and estrogen-deficient bone niches differ greatly as host environments for disseminated cancer cells due to the acute sensitivity of bone and marrow cells to changes in endocrine status. Estrogen acts directly on bone cells to regulate the lifespan of both osteoclasts and osteoblast, and inhibits T-cell production of inflammatory cytokines, which can further drive osteoclast activation and bone resorption [21,29]. Increased bone resorption has been demonstrated in preclinical models, including OVX, to accelerate cancer progression in bone [29-31] presumably via release of matrix-derived growth factors, (e.g., TGF $\beta$ , IGF, FGF, PDGF), which stimulate tumor growth and expression of osteolytic factors that perpetuate a feed-forward cycle of bone destruction [19]. Using an ER-negative breast cancer cell line to avoid direct tumor growth inhibitory effects, our studies support the postulate that

estrogen depletion by AI treatment alters the bone microenvironment in ways that can indirectly promote cancer cell homing, growth, and/or an osteolytic phenotype in bone. The assertion that AI-induced bone loss increased metastatic tumor growth was further supported by the finding that blockade of bone resorption by zoledronic acid reduced tumor burden in bone.

Direct anti-cancer effects of bisphosphonates have been pursued with relatively little evidence that physiologically relevant doses can directly elicit cancer cell apoptosis [32,33]. Although direct anti-tumor effects of bisphosphonates have been shown *in vitro* [33], their anti-cancer activity *in vivo* continues to be attributed to indirect effects via inhibition of osteoclastic bone resorption [29]. Recent clinical reports have demonstrated differential anti-cancer effects of bone-targeted anti-resorptives in breast cancer patients depending on menopausal status. In the AZURE, ZO-FAST and ABCSG-12 trials, zoledronic acid consistently improved disease-free survival in breast cancer patients, however, this effect was limited to 1) postmenopausal women and 2) premenopausal women undergoing AI therapy treatment (chemical menopause) [34-36], suggesting that the anti-tumor effects of zoledronic acid were reserved for estrogen deficient populations in a high bone turnover state. In light of our studies and the clinical link between bone loss and cancer progression, it will be important to consider the skeletal health not only of cancer patients undergoing AI therapy, but of patients undergoing any therapeutic intervention known to adversely affect skeletal health (e.g., GnRH agonists, glucocorticoids, radiation therapy).

We utilized the triple-negative MDA-MB-231 human breast cancer cell line to assess the impact of the microenvironment on tumor growth in the absence of effects on ER signaling. By contrast, adjuvant AI therapy in the clinical setting is prescribed to breast cancer patients with ER-positive primary tumors [7]. Clinical reports, however, indicate that in many cases ER status at the primary tumor site does not match the ER status of disseminated tumor cells [37], making our model relevant in the setting of advanced disease where metastatic tumor cell ER expression is lost. Once the metastatic process has been initiated, the tumor-promoting effects

of AI treatment-induced bone loss may negate the benefit of AI-induced tumor suppression at the primary site. Use of an ER-positive breast cancer model (e.g., MCF-7) would be useful in determining the relative importance of the benefit of direct tumor growth suppression versus the risk of bone resorption-induced disease progression in the context of AI therapy. Disease stage at the onset of AI treatment is relevant. Clinical data demonstrate that disease-free survival is approximately five times longer in patients receiving AIs with early stage disease compared to advanced metastatic breast cancer [38] where presumably the growth inhibitory effects of AIs are overridden by signals from the microenvironment. Breast cancer mortality results from tumor metastases rather than primary tumor growth [19], and bone is the preferred metastatic destination for breast cancer [39]. Thus, the prevention of bone loss in early stage breast cancer patients at the very onset of AI treatment could be of importance.

AI-induced arthralgia and muscle weakness are poorly characterized, yet are often so unmanageable that patients discontinue adjuvant AI therapy [9-13]. The identification of the molecular mechanism(s) underlying AI related muscle dysfunction could be critical in the development of interventions that can restore quality of life and improve drug compliance. In our studies zoledronic acid partially improved muscle function in AI treated mice with bone metastases, suggesting that osteoclastic bone resorption played a role in reduced skeletal muscle contractility in the setting of AI therapy. Recent work reported by our group identified bone-derived TGF $\beta$  as the mediator of muscle weakness in mice with bone metastases through the up-regulation of NADPH oxidase 4 production of reactive oxygen species leading to oxidation of the ryanodine receptor (RyR1) calcium channel complex in muscle resulting in SR Ca<sup>2+</sup> leak and muscle weakness [24]. Release of bone-derived TGF $\beta$  during AI therapy-induced bone loss could have downstream effects on muscle contractility via a similar mechanism, a hypothesis currently under investigation in our laboratory. We speculate that AI-induced muscle weakness is likely multi-faceted in light of the finding that bisphosphonate treatment alone did not restore muscle function to the level of non-tumor control mice. It is possible that AIs elicit

direct toxic effects on myocytes, a postulate that has yet to be tested. Selective estrogen receptor modulators (SERMs; e.g., tamoxifen), which interact with the ER and inhibit its activity in breast tissue while preserving bone have also associated with muscle weakness [14], suggesting that inhibition of ER signaling in muscle impacts muscle contractility in the absence of high bone turnover. Furthermore, muscle weakness associated with declining estrogen levels during menopause in healthy women can be rescued by hormone replacement therapy [40-42], providing further proof that ER signaling blockade contributes to muscle weakness in the AI-treated patient. Relevant non-tumor models and *in vitro* studies will be useful in determining the relative role of bone loss, ER signaling blockade, and potential direct drug toxicities on muscle function following AI and SERM therapy.

In summary, the causes of AI-induced musculoskeletal complications and the consequences of AI-induced bone loss are poorly characterized. Bone-derived factors released during an elevated state of osteoclastic bone resorption are known to have adverse effects on muscle function and can alter the bone microenvironment to favor breast cancer cell progression and perpetuate osteolysis. Our studies demonstrated that modulation of the bone microenvironment impacted tumor growth locally and muscle function systemically in AI treated mice. These findings emphasize the importance of considering the musculoskeletal health of cancer patients when selecting estrogen deprivation treatment options and the need to further investigate non-estrogenic therapeutic agents that can improve musculoskeletal outcomes in cancer patients.

## **MATERIALS AND METHODS**

### **Animals**

The Institutional Animal Care and Use Committee at Indiana University approved animal protocols for these studies in accordance with the National Institutes of Health Guide for the Care and Use of Laboratory Animals. Three-week female athymic nude mice were purchased

from Harlan Laboratories (Indianapolis, IN) and housed in plastic cages with access to water and mouse chow *ad libitum* and maintained on a 12h light/dark schedule at  $22 \pm 2^{\circ}\text{C}$ . After one week of acclimation, mice were anesthetized with a ketamine/xylazine cocktail and underwent bilateral ovariectomy (OVX) or a sham surgery under sterile conditions. Aromatase inhibitor (letrozole, 10ug/d), zoledronic acid (Zometa; 5 $\mu\text{g/kg}$  3x/week), and vehicle (PBS, 50 $\mu\text{l/d}$ ) treatments were administered daily via subcutaneous injection 24h after surgery and continued for the duration of the study. Blood was collected by retro-orbital puncture three days prior to surgery (baseline) and three weeks post surgery. Serum 17 $\beta$ -estradiol was measured by ELISA (Calbiotech) and expressed as percent of baseline.

### **Bone microcomputed tomography ( $\mu\text{CT}$ )**

Bone  $\mu\text{CT}$  was performed at the proximal metaphysis of the tibia using a high-resolution imaging system ( $\mu\text{CT40}$ ; SCANCO Medical AG) on isoflurane-anesthetized mice. Bone  $\mu\text{CT}$  scans were acquired using a 17 $\mu\text{m}^3$  isotropic voxel size, 55kVp peak X-ray tube potential, 200ms integration time, and were subjected to Gaussian filtration. Trabecular bone microarchitecture was evaluated in the proximal metaphysis of the tibia in a region that began 0.4mm distal to the growth plate and extended distally 1.0mm. A threshold of 170mg HA/cm<sup>3</sup> was used to segment bone from surrounding soft tissue. Trabecular bone outcomes included trabecular bone volume fraction (BV/TV; %), trabecular thickness (Tb.th; mm), trabecular number (Tb.N; mm<sup>-1</sup>), trabecular separation (Tb.Sp; mm), and connectivity density (Conn.D; mm<sup>-3</sup>). Scan acquisition and analyses were conducted in accordance with guidelines for use of  $\mu\text{CT}$  in rodents [43].

### **Dual energy X-ray absorptiometry (DXA)**

*In vivo* measurement of fat mass, lean mass and bone mineral density (BMD) was performed on anesthetized mice (ketamine/xylazine) using a PIXImus II densitometer (GE

Lunar, Madison, WI) calibrated with a phantom of defined density. Body composition and BMD were measured at baseline on the day of surgery, at week six post-surgery, and at the termination of the study (week nine post-surgery), and data were expressed as percent change over time.

### **Intra-cardiac inoculation procedure**

Three weeks after OVX and sham surgeries, mice were inoculated in the left cardiac ventricle with MDA-MB-231 tumor cells, as previously described [26]. Briefly, tumor cell inoculation was performed percutaneously into the left cardiac ventricle of anesthetized mice in a supine position with a 26-gauge needle attached to a 1mL syringe containing  $1 \times 10^5$  cells suspended in 0.1mL sterile PBS. Visualization of bright red blood entering the hub of the needle in pulsatile fashion was indicative of correct needle placement into the left cardiac ventricle. Mice were followed for the development of osteolytic bone lesions by radiography on days 23 and 32 of the experiment. Osteolytic lesions were visualized in anesthetized mice in prone position using a digital X-ray imager (Kubtec) at 2.7x magnification. Lytic lesion area, reported as total lesion area ( $\text{mm}^2$ ) per animal in hind limb and forelimb long bones, was analyzed in a blinded fashion using ImageJ 1.48r software (National Institutes of Health).

### **Histology**

Hind limbs were removed from mice at the time of experimental termination, fixed in 10% neutral-buffered formalin for 48h and stored in 70% ethanol. Tibiae, femora, and humeri were decalcified in 10% EDTA for two weeks, processed using an automated tissue processor (Excelsior, Thermoelectric), and embedded in paraffin. Mid-sagittal  $4.5\mu\text{m}$  sections were stained with hematoxylin and eosin (H&E) with orange G and phloxine to visualize new bone, and with tartrate-resistant acid phosphatase (TRAP) to visualize osteoclasts. Total tumor area was measured in H&E-stained mid-sagittal sections of the tibiae, femora, and humeri at 10x

magnification without knowledge of experimental groups. Osteoclast cells were quantified in the mid-sagittal sections of tibiae in tumor-bearing hind limbs. Briefly, TRAP-positive multinucleated cells were quantified at 40x magnification along the perimeter of the tumor where the cancer cells interfaced directly with bone surfaces. Data were expressed as number of osteoclasts per mm of tumor-bone interface (OcN/mm), as previously described [26]. All sections were viewed on a Leica DM LB compound microscope outfitted with a Q-Imaging Micropublisher Cooled CCD color digital camera (Nuhsbaum Inc., McHenry, IL). Images were captured and analyzed using BioQuant Image Analysis Software version 13.2 (BIOQUANT Image Analysis Corporation, Nashville, TN).

### **Measurement of muscle specific force**

*Ex vivo* contractility of the extensor digitorum longus (EDL) muscles was determined as previously described [24]. Briefly, EDL muscles were dissected from hind limbs and stainless steel hooks were tied to the tendons of the muscles using 4-0 silk sutures and the muscles were mounted between a force transducer (Aurora Scientific) and an adjustable hook. The muscles were immersed in a stimulation chamber containing O<sub>2</sub>/CO<sub>2</sub> (95/5%) bubbled Tyrode solution (121 mM NaCl, 5.0 mM KCl, 1.8 mM CaCl<sub>2</sub>, 0.5 mM MgCl<sub>2</sub>, 0.4 mM NaH<sub>2</sub>PO<sub>4</sub>, 24 mM NaHCO<sub>3</sub>, 0.1 mM EDTA, 5.5 mM glucose). The muscle was stimulated to contract using a supramaximal stimulus between two platinum electrodes. Data were collected via Dynamic Muscle Control/Data Acquisition (DMC) and Dynamic Muscle Control Data Analysis (DMA) programs (Aurora Scientific). The force–frequency relationships were determined by triggering contraction using incremental stimulation frequencies (0.5ms pulses at 1–150 Hz for 350ms at supra-maximal voltage). Between stimulations the muscle was allowed to rest for 3 min. At the end of the force measurement, the length and weight of the muscle was measured. To quantify the specific force, the absolute force was normalized to the muscle size calculated as the muscle



weight divided by the length using a muscle density constant of 1.056 kg/m<sup>3</sup> [28]. The investigators were blinded to treatment of subjects.

### **Statistical analyses**

Differences were determined by one-way or two-way ANOVA, as appropriate, with Tukey's multiple comparisons test (GraphPad, Prism 6.0f). Results are expressed as mean  $\pm$ SEM and  $p < 0.05$  was considered significant.

### **GRANT SUPPORT**

This work was supported by the Department of Defense Breast Cancer Research Program BC134025 (LEW) and BC043416 (WMK).

### **CONFLICT OF INTEREST**

The authors declare no conflict of interest.

### **REFERENCES**

1. Jemal A, Siegal R, Xu J, Ward E. Cancer statistics. CA Cancer J Clin. 2010; 60: 277-300.
2. Clark GM, Osborne CK, McGuire WL. Correlations between estrogen receptor, progesterone receptor, and patient characteristics in human breast cancer. J Clin Oncol. 1984; 2: 1102-1109.
3. Fisher B, Costantino J, Redmond C, Poisson R, Bowman D, Couture J, Dimitrov NV, Wolmark N, Wickerman L, Fisher ER, Margoless R, Robidoux A, Shibata H, et al. A randomized clinical trial evaluating tamoxifen in the treatment of patients with node-negative breast cancer who have estrogen-receptor positive tumors. N Engl J Med. 1989; 320: 479-484.
4. Goss PE, Ingle JN, Martino S, Robert NJ, Muss HB, Piccart MJ, Castiglione M, Tu D, Shepherd LE, Pritchard KI, Livingston RB, Davidson NE, Norton L, et al. A randomized trial of letrozole in postmenopausal women after five years of tamoxifen therapy for early-stage breast cancer. N Engl J Med. 2003; 349: 1793-1802.
5. Simpson ER, Davis SR. Minireview: aromatase and the regulation of estrogen biosynthesis – some new perspectives. Endocrinology. 2001; 142: 4589-4594.

6. Coates AS, Keshaviah A, Thürlimann B, Mouridsen H, Mauriac L, Forbes JF, Paridaens R, Castiglione-Gertsch M, Gelber RD, Colleoni M, Láng I, Del Mastro L, Smith I, et al. Five years of letrozole compared with tamoxifen as initial adjuvant therapy for postmenopausal women with endocrine-responsive early breast cancer: update of study BIG 1-98. *J Clin Oncol*. 2007; 25: 486-492.
7. Burstein HJ, Prestrud AA, Seidenfeld J, Anderson H, Buchholz TA, Davidson NE, Gelmon KE, Giordano SH, Hudis CA, Malin J, Mamounas EP, Rowden D, Solky AJ, et al. American Society of Clinical Oncology clinical practice guidelines: Update on adjuvant endocrine therapy for women with hormone receptor-positive breast cancer. *J Clin Oncol* 2010; 28: 3784-3796.
8. Goss PE, Ingle JN, Pritchard KI, Robert NJ, Muss H, Gralow J, Gelmon K, Whelan T, Strasser-Weippl K, Rubin S, Sturtz K, Wolff AC, Winer E, et al. Extending aromatase-inhibitor adjuvant therapy to 10 years. *N Engl J Med*. 2016; 375: 209-219.
9. Henry NL, Giles JT, Ang D, Mohan M, Dadabhoy D, Robarge J, Hayden J, Lemler S, Shahverdi K, Powers P, Li L, Flockhart D, Stearns V, Hayes DF, et al. Prospective characterization of musculoskeletal symptoms in early breast cancer patients treated with aromatase inhibitors. *Breast Cancer Res Treat*. 2008; 111: 365-372.
10. Lintermans A, Van Calster B, Van Hoydonck M, Pans S, Verhaeghe J, Westhovens R, Henry NL, Wildiers H, Paridaens R, Dieudonné AS, Leunen K, Morales L, Verschueren K, et al. Aromatase inhibitor-induced loss of grip strength is body mass index dependent: hypothesis-generating findings for its pathogenesis. *Annals Oncol*. 2011; 22: 1763-1769.
11. Dent SF, Gaspo R, Kissner M, Pritchard KI. Aromatase inhibitor therapy: toxicities and management strategies in the treatment of postmenopausal women with hormone-sensitive early breast cancer. *Breast Cancer Res Treat*. 2011; 126: 295-310.
12. Donnellan PP, Douglas SL, Cameron DA, Leonard RC. Aromatase inhibitors and arthralgia. *J Clin Oncol*. 2001; 19: 2767.
13. Henry NL, Azzouz F, Desta Z, Li L, Nguyen AT, Lemler S, Hayden J, Tarpinian K, Yakim E, Flockhart DA, Stearns V, Hayes DF, Storniolo AM. Predictors of aromatase inhibitor discontinuation as a result of treatment-emergent symptoms in early-stage breast cancer. *J Clin Oncol*. 2012; 30: 936-942.
14. Buzdar AU. Clinical features of joint symptoms observed in the 'Arimedex,' Tamoxifen, Alone or in Combination (ATAC) trial. *J Clin Oncol* 2006; 24(18s): 551.
15. Gross PE, Ingle JN, Ales-Martinez JE, Cheung AM, Chlebowski RT, Wactawski-Wende J, McTieran A, Robbins J, Johnson KC, Martin LW, Winkquist E, Sarto GE, Garber JE, et al. Exemestane for breast-cancer prevention in post-menopausal women. *N Engl J Med*. 2010; 364: 2381-91.
16. Henry NL, Giles JT, Stearns V. Aromatase inhibitors-associated musculoskeletal symptoms: etiology and strategies for management. *Oncology* 2008; 22: 1401-1408.
17. Brown SA, Guise TA. Cancer treatment-related bone disease. *Crit Rev Eukaryot Gene Expr*. 2009; 19: 47-60.
18. Saad F, Adachi JD, Brown JP, Canning LA, Gelmon KA, Josse RG, Pritchard KI. Cancer treatment-induced bone loss in breast and prostate cancer. *J Clin Oncol*. 2008; 26: 5466-5476.

19. Weilbaecher KN, Guise TA. Cancer to bone: a fatal attraction. *Nature Rev Cancer*. 2011; 11: 411-425.
20. Bonfil RD, Cher ML. Proteolytic enzymes in metastatic bone disease. *IBMS BoneKEy*. 2011; 8: 16-36.
21. Frenkel B, Hong A, Baniwal SK, Coetzee GA, Ohlsson C, Khalid O, Gabet Y. Regulation of adult bone turnover by sex steroids. *J Cell Physiol*. 2010; 224: 305-310.
22. Mendias CL, Gumucio JP, Davis ME, Bromley CW, Davis CS, Brooks SV. Transforming growth factor-beta induces skeletal muscle atrophy and fibrosis through the induction of atrogin-1 and scleraxis. *Muscle Nerve*. 2012; 45: 55-59.
23. Regan JN, Waning DL, Guise TA. Skeletal muscle Ca(2+) mishandling: Another effect of bone-to-muscle signaling. *Semin Cell Dev Biol*. 2016; 49: 24-29.
24. Waning DL, Mohammad KS, Reiken SR, Wenjun X, Anderssen DC, John S, Chiechi A, Wright LE, Umanskaya A, Niewolna M, Trivedi T, Charkhzarrin S, Khatiwada P, et al. TGFβ mediates muscle weakness associated with bone metastases. *Nature Med*. 2015; 21: 1262-1271.
25. Evans JS, Varney RF, Koch FC. The mouse uterine weight method for the assay of estrogens. *Endocrinology*. 1941; 28: 747-752.
26. Wright LE, Ottewell PD, Rucci N, Peyruchaud O, Pagnotti GM, Chiechi A, Buijs JT, Sterling JA. Murine models of breast cancer bone metastases. *BoneKEy Rep*. 2016; 5: 804.
27. Rodan GA, Fleisch HA. Bisphosphonates: mechanism of action. *J Clin Invest*. 1996; 97: 2692-2696.
28. Yamada T, Place N, Kosterina N, Ostberg T, Zhang SJ, Grundtman C, Erlandsson-Harris H, Lundberg IE, Glenmark B, Bruton JD, Westerblad H. Impaired myofibrillar function in the soleus muscle of mice with collagen-induced arthritis. *Arthritis Rheum*. 2009; 60: 3280-3289.
29. Wright LE, Guise TA. The microenvironment matters: estrogen deficiency fuels cancer bone metastases. *Clin Cancer Res*. 2014; 20: 2817-2819.
30. Ottewell PD, Wang N, Brown HK, Reeves KJ, Fowles CA, Croucher PI, Eaton CI, Holen I. Zoledronic acid has differential antitumor activity in pre- and postmenopausal bone microenvironment in vivo. *Clin Cancer Res*. 2014; 20: 2922-2932.
31. Schneider A, Kalikin LM, Mattos AC, Keller ET, Allen MJ, Pienta KJ, McCauley LK. Bone turnover mediates preferential localization of prostate cancer in the skeleton. *Endocrinology*. 2005; 146: 1727-1736.
32. Ottewell PD, Monkkonen J, Jones M, Lefley DV, Coleman RE, Holen I. Antitumor effects of doxorubicin followed by zoledronic acid in a mouse model of breast cancer. *J Natl Cancer Inst*. 2008; 100: 1167-1178.
33. Jagdev SP, Coleman RE, Shipman CM, Rostami-H A, Croucher PI. The bisphosphonate, zoledronic acid, induces apoptosis of breast cancer cells: evidence for synergy with paclitaxel. *Br J Cancer*. 2001; 84: 1126-1134.
34. Coleman RE, Marshall H, Cameron D, Dodwell D, Burkinshaw R, Keane M, Gil M, Houston SJ, Grieve RJ, Barrett-Lee PJ, Ritchie D, Pugh J, Gaunt C, et al. Breast-cancer adjuvant therapy with zoledronic acid. *N Engl J Med*. 2011; 365: 1396-1405.

35. Coleman R, de Boer R, Eidtmann H, Llombart A, Davidson N, Neven P, von Minckwitz G, Sleeboom HP, Forbes J, Barrios C, Frassoldati A, Campbell I, Pajja O, et al. Zoledronic acid (zoledronate) for postmenopausal women with early breast cancer receiving adjuvant letrozole (ZO-FAST study): final 60-month results. *Ann Oncol.* 2013; 24: 398-405.
36. Gnant M, Mlineritsch B, Stoeger H, Luschin-Ebengreuth G, Heck D, Menzel C, Jakesz R, Seifert M, Hubalek M, Pristauz G, Bauernhofer T, Eidtmann H, Eiermann W, et al. Adjuvant endocrine therapy plus zoledronic acid in premenopausal women with early-stage breast cancer: 62-month follow-up from the ABCSG-12 randomized trial. *Lancet Oncol.* 2011; 12: 631–641.
37. Fehm T, Hoffmann O, Aktas B, Becker S, Solomayer EF, Wallwiener D, Kimmig R, Kasimir-Bauer S. Detection and characterization of circulating tumor cells in blood of primary breast cancer patients by RT-PCR and comparison to status of bone marrow disseminated cells. *Breast Cancer Res.* 2009; 11: R59.
38. Gradishar WJ. Safety considerations of adjuvant therapy in early breast cancer in postmenopausal women. *Oncology.* 2005; 69: 1-9.
39. Tubiana-Hulin M. Incidence, prevalence and distribution of bone metastases. *Bone.* 1991; 12: S9-10.
40. Maltais ML, Desroches J, Dionne IJ. Changes in muscle mass and strength after menopause. *J Musculoskelet Neuronal Interact.* 2009; 9: 186-197.
41. Phillips SK, Rook KM, Siddle NC, Bruce SA, Woledge RC. Muscle weakness in women occurs at an earlier age than in men, but strength is preserved by hormone replacement therapy. *Clin Sci (Lond).* 1993; 84: 95-8.
42. Skelton DA, Phillips SK, Bruce SA, Naylor CH, Woledge RC. Hormone replacement therapy increases isometric muscle strength of adductor pollicis in post-menopausal women. *Clin Sci (Lond).* 1999; 96: 357-364.
43. Bouxsein ML, Boyd SK, Christiansen BA, Guldberg RE, Jepsen KJ, Müller R. Guidelines for assessment of bone microstructure in rodents using micro-computed tomography. *J Bone Miner Res.* 2010; 25: 1468-1486.

## FIGURE LEGENDS

**Figure 1: Study design. Panel A.** Female BALB/c athymic nude (n=20/group) mice were randomized into five treatment groups 1) sham + vehicle (PBS), 2) sham + letrozole (Let), 3) ovariectomized (OVX) + vehicle, 4) OVX + letrozole, and 5) OVX + letrozole + zometa (Zol).

**Panel B.** At four-weeks of age, mice underwent sham surgery or OVX, and drug treatments commenced 24 hours later. After changes in bone volume and microarchitecture were assessed by micro-computed tomography ( $\mu$ CT) three weeks post-surgery, groups were inoculated in the left cardiac ventricle with  $1 \times 10^5$  MDA-MB-231 human breast cancer cells. Mice were followed for

six weeks for the development of bone metastases and tissues were collected following euthanasia at 13-weeks of age.

**Figure 2: Impact of ovariectomy (OVX) and aromatase inhibitor (letrozole; Let) on circulating 17 $\beta$ -estradiol and on uterine atrophy in nude mice.** Four-week female athymic nude mice underwent OVX or sham surgery and were treated with vehicle or aromatase inhibitor (letrozole, Let; 10 $\mu$ g/day)  $\pm$  bisphosphonate (zoledronic acid, Zol; 5 $\mu$ g/kg 3x/week; n=20/group). **Panel A.** Serum was collected via retro-orbital puncture at baseline and three weeks after sham/OVX surgery and commencement of drug treatments. Serum 17 $\beta$ -estradiol was measured by immuno-assay (Calbiotech) as per manufacturer protocol, and results are expressed as % of baseline. **Panel B.** At the termination of the study nine weeks post-surgery, uteri were dissected and weighed. Results are expressed as mean  $\pm$  SEM and differences were determined by one-way ANOVA with Tukey's multiple comparisons test where \*p<0.05, \*\*p<0.01, \*\*\*p<0.001, and \*\*\*\*p<0.0001.

**Figure 3: Bone volume and microarchitecture were compromised in nude mice after three weeks of estrogen deprivation treatment.** Three weeks after OVX/sham surgery and the commencement of drug treatments, mice were anesthetized with isoflurane and bone microarchitecture was assessed in the proximal tibia by micro-computed tomography ( $\mu$ CT40; SCANCO Medical AG). **Panel A.** Trabecular bone volume (BV/TV), **panel B.** connectivity density (1/mm<sup>3</sup>), **panel C.** trabecular number (1/mm), **panel D.** trabecular separation (mm), **panel E.** trabecular thickness (mm), and **panel F.** structure model index are expressed as mean  $\pm$  SEM and differences were determined by one-way ANOVA with Tukey's multiple comparisons test where \*p<0.05, \*\*p<0.01, \*\*\*p<0.001, and \*\*\*\*p<0.0001. **Panel G.** Representative reconstructed images of  $\mu$ CT scans showing trabecular bone at the proximal tibia were selected with a BV/TV % most representative of the group mean.

**Figure 4: Changes in body composition and bone mineral density (BMD) in estrogen deficient tumor-bearing nude mice.** Three weeks after the beginning of surgery and drug treatments, groups were inoculated in the left cardiac ventricle with  $1 \times 10^5$  MDA-MB-231 human breast cancer cells and followed for six weeks for the development of bone metastases. **Panel A.** Body weight was measured weekly. **Panel B.** Lean mass, **panel C.** fat mass, **panel D.** total body BMD, **panel E.** BMD of the lumbar vertebrae (L4-L6), **panel F.** distal femur BMD, and **panel G.** proximal tibia BMD were measured at baseline, six weeks, and nine weeks after the beginning of treatments by dual energy X-ray absorptiometry (DXA). Data are expressed as mean % of baseline  $\pm$ SEM, and differences were determined by two-way ANOVA with Tukey's multiple comparisons test at week nine where \* $p < 0.05$ , \*\* $p < 0.01$ , \*\*\* $p < 0.001$ , and \*\*\*\* $p < 0.0001$ .

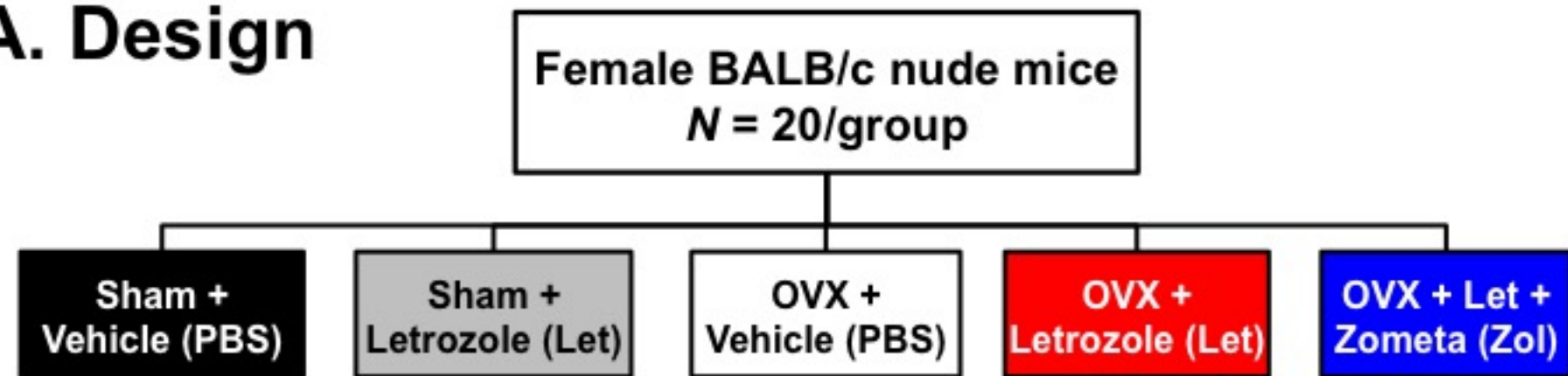
**Figure 5: Osteolytic bone metastases assessed by radiography in estrogen deficient nude mice.** **Panel A.** Osteolytic lesions were measured in anesthetized mice in prone position on d23 and d32 post tumor inoculation using a digital X-ray imager (Kubtec) at 2.7x magnification. Lytic lesion area is reported as total lesion area ( $\text{mm}^2$ ) per animal in hind limb and forelimb long bones. **Panel B.** Representative X-rays showing radiolucent lytic lesions (arrows) were selected with lesion areas most representative of the group mean.

**Figure 6. Histological assessment of tumor-bearing bone of estrogen deficient nude mice.** **Panel A.** Tartrate-resistant acid phosphatase (TRAP)-positive multi-nucleated cells were quantitated at the bone-tumor interface in mid-sagittal sections of the tibia and expressed as number of osteoclasts per mm of interfacing surface (OcN/mm). **Panel B.** Mid-sagittal sections were stained with hematoxylin and eosin (H&E) and total tumor area was measured in the tibia, femur and humerus at 10x magnification. Tumor area is expressed as the combined total tumor area per animal ( $\text{mm}^2$ ). **Panel C.** Representative histological images (H&E) showing tumor cells

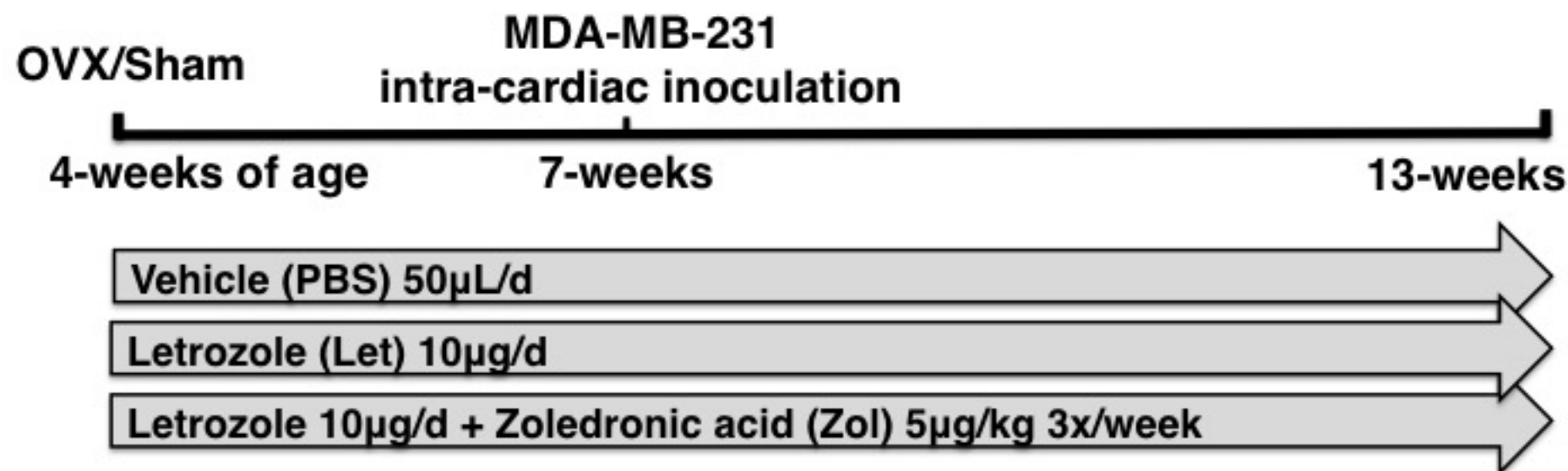
(T) in the distal femur and proximal tibia were selected with tumor areas most representative of the group mean. Differences were determined by one-way ANOVA with Tukey's multiple comparisons test where  $*p < 0.05$  and  $***p < 0.001$ .

**Figure 7: *Ex vivo* contractility of the EDL muscle. Panel A.** *Ex vivo* muscle specific force of the extensor digitorum longus (EDL) muscle was measured in tumor and non-tumor bearing mice. Data are expressed as mean force ( $\pm$ SEM) normalized to muscle size, and differences were determined by two-way ANOVA with Tukey's multiple comparisons test performed at 150Hz where  $*p < 0.05$  and  $****p < 0.0001$ . **Panels B-E.** Muscles of the hind limb were dissected and weighed, including the EDL, tibialis anterior, gastrocnemius, and soleus. Differences were determined by one-way ANOVA with Tukey's multiple comparisons test where  $*p < 0.05$ .

## A. Design

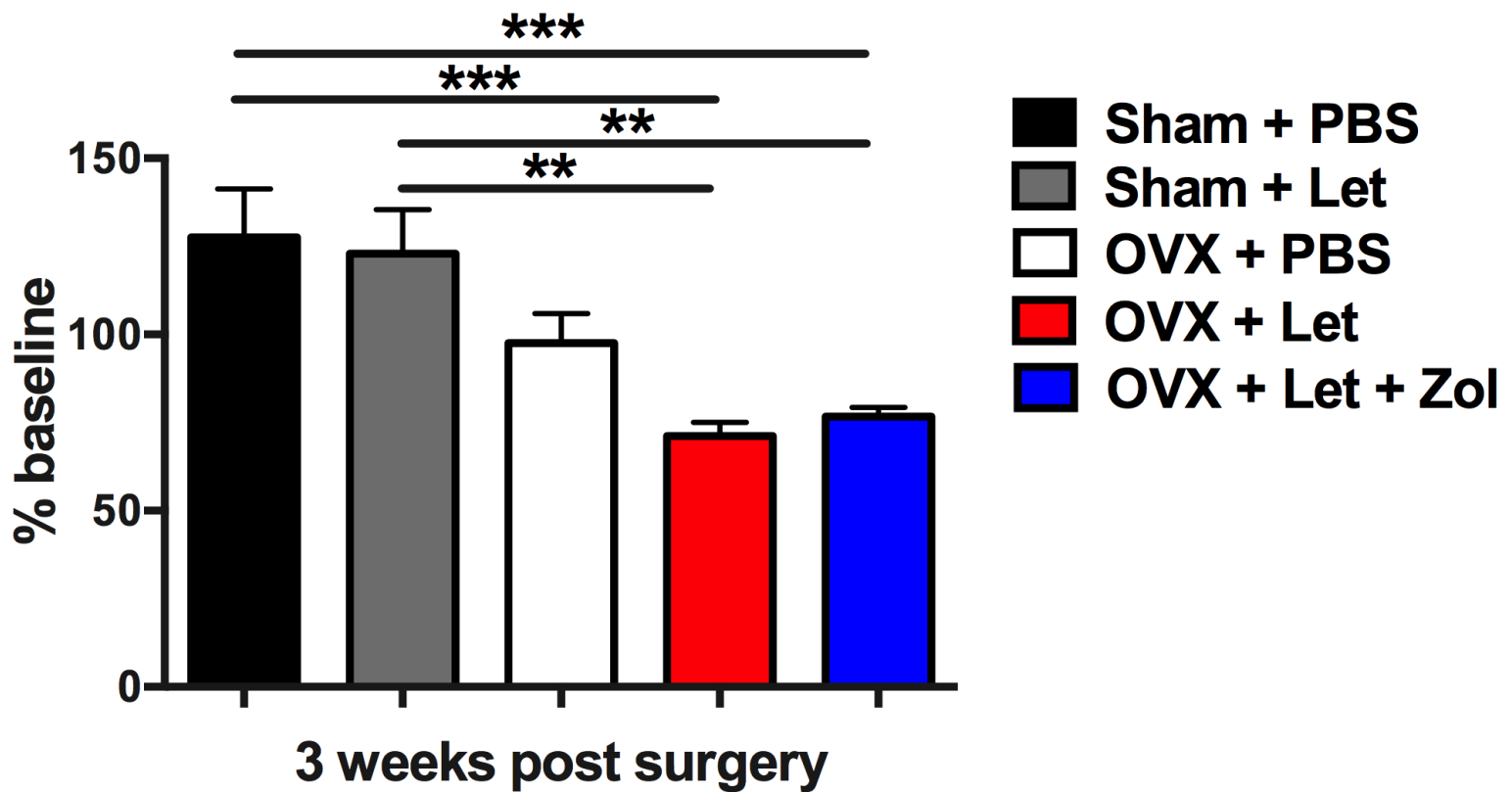


## B. Timeline

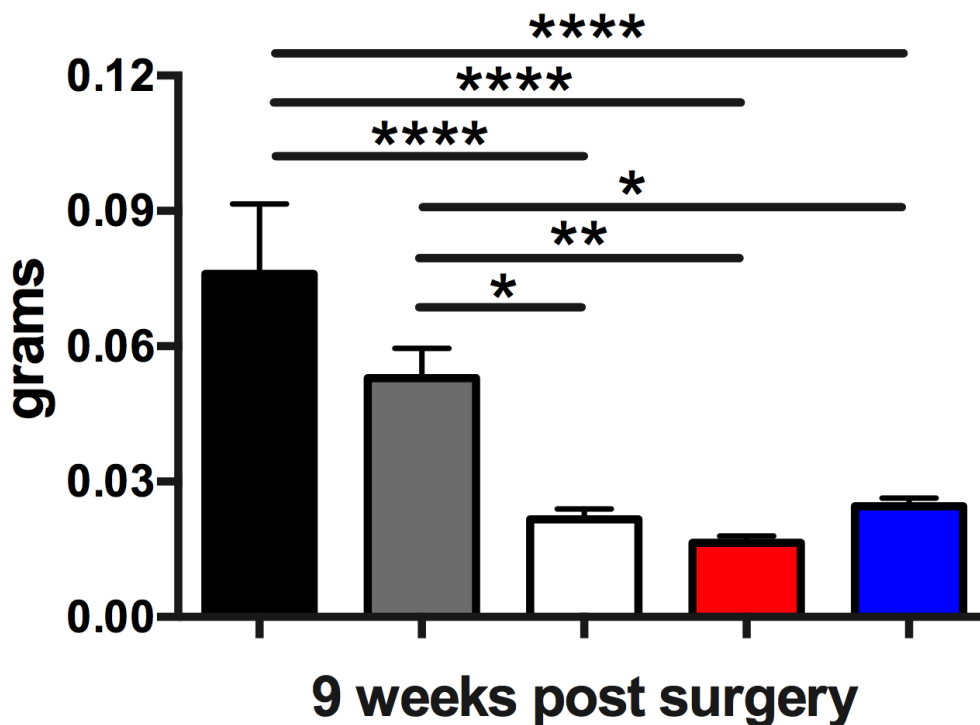




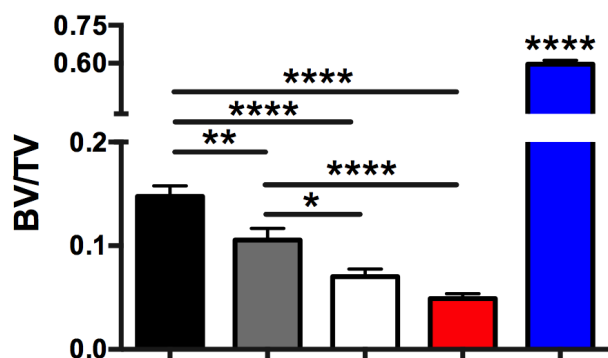
## A. $17\beta$ -Estradiol



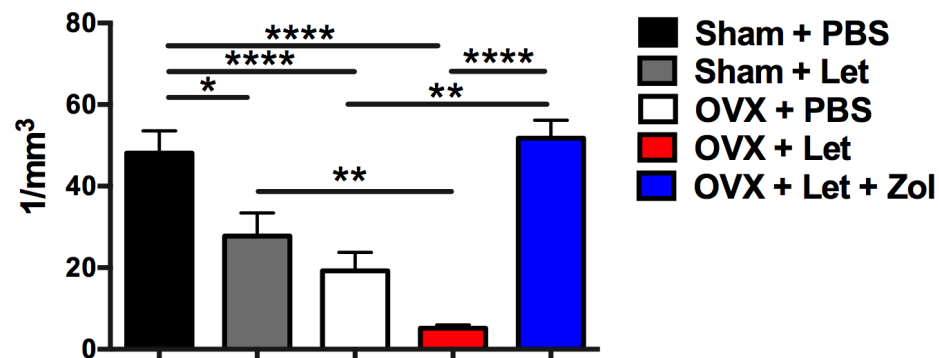
## B. Uterine weight



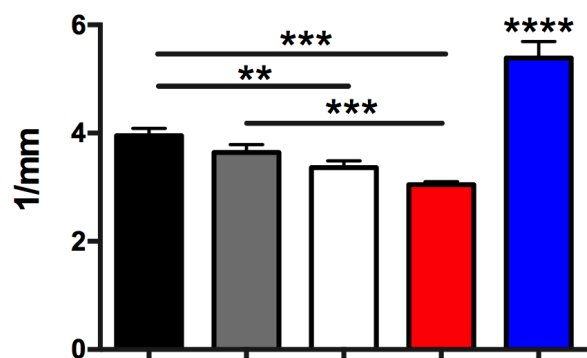
**A. Bone volume fraction**



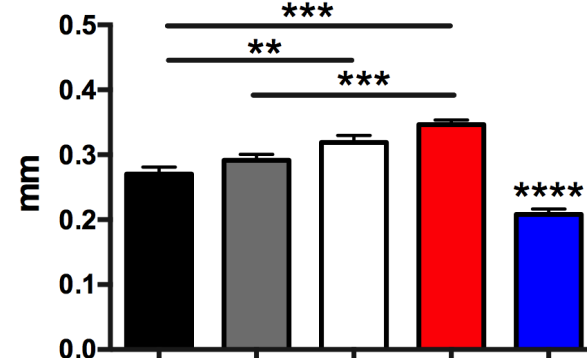
**B. Connectivity density**



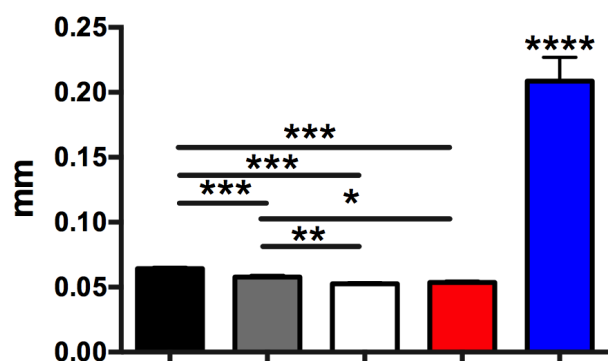
**C. Trabecular number**



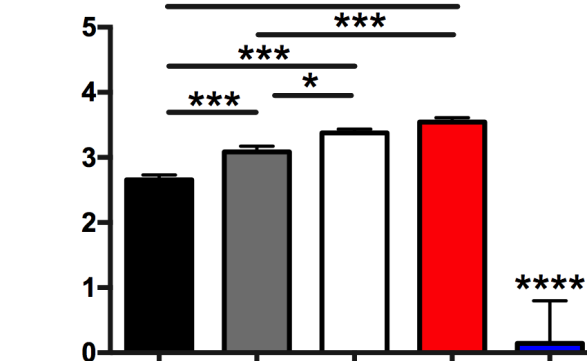
**D. Trabecular separation**

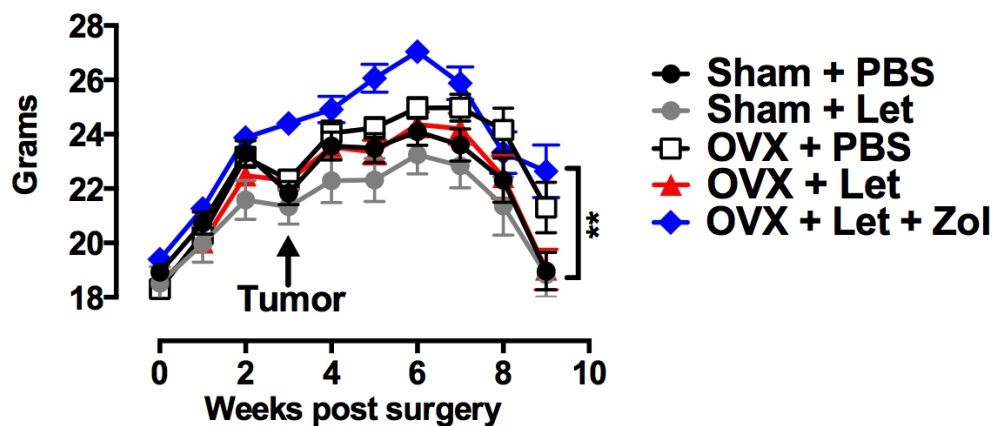
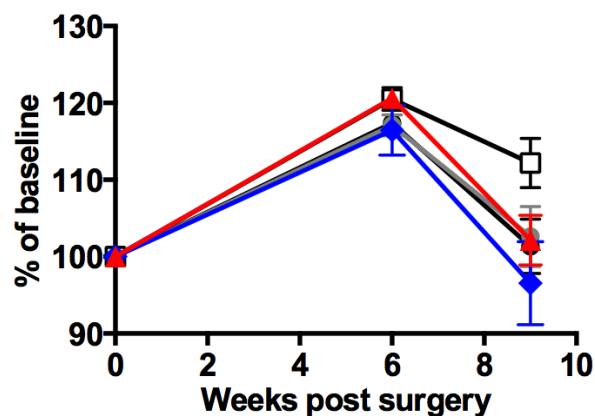
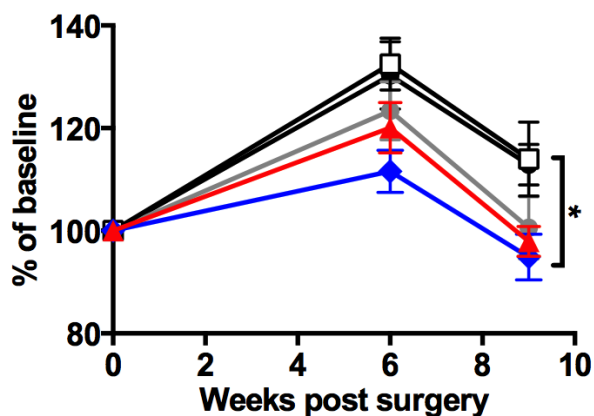
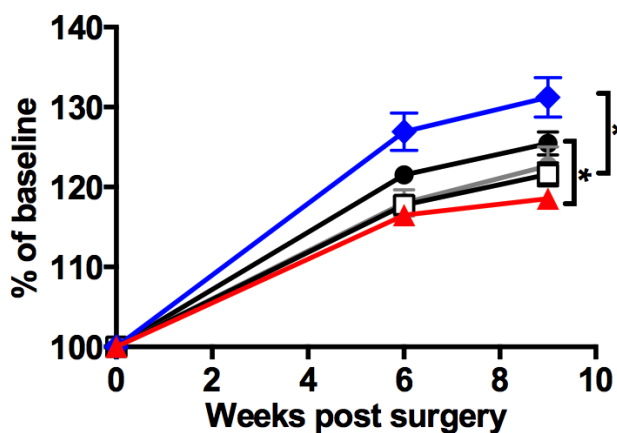
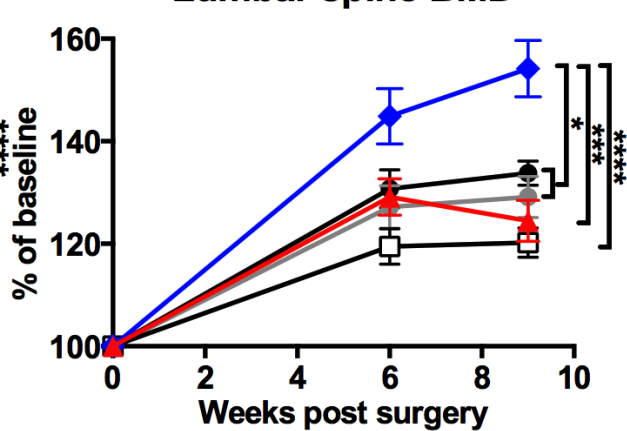
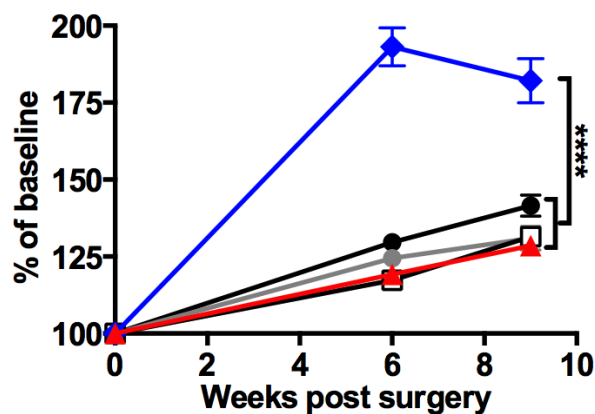
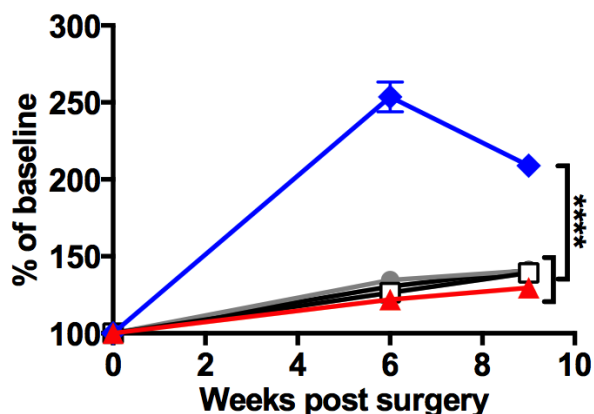


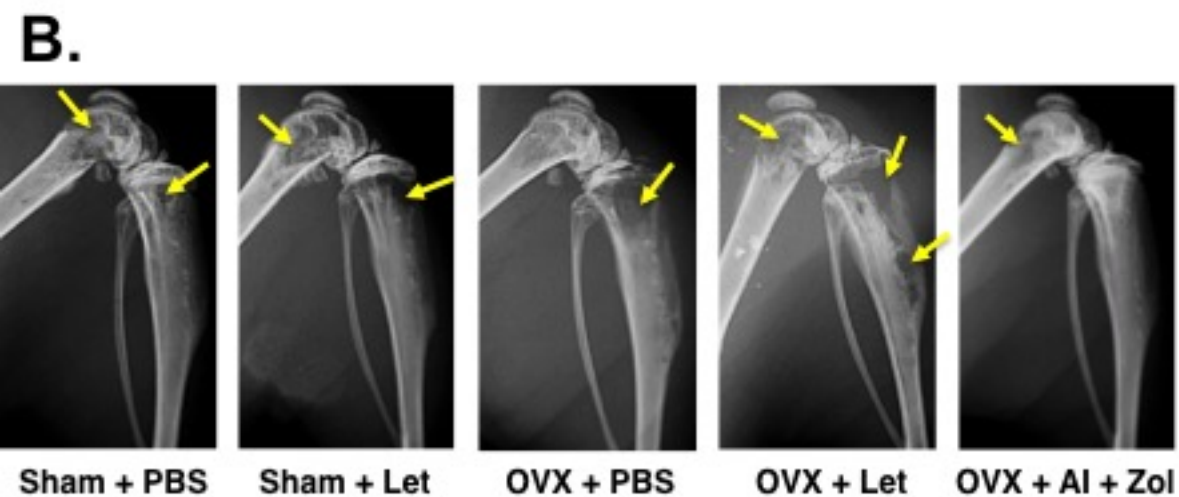
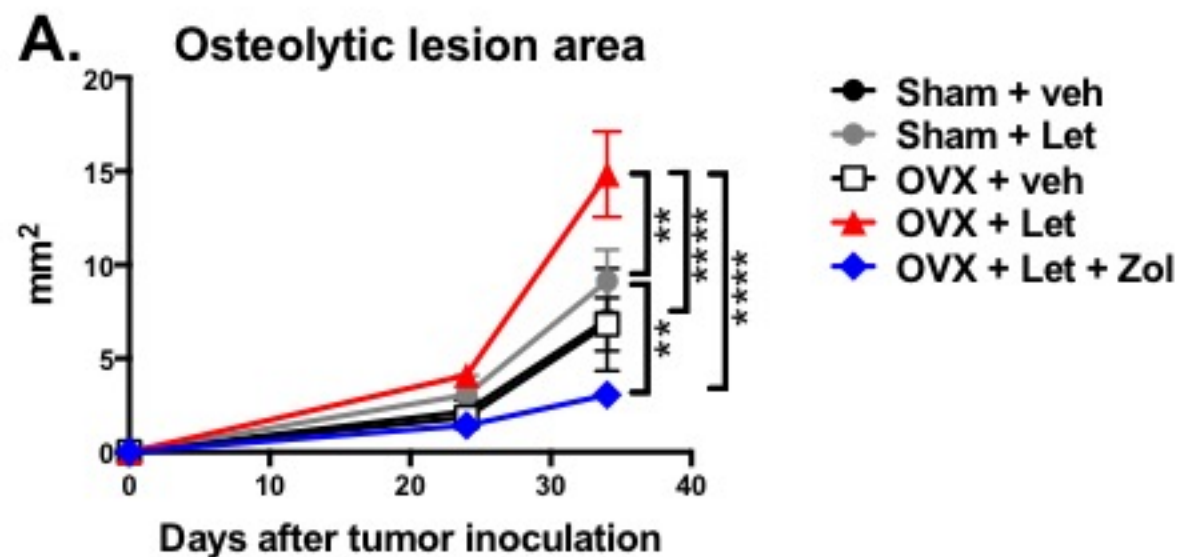
**E. Trabecular thickness**

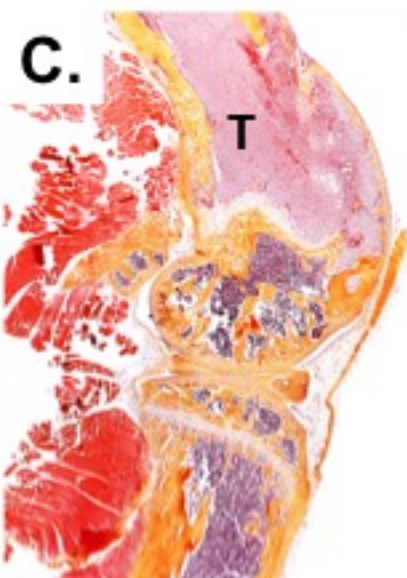
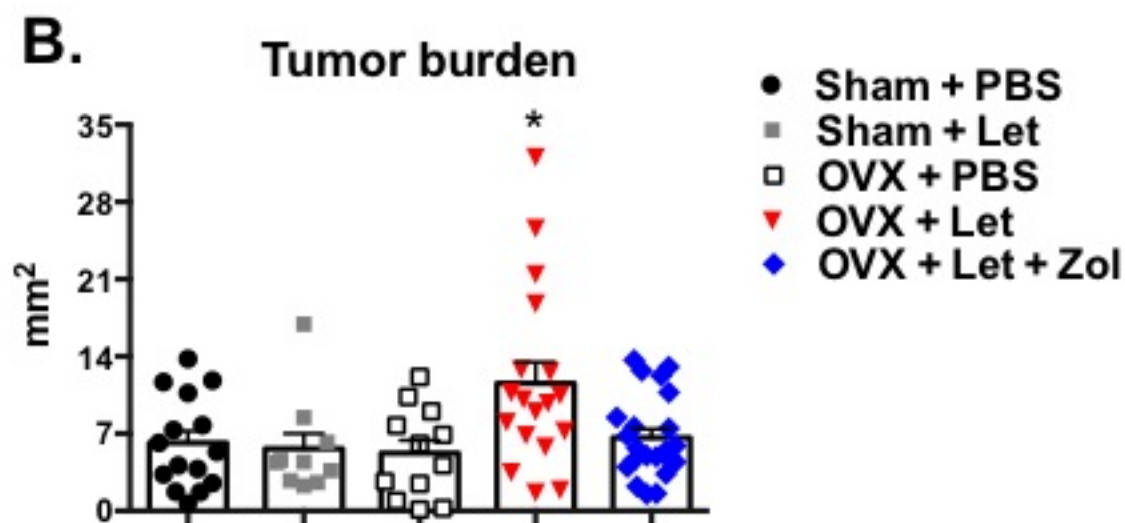
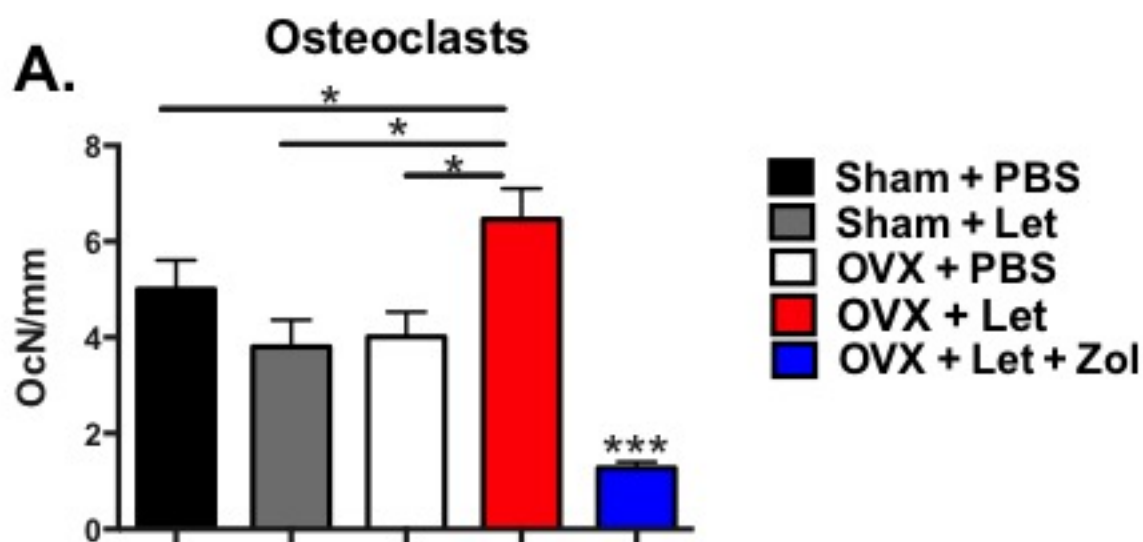


**F. Structure model index**

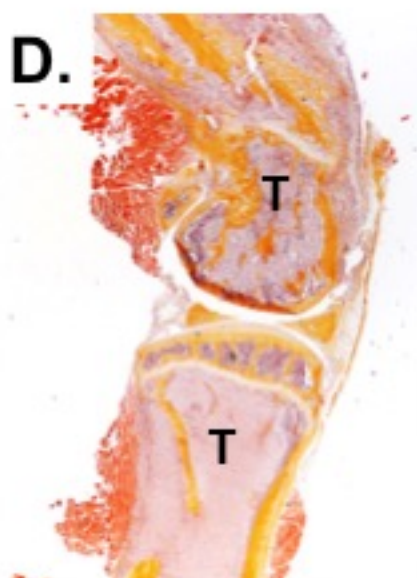


**A.****Body weight****B.****Lean mass****C.****% Fat mass****D.****Total skeletal BMD****E.****Lumbar spine BMD****F.****Distal femur BMD****G.****Proximal tibia BMD**

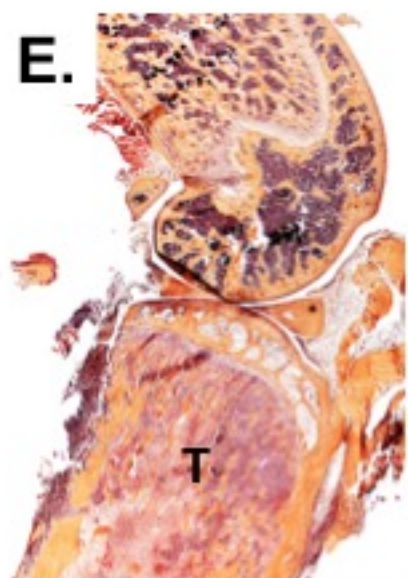




Sham + PBS

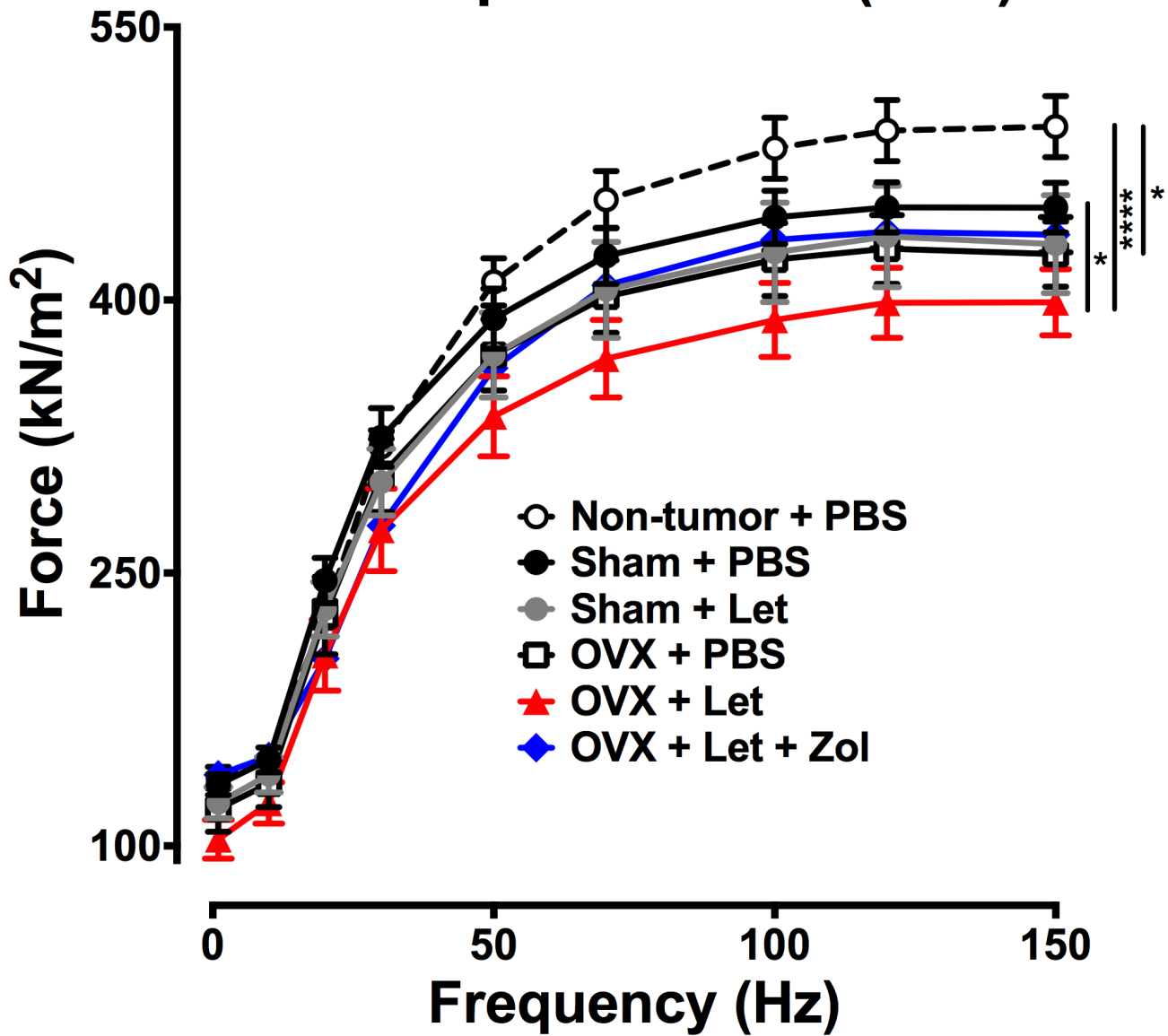


OVX + Let

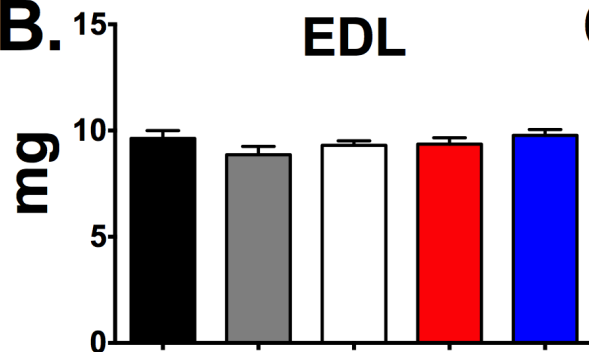


OVX + Let + Zol

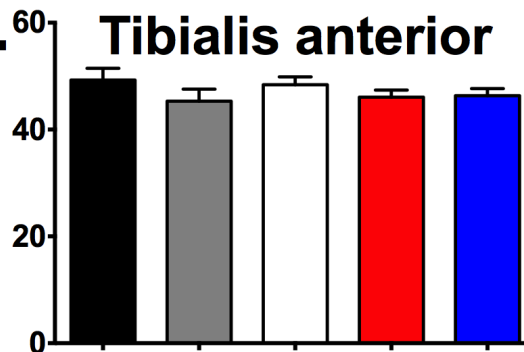
# A. Muscle specific force (EDL)



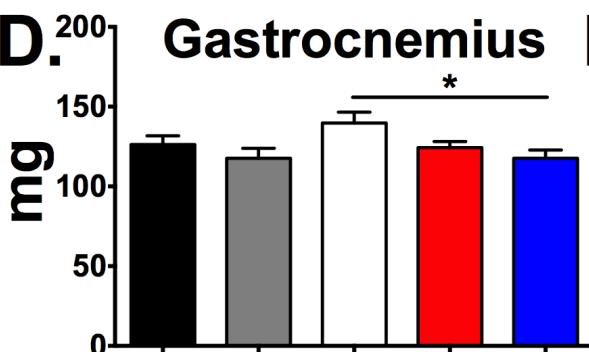
## B. EDL



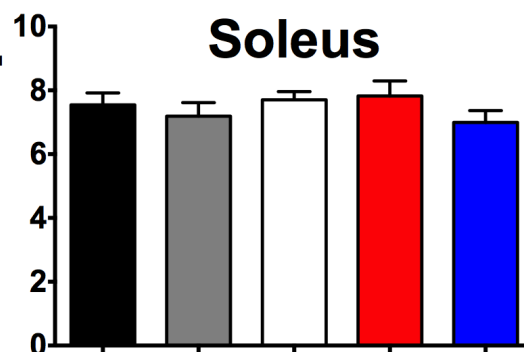
## C. Tibialis anterior



## D. Gastrocnemius



## E. Soleus



## LABORATORY METHODS

# Murine models of breast cancer bone metastasis

Laura E Wright<sup>1</sup>, Penelope D Ottewell<sup>2</sup>, Nadia Rucci<sup>3</sup>, Olivier Peyruchaud<sup>4</sup>,  
Gabriel M Pagnotti<sup>5</sup>, Antonella Chiechi<sup>1</sup>, Jeroen T Buijs<sup>6</sup> and Julie A Sterling<sup>7,8</sup>

<sup>1</sup>Division of Endocrinology, Department of Medicine, Indiana University, Indianapolis, IN, USA. <sup>2</sup>Department of Oncology, Mellanby Center for Bone Research, University of Sheffield, Sheffield, UK. <sup>3</sup>Department of Biotechnological and Applied Clinical Sciences, University of L'Aquila, L'Aquila, Italy. <sup>4</sup>Physiopathologie, Diagnostic et Traitements des Maladies Osseuses, INSERM, UMR\_S1033, Lyon, France. <sup>5</sup>Department of Biomedical Engineering, Stony Brook University, Stony Brook, NY, USA. <sup>6</sup>Department of Thrombosis & Hemostasis, Leiden University Medical Center, Leiden, The Netherlands. <sup>7</sup>Department of Medicine, Division of Clinical Pharmacology, Vanderbilt University, Nashville, TN, USA. <sup>8</sup>Department of Veterans Affairs, Tennessee Valley Healthcare System, Nashville, TN, USA.

Bone metastases cause significant morbidity and mortality in late-stage breast cancer patients and are currently considered incurable. Investigators rely on translational models to better understand the pathogenesis of skeletal complications of malignancy in order to identify therapeutic targets that may ultimately prevent and treat solid tumor metastasis to bone. Many experimental models of breast cancer bone metastases are in use today, each with its own caveats. In this methods review, we characterize the bone phenotype of commonly utilized human- and murine-derived breast cell lines that elicit osteoblastic and/or osteolytic destruction of bone in mice and report methods for optimizing tumor-take in murine models of bone metastasis. We then provide protocols for four of the most common xenograft and syngeneic inoculation routes for modeling breast cancer metastasis to the skeleton in mice, including the intra-cardiac, intra-arterial, orthotopic and intra-tibial methods of tumor cell injection. Recommendations for *in vivo* and *ex vivo* assessment of tumor progression and bone destruction are provided, followed by discussion of the strengths and limitations of the available tools and translational models that aid investigators in the study of breast cancer metastasis to bone.

*BoneKEy Reports* 5, Article number: 804 (2016) | doi:10.1038/bonekey.2016.31

## Introduction

Breast cancer metastasis to the skeleton and subsequent bone destruction often result in severe bone pain, fragility fractures, nerve compression syndromes and hypercalcemia of malignancy resulting in significant morbidity and mortality.<sup>1,2</sup> Elucidation of the molecular mechanisms that mediate breast cancer bone metastases and cancer-induced bone destruction has begun to reveal potential therapeutic targets that may lead to improved patient survival and quality of life; however, further investigation is necessary to address this currently irreversible late-stage complication of malignancy. Therefore, it is of utmost importance for investigators to establish well-characterized *in vivo* models of breast cancer bone metastasis.

Unlike the study of postmenopausal osteoporosis where the ovariectomy model is the clear FDA-mandated choice,<sup>3</sup> there are numerous murine models of breast cancer metastasis to bone, each with its own benefits and limitations. Because

spontaneous metastasis to the skeleton from primary tumors in animals is rare,<sup>2</sup> and no single model reproduces all of the genetic and phenotypic changes of human breast cancer bone metastasis, researchers must select a model or a combination of models that best suits the aspect of the metastatic disease that they wish to investigate. Here we (1) identify the most commonly utilized breast cancer cell lines that elicit osteolytic, osteoblastic or mixed phenotypes in bone, (2) provide protocols for tumor cell inoculation routes that model metastatic disease in the skeleton and (3) explore methods for the post-inoculation monitoring of breast cancer progression in bone.

## Modeling osteolytic breast cancer bone metastases

Inoculation of bone trophic tumor cells directly into the blood stream provides a useful tool for investigating the processes associated with breast cancer cell homing, colonization and subsequent metastatic tumor growth and osteolytic lesion

Correspondence: Dr LE Wright, Division of Endocrinology, Department of Medicine, Indiana University, 980 West Walnut Street Walther Hall R3, Room C132, Indianapolis, IN 46202, USA.  
E-mail: laewrig@iu.edu

Received 21 October 2015; accepted 2 April 2016; published online 11 May 2016



formation in bone. Intra-cardiac inoculation of human triple negative MDA-MB-231 adenocarcinoma cells into immune-compromised mice (i.e., BALB/c nude, MF1 nude and NOD/SCID) results in tumor cell dissemination through the arterial vascular system and homing primarily to long bones, spine, jaw and lungs (**Figure 1a; Table 1**).<sup>4,5</sup> In syngeneic tumor models where murine-derived cell lines are inoculated into a murine host, a bone metastatic profile can be observed with varying degrees of success following intra-cardiac injection of 4T1 or PyMT MMTV mammary cancer cells into immune competent BALB/c or FVB/N mice, respectively (**Table 1**).<sup>6,7</sup>

Visceral metastases, particularly to the lung, can significantly shorten the life span of a mouse and thus limit the experimental time frame during which skeletal metastases can be studied *in vivo*. MDA-MB-231 and 4T1 cell lines have therefore been manipulated in the laboratory to produce bone-seeking sub-lines that favor homing to and colonization of mouse tibiae and femurs with a reduced propensity to metastasize to the lung. Bone-seeking sub-lines, often referred to in the literature as MDA-MB-231-B02, MDA-MB-231-1833, MDA-MB-231-B, MDA-IV and MDA-MB-231-bone, form tumors in the long bones of up to 90% of mice following intra-cardiac inoculation in BALB/c nude mice.<sup>8–12</sup> Intra-cardiac inoculation of the subline

4T1-2 cells into BALB/c mice results in bone metastases in 70–80% of animals (**Table 1**).<sup>13</sup>

Direct intra-tibial injection of a number of breast cancer cell lines including MDA-MB-231, MDA-MB-436 and SUM1315 into immunocompromised mice and 4T1 and PyMT MMTV cell lines into immune competent BALB/c and FVB/N mice results in the development of osteolytic mammary tumors in bone with minimal impact outside of bone marrow engraftment (**Figure 1b; Table 1**).<sup>7,14,15</sup> The intra-tibial model bypasses the early stages of metastasis including homing to the bone microenvironment and is therefore useful for a more direct assessment of tumor–bone interactions, particularly when interested in studying genetic manipulations of the host or tumor cells of interest.

Intra-cardiac, intra-arterial and intra-tibial inoculation of cancer cells provide useful tools for examining the later stages of breast cancer bone metastasis; however, these aforementioned models do not permit investigation into the stages that precede the colonization of breast cancer in bone, including primary tumor growth or the dissemination of tumor cells through intravascularization. The 4T1 mouse mammary cancer cell line was derived from a BALB/c spontaneous mammary carcinoma,<sup>16</sup> and orthotopic inoculation of 4T1 cells into the



**Figure 1** Radiographs of the distal femur and proximal tibia of mice with breast cancer bone metastases. Representative images are presented of (a). MDA-MB-231 breast cancer bone metastases 4 weeks post inoculation of 100 000 cells via intra-cardiac route, (b). ZR-75-1 breast cancer bone metastases 25 weeks post inoculation of 100 000 cells via intra-cardiac route, (c). 4T1 breast cancer bone metastases 4 weeks post inoculation of 10 000 cells via intra-tibial route, and (d). MCF-7 breast cancer bone metastases 20 weeks post inoculation of 100 000 cells via intra-tibial route.



**Table 1** Human and mouse mammary cancer cell lines that form osteolytic bone lesions following inoculation into mice

Cell line	Species	Origin	Subline	Mouse strain	Inoculation route	Metastatic site(s)	Time to lesion formation
MDA-MB-231	Human	Human mammary adenocarcinoma isolated from a pleural effusion from a 51-year-old Caucasian female	Parental	BALB/c nude	Intra-cardiac	Mouse long bones, spine and jaw	2–3 weeks
				MF1 nude	Intra-tibial	Mouse tibiae	1–3 weeks
				NOD/SCID	Orthotopic	Mouse tibiae	7 weeks
			MDA-MB-231-BO2	BALB/c nude	Intra-cardiac	Mouse long bones, spine and jaw	2–3 weeks
					Intra-tibial	Mouse tibiae	1–3 weeks
					Intra-arterial	Mouse long bones	2–3 weeks
			MDA-MB-231-IV	BALB/c nude	Intra-cardiac	Mouse long bones, spine and jaw	2–3 weeks
					Intra-tibial	Mouse tibiae	1–3 weeks
					Intra-arterial	Mouse tibiae	2–3 weeks
		Intra-venous	Mouse long bones	2–3 weeks			
		Orthotopic	Mouse long bones	10–14 weeks			
			Human bone X-plants				
MDA-MB-436	Human	Human mammary adenocarcinoma isolated from a pleural effusion from a 43-year-old Caucasian female	Parental	MF1 nude BALB/c nude NOD/SCID	Intra-osseous	Mouse tibiae	2–3 weeks
SUM1315	Human	Isolated from a metastatic nodule of a Caucasian female patient with ductal carcinoma	Parental	NOD/SCID	Intra-tibial Orthotopic	Mouse tibiae Human bone X-plants	3–4 weeks 8–12 weeks
4T1	Mouse	Isolated from a stage 1 V mammary tumor from a female BALB/c cfC3H mouse	Parental	BALB/c cfC3H	Intra-cardiac Intra-tibial Orthotopic	Mouse long bones, spine, jaw and lungs	2–3 weeks
						Mouse tibiae	1–3 weeks
						Mouse long bones, jaw and lungs	3–6 weeks
	4T1-2	BALB/c cfC3H	Intra-cardiac Intra-tibial Orthotopic	Mouse long bones, spine, jaw and lungs	2–3 weeks		
				Mouse tibiae	1–3 weeks		
				Mouse long bones, jaw and lungs	3–4 weeks		
PyMT MMTV	Mouse	Isolated from mammary tumour induced by MMTV viral oncogene in FVB/N female mouse	Parental	FVB/N	Intra-cardiac Intra-tibial	Mouse long bones, spine, jaw and lungs Mouse tibiae	2–3 weeks 1–2 weeks
KEP	Mouse	Mouse invasive lobular carcinoma derived from a Keratin14-driven E-cadherin/p53 (KEP) knock out primary mammary carcinoma	KEP/Luc KEP/Luc	RAG <sup>-/-</sup> ; IL2R <sup>γc</sup> <sup>-/-</sup>	Orthotopic	Spine	3–5 weeks
				BALB/c	Intra-cardiac	Mouse long bones and spine	2–4 weeks
					Orthotopic	Mouse long bones and spine	6–9 weeks
					BALB/c nude	Intra-tibial	Mouse long bones and spine Mouse tibiae

mammary fat pad of BALB/c mice results in spontaneous metastasis to lungs (~60% of mice) and bone (~20–30% of mice; **Table 1**).<sup>17</sup> Incidence of bone metastasis can be increased to 50–70% by utilizing the bone-seeking 4T1-2 subline.<sup>18,19</sup> This syngeneic model has the benefit of utilizing an immune competent mouse.

Recently, it was shown that orthotopic inoculation of luciferase-transduced murine invasive lobular breast carcinoma cells (KEP cells) resulted in the formation of bone metastases in the appendicular and axial skeleton within 3 weeks after resection of the orthotopic tumor with minimal lung involvement in BALBc nude mice (**Table 1**).<sup>20</sup> Although MDA-MB-231 do not metastasize to murine bone from the orthotopic site in BALB/c nude and NOD SCID mice, distant metastases at skeletal sites were observed when using NSG mice,<sup>21</sup> suggesting the importance of NK cells in regulating the metastatic process.

Spontaneous metastasis of an orthotopic human breast cancer tumor to bone can be achieved in an immune-compromised mouse using a unique model that incorporates human-derived bone X-plants. In recent studies, orthotopic

inoculation of human-derived SUM-1315 or MDA-MB-231-IV cells into the mammary fat pad of NOD SCID mice 4 weeks following ectopic implantation of human bone resulted in spontaneous metastasis of human breast cancer cells specifically to the human bone grafts in 40–60% of animals (**Table 1**).<sup>22,23</sup>

### Modeling osteoblastic breast cancer bone metastases

Although patients with breast cancer usually develop osteolytic bone metastases, as many as 25% will present with osteoblastic bone metastases.<sup>24</sup> The human breast cancer cell lines ZR-75-1 and MCF-7 can be utilized to establish an osteoblastic bone metastatic phenotype in mice.

ZR-75-1 cultures were initially derived from a malignant ascetic effusion in a 63-year-old Caucasian female with ductal carcinoma. ZR-75-1 cells possess receptors for all four classes of steroid hormones and are thus responsive to estradiol stimulation.<sup>25,26</sup> Mice inoculated via intra-cardiac route with ZR-75-1 cells develop osteoblastic bone metastases in the long bones; however, bone metastases are typically not detectable by X-ray for 12–25 weeks post inoculation (**Figure 1c**; **Table 2**).

**Table 2** Human mammary cancer cell lines that form osteoblastic bone lesions following inoculation into mice

Cell line	Species	Origin	Subline	Mouse strain	Inoculation route	Metastatic site(s)	Time to lesion formation
MCF-7	Human	Human mammary adenocarcinoma isolated from a pleural effusion in a 69-year-old Caucasian female	Parental	BALB/c nude	Intra-cardiac Intra-tibial	Mouse long bones Mouse tibiae	20–25 weeks 1–3 weeks
			MCF-7/Neu	BALB/c nude	Intra-cardiac Intra-tibial	Mouse long bones Mouse tibiae	10–12 weeks 1–3 weeks
ZR-75-1	Human	Human ductal carcinoma derived from a malignant ascetic effusion in a 63-year-old Caucasian female	Parental	BALB/c nude	Intra-cardiac	Mouse long bones and spine	12–25 weeks

Human MCF-7 breast cancer cells were derived from a metastatic pleural effusion in a 69-year-old Caucasian female with breast carcinoma.<sup>27</sup> MCF-7 cells retain characteristics of differentiated mammary epithelium and possess estrogen receptors.<sup>27,28</sup> Intra-cardiac inoculation of MCF-7 cells in immune-compromised mice results in mixed osteolytic/osteoblastic bone metastases in the long bones after 20–25 weeks (**Table 2**). In order to speed metastatic progression, the MCF-7 cell line has been stably transfected with the oncogene Neu, and this cell line establishes mixed osteolytic and osteoblastic bone metastases in immunocompromised mice within 10–12 weeks after intra-cardiac inoculation.<sup>29</sup> Because ER + MCF-7 cell growth is estrogen dependent mice should be implanted subcutaneously with slow-release estradiol pellets (0.25 mg) prior to intra-cardiac tumor cell inoculation in order to more closely mimic a pre-menopausal tumor environment and speed the progression of tumor growth in bone.<sup>30,31</sup> MCF-7 and MCF-7/Neu cells are also commonly utilized to establish bone lesions in mice via the intra-tibial inoculation route, with lesions developing in a shorter time span of 1–3 weeks post injection (**Figure 1d**; **Table 2**). Estradiol supplementation is typically not introduced when MCF-7 cells are directly implanted into bone.

## Materials and Methods

This section begins by detailing recommendations for the preparation of breast cancer cells and pre-operative care instructions for the handling of mice prior to inoculation. Four of the most commonly utilized cell inoculation routes resulting in breast cancer bone metastases are then described, including lists of necessary materials for each technique. Recommendations for the post-inoculation monitoring of animals and assessment of tumor progression in bone *in vivo* and *post mortem* are then described.

### Breast cancer cell preparation

Manufacturer specifications should guide the user as to the appropriate growth conditions for the cell line of interest. As a general rule for all tumor cell inoculation routes, prepare cells from a fresh batch of low passage number. Split cells 1–2 days prior to the injections such that they reach ~80% confluence on the day of inoculation. Overcrowding of tumor cells can affect their metastatic potential *in vivo*; therefore, cell confluence prior to inoculation must be monitored judiciously. Wash flasks briefly with the appropriate cold cell culture media or phosphate-buffered saline (PBS), trypsinize (0.15% Trypsin EDTA) at 37 °C, and remove cells with ice-cold media containing 10% fetal bovine serum (FBS). Centrifuge (200g, 5 min) and suspend the cell pellet in ice-cold PBS for quantitation. Re-suspend the cells at the desired concentration (**Table 3**) in cold PBS and keep the cell suspension for no more than 30 min on ice until the moment of inoculation. Prepare cells in small batches (enough for 1–2 cages or 5–10 animals) and keep on ice to minimize clumping and risk of embolism during the *in vivo* inoculation.

Because of volumetric limitations of the mouse circulation 100 µl is the recommended injection volume using the intra-cardiac or intra-arterial routes.

Reagents for tumor cell preparation

- (1) PBS (without Ca<sup>2+</sup> and Mg<sup>2+</sup>)
- (2) 0.15% Trypsin EDTA
- (3) Cold Dulbecco's Modified Eagle Medium (or other media) with 10% FBS

### Pre-operative management of mice

For the intra-cardiac, intra-arterial and intra-venous metastasis models, mice are inoculated between 4 and 6 weeks of age, as tumor-take is markedly reduced after 6 weeks. For the intra-tibial injection, 6- to 8-week-old mice are typically used, as tibiae of younger mice are small and difficult to inject accurately. A ketamine/xylazine cocktail (100 mg kg<sup>-1</sup> and 10 mg kg<sup>-1</sup>, respectively) or isoflurane (2.5% isoflurane at 2–3 l min<sup>-1</sup> O<sub>2</sub>) may be utilized for anesthesia during the inoculation of tumor cells depending on the laboratory's preference. Many groups, however, experience improved survival rates following intra-cardiac inoculation with the use of isoflurane (vs ketamine/xylazine), likely due to increased vascular tone and body temperature. If the mouse strain selected is furred, it may be important to shave the mouse at the site of inoculation for better visualization of anatomical landmarks.

### Cellular inoculation routes for modeling breast cancer bone metastases in mice

**Intra-cardiac inoculation of breast cancer cells.** Once a mouse has been properly anesthetized and is unresponsive to pinch, place it on a sterile surface in supine position ensuring that the vertebral column is straight. Tape the forelimbs away from the torso at a slightly angled and upward position (**Figure 2a**). Prior to inoculation, clean the chest of the animal thoroughly with betadine and wipe with an alcohol pad or as per the institutional standard operating procedures. Once the chest has been sterilized, gently place one hand on the chest of the mouse to tighten the skin and mark the top of the sternum and the xyphoid process (distal sternum) with a permanent marker (**Figure 2a**). Make a third mark in the middle of these two landmarks and slightly to your right (animal's left) just over the heart in the third intercostal space (**Figure 2a**). This mark identifies the location of the left cardiac ventricle where you will insert the needle for tumor cell inoculation.

With intra-cardiac inoculation, prepare the needle by leaving a small air space in the top of the syringe before slowly drawing up the desired volume of cell suspension into the syringe (**Figure 2b**). This air space will permit a small influx of bright red oxygenated blood into the syringe hub when properly inserted into the left cardiac ventricle. Hold the skin of the mouse tight with one hand and insert the needle perpendicularly into the middle marking (**Figure 2c**). When the needle has entered the left cardiac ventricle, watch for the pulse of blood to appear in the hub of the needle. The appearance of air bubbles in the needle hub upon insertion

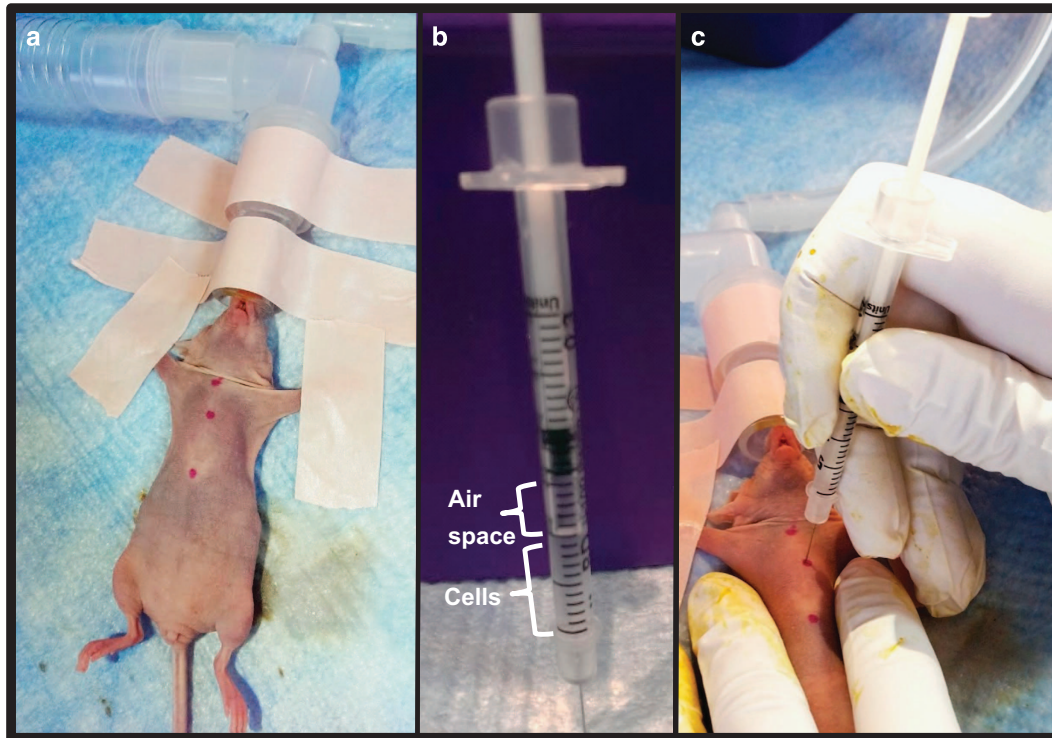


**Figure 2** Inoculation of breast cancer cells in the left cardiac ventricle of a mouse. (a) Sterilize the chest of an anesthetized mouse and mark the top of the sternum and the xyphoid process (distal sternum) with a permanent marker. Make a 3rd mark in the middle of these two landmarks and slightly to your right (animal's left) just over the heart in the third intercostal space. (b) Prepare the needle by leaving a small air space in the top of the syringe before slowly drawing up the desired volume of cell suspension into the syringe. This air space will permit a small influx of bright red oxygenated blood into the syringe hub when properly inserted into the left cardiac ventricle. (c) Once the needle is correctly positioned in the left cardiac ventricle, inject the cell suspension slowly into the left ventricle being careful not to move the needle or press it deeper into the thoracic cavity.

indicates that it has likely entered the lungs and will need to be removed and repositioned. If you do not see a red pulse of blood in the needle hub but are confident that you are in the correct location, you can pull up slightly on the syringe plunger to verify your position in the cardiac ventricle. If there is still no visible red pulse, the needle can be slowly and slightly adjusted up or down. When small adjustments are futile, remove and reposition the insertion point completely or set the mouse aside temporarily. Extended anesthesia can cause vasoconstriction and reduce the animal's blood pressure such that the pulse of blood into the needle's hub becomes less noticeable.

Once the needle is correctly positioned in the left cardiac ventricle, inject the cell suspension slowly into the left ventricle being careful not to move the needle or press it deeper into the thoracic cavity. Keep a close eye on the cell suspension in the syringe and do not inject the air bubble at the top of the syringe (**Figure 2b**). As soon as the cells have been inoculated, quickly remove the needle, apply slight pressure at the injection site for a few seconds and place the mouse on a heating pad until fully awake. Once mice have fully recovered, monitor their behavior for 24 h and watch for potential signs of embolism or distress.

#### Materials for intra-cardiac inoculation

- (1) Anesthetized mouse (immune compromised if using human cells)
- (2) Cellular suspension
- (3) 0.5–1 cc insulin syringe, 27–29G, 0.5 inch
- (4) Surgical tape
- (5) Betadine and alcohol swabs
- (6) Permanent marker
- (7) Water recirculating heating pad

**Intra-arterial inoculation of breast cancer cells in the tail.** Once a mouse has been anesthetized with isoflurane, place it on a sterile surface in supine position and tape the torso of the mouse to the table for

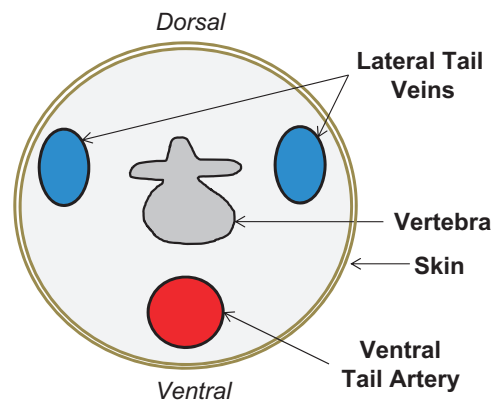


**Figure 3** Schematic representation of the tail vasculature of a mouse.

stability. Use a heating pad or lamp to dilate the vessels within the tail for 2–3 min in order to facilitate greater ease of inoculation. Alternatively, the tail can be placed in warm water (30–35 °C). Using an alcohol pad, disinfect the tail vigorously, which will also help dilate the vessels within the tail and facilitate inoculation. Keep the tail clinged between the forefinger and thumb and insert the needle (beveled edge facing up) horizontally across the proximal section of the tail into the artery (**Figure 3**). Once the needle has entered the artery, the opposite hand is used to retract the syringe plunger slightly to inspect for a tight fitting within the artery and inspect the barrel of the syringe for a small amount of blood, which should appear at the needle hub. This will not occur if the needle has not breached the epithelial membrane of the artery or if the syringe has protruded through the artery. Once the syringe is properly



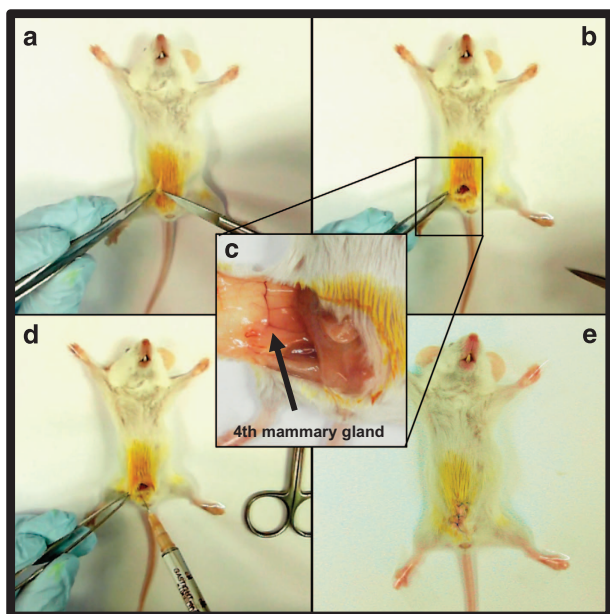


**Figure 4** Inoculation of breast cancer cells in the 4th mammary fat pad of a mouse. (a, b) Place an anesthetized mouse in supine position on a sterile surface and tape the forelimbs and hind limbs away from the torso. Prior to inoculation, clean the inguinal surface of the animal thoroughly with betadine and alcohol. Using sterile surgical instruments, create a small incision in the skin adjacent to the 4th mammary fat pad. (c, d) Insert the needle into the fourth mammary gland fat pad and slowly inoculate the tumor cell suspension. The fourth mammary gland fat pad is located at the intersection of three prominent blood vessels. (e) After the injection of cells, close the wound with 4–6 sutures, administer an analgesic as per institutional guidelines and place the mouse on a heating pad until fully awake.

seated within the artery, depress the plunger slowly in order to minimize cell lysis resulting from fluid shear. The needle should ideally pierce the artery just once in order for the cell bolus to be delivered in its entirety. However, when small adjustments are futile, remove the needle completely and reposition the insertion point proximally to the initial site of injection. Once mice have fully recovered, monitor their behavior for 24 h and watch for potential signs of embolism, pain, or distress.

#### Materials for intra-arterial tail inoculation

- (1) Anesthetized mouse (immune compromised if using human cells)
- (2) Cellular suspension
- (3) 0.5–1 cc insulin syringe, 27–29G, 0.5 inch
- (4) Surgical tape
- (5) Betadine and alcohol swabs
- (6) Water recirculating heating pad

**Orthotopic (mammary fat pad) inoculation of breast cancer cells.** Place an anesthetized mouse in supine position on a sterile surface and tape the forelimbs and hind limbs away from the torso (**Figure 4a**). Prior to inoculation, clean the inguinal surface of the animal thoroughly with betadine and wipe with an alcohol pad or as per the institutional standard operating procedures. Using sterile surgical instruments, create a small incision in the skin adjacent to the fourth mammary fat pad (**Figures 4b and c**). Insert the needle into the fourth mammary gland fat pad and slowly inoculate the tumor cell suspension (**Figures 4d and e**; Supplementary Video 1). The 4th mammary gland fat pad is located at the intersection of three prominent blood vessels (**Figure 4c**). As with all techniques, it may be important for investigators to practice and familiarize themselves with the necessary anatomical landmarks prior to initiation of a multi-animal study. After the injection of cells, close the wound with 4–6 unconnected sutures, administer an analgesic as per

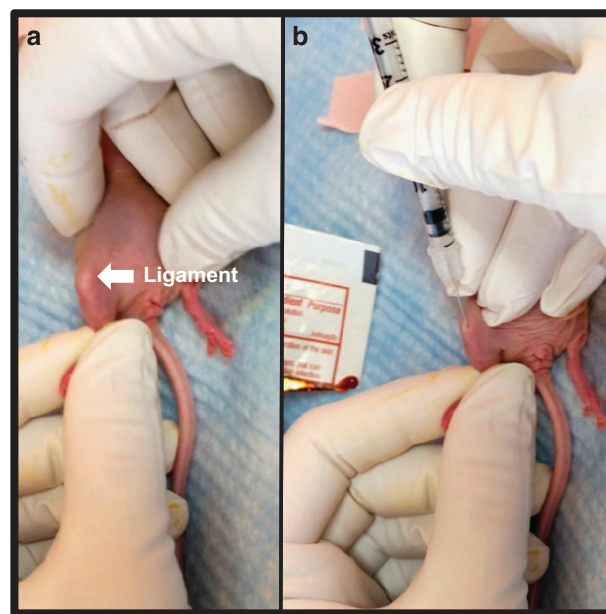


**Figure 5** Inoculation of breast cancer cells in the proximal tibia of a mouse. (a) After sterilizing the hind limbs of an anesthetized mouse, bend the knee to nearly 90°. While holding the hind limb between the thumb and index finger, locate the patellar ligament between the knee and the tibia, which should be visible through the skin as a white longitudinal structure. (b) Holding the needle parallel to the tibia in the dominant hand, push the needle through the center of the patellar ligament and into the proximal end of the tibia. Resistance will be felt once the needle reaches the bone. Twist the needle slightly to drill through the growth plate until the needle can be felt giving way. Once inserted into the bone approximately 2–3 mm, inject the cell suspension slowly and then withdraw the needle using the same drilling motion used to enter the bone.

institutional guidelines and place the mouse on a heating pad until fully awake.

In order to limit the occurrence of spontaneous tumor metastases to the lungs when using murine-derived cells (for example, 4T1), primary tumors can be surgically resected from anesthetized mice when tumors reach ~1 cm<sup>3</sup>. Animals can then be followed for 3–4 additional weeks for the development of bone metastases.

Some laboratories have reported that orthotopic implantation of the human-derived breast cancer cell lines SUM-1315 and MDA-MB-231-IV into immune-compromised mice can elicit spontaneous metastasis to bone when preceded by engraftment of human bone plugs.<sup>22,23</sup> In this model, 5 mm bone biopsy cores obtained from human femoral heads (within 2–4 h of removal from the patient) can be implanted under the skin on the posterior surface of the animal prior to tumor cell inoculation in the mammary fat pad. Four weeks after bone plug implantation, the human bone grafts become vascularized and bone marrow resembles that of normal bone.<sup>22,23</sup> Orthotopic injection of human-derived tumor cells can then proceed as described, and the human bone plugs are then excised at the termination of the study (~8–14 weeks) and evaluated for the presence of breast cancer metastases.

#### Materials for orthotopic inoculation

- (1) Anesthetized mouse (immune compromised if using human cells)
- (2) Cellular suspension
- (3) 0.1 cc Hamilton syringe, 25–27G, 0.5 inch
- (4) Tape
- (5) Betadine and alcohol swabs
- (6) Sterile scissors and forceps
- (7) Suture
- (8) Water recirculating heating pad
- (9) Analgesic

**Intra-tibial inoculation of breast cancer cells.** Prepare a syringe with the desired tumor cell suspension and set aside until ready to inject. After sterilizing the hind limbs, bend the knee to nearly 90° (**Figure 5a**). While holding the hind limb between the thumb and index finger, locate the patellar ligament between the knee and the tibia, which should be visible through the skin as a white longitudinal structure. Some laboratories choose to make a 2–3 mm incision through the skin on the knee to more easily visualize the tibia and patellar ligament; however, with practice this may not be necessary. Holding the needle parallel to the tibia in the dominant hand, push the needle through the center of the patellar ligament and into the proximal end of the tibia (**Figure 5b**). Resistance will be felt once the needle reaches the bone. Twist the needle slightly to drill through the growth plate until the needle can be felt giving way. Once inserted into the bone ~2–3 mm, attempt to move the needle slightly from side to side. When the needle is in the tibia, it will not be easily moved. If it moves freely from side to side, the needle is most likely embedded primarily in muscle and the insertion will need to be repeated. When the needle is accurately placed inside the marrow cavity of the tibia, inject the cell suspension slowly and then withdraw the needle using the same drilling motion used to enter the bone. In the event that the needle becomes clogged when penetrating or drilling through the top of the tibia, remove the original needle and re-insert a new needle, trying to follow the route created by the first needle. Once complete, use the same technique to inject the contralateral tibia with sterile PBS or desired vehicle to serve as a sham control. Bleeding rarely occurs; however, if blood does appear, apply pressure at the site. Administer an analgesic as per institutional guidelines, place the mouse on a heating pad and monitor until active.

Although cells can be inoculated into the tibia at any age, it is more difficult to penetrate the tibia in older animals once the growth plates have mineralized (>8-week old). On the other hand, very young mice can present injection difficulties due to the small size of the tibia; most laboratories therefore select 4- to 6-week-old mice for the intra-tibial inoculation route. If the mouse strain selected is furred, shave or wet the hair on the hind limb prior to the inoculation in order to better visualize the patellar ligament and other landmarks in the knee.

Materials for intra-tibial inoculation

- (1) Anesthetized mouse (immune compromised if using human cells)
- (2) Cellular suspension
- (3) 0.1 cc Hamilton syringe, 25–27G, 0.5 inch
- (4) Betadine and alcohol swabs
- (5) Water recirculating heating pad
- (6) Analgesic

### Assessment of tumor progression in bone

Throughout a bone metastasis experiment, mice should be monitored daily for changes in activity levels, mobility and onset of cachexia, which is a paraneoplastic syndrome characterized in mice by loss of body weight, muscle atrophy and weakness, arched appearance and lethargy.<sup>32,33</sup> Mice should be euthanized when >10–20% body weight is lost, tumor progression impairs mobility (for example, long bone fracture, head-tilt, paraplegia) or an animal appears to be in respiratory distress. A subset of mice may require euthanasia sooner than other mice in large studies. With the exception of survival studies, it is important that mice be euthanized on the same day or as close to the same day as possible such that the experimental time frame is identical for all mice, thus permitting an accurate comparison of tumor progression between groups.

Osteolytic lesion area and abnormal bone remodeling can be visualized and assessed weekly *in vivo* using a cabinet X-ray machine (**Figure 6a**; **Table 4**). Because X-ray analysis is an assessment of overt osteolytic lesion formation and provides only indirect information on tumor cell growth, cancer cell lines are commonly transfected with bioluminescent proteins permitting *in vivo* visualization and quantitation

of tumor growth at metastatic sites using bioluminescence imaging (BLI; **Table 4**).<sup>11,20,34</sup> BLI serves as an ideal complement to X-ray analysis of osteolysis, as it provides information on the presence of extra-skeletal metastases as well as micrometastases in bone, which precede bone destruction. Although not utilized to quantitate skeletal tumor burden, intra-vital microscopy may be useful for studying individual tumor cell motility and behavior in the bone microenvironment.<sup>35</sup>

At the termination of the study, mice should be subjected to necropsy and examined closely for gross evidence of metastatic foci outside of bone. For an intra-cardiac tumor inoculation study, evidence of tumor growth in the mediastinum surrounding the heart indicates that tumor cells were not accurately injected into the left cardiac ventricle, and the mouse should be excluded from the study. Fix all vital organs for future analysis. Carefully cut and scrape away skeletal muscle from the forelimbs, hind limbs and vertebral column, and fix the skeletal samples. Prior to decalcification of the bones, high-resolution *ex vivo* bone microcomputed tomography ( $\mu$ CT) can be performed to assess osteolytic or osteoblastic bone destruction and BV/TV at the distal femur, proximal tibia or lumbar vertebrae (**Figure 6b**).

Following decalcification, paraffin-embedded bone should be sectioned and stained with hematoxylin/eosin (H&E), and tumor burden ( $\text{mm}^2$ ) should be measured in long bones and spine using image analysis software (**Figure 6c**). Osteoblast numbers may also be quantitated in H&E stained sections. Histological sections should also be stained for tartrate-resistant acid phosphatase activity in order to assess the total osteoclast number relative to the bone surface and the osteoclast number at the bone and tumor interface, all of which are known to increase with cancer-induced osteolysis (**Figure 6d**; **Table 4**).<sup>36–37</sup> Finally, serum can be assayed for the presence of bone turnover markers, hormones, inflammatory factors or growth factors of interest.

When applicable, quantification of spontaneous metastases to lung, liver, brain or adrenals can be performed in paraffin-embedded organs collected at necropsy. For these analyses, 5  $\mu\text{m}$  sections can be cut every 200  $\mu\text{m}$  through the organ and stained with H&E. The number and area of metastatic foci for each section can then be determined using image analysis software, and results can be expressed as the total metastatic foci number per organ and as total metastatic area per organ.

### Discussion

When considering skeletal metastasis models with the intention of studying breast cancer osteolysis, a common choice is the intra-cardiac injection of human breast cancer cells in immune-compromised mice.<sup>38–40</sup> Alternatively, these human cells can be directly implanted into bone, bypassing earlier steps in the metastatic process. A benefit of the former model is that tumor cells detected in bone have themselves ‘seeded the soil,’ thus replicating the more natural progression of disseminated tumor cells formation of micrometastases, which progress in size over time, as occurs in humans. The necessity of using immune cell-deficient mice when inoculating human cell lines is typically seen as a limitation because it does not accurately model the immune competent human patient. It can, however, be seen as an advantage, as it eliminates possible confounding effects related to the animal’s immune response and permits the study of human cells in a very permissive host environment.

The pathogenesis of breast cancer bone destruction in the intra-cardiac MDA-MB-231 model is relatively similar to the human condition. Upon inoculation, breast cancer cells circulate in the vasculature, home to the bone compartment, and micrometastases can be detected by BLI in distant skeletal sites in as early as 1 week after injection.<sup>41</sup> As the tumor cells proliferate in the bone microenvironment, tumor-derived



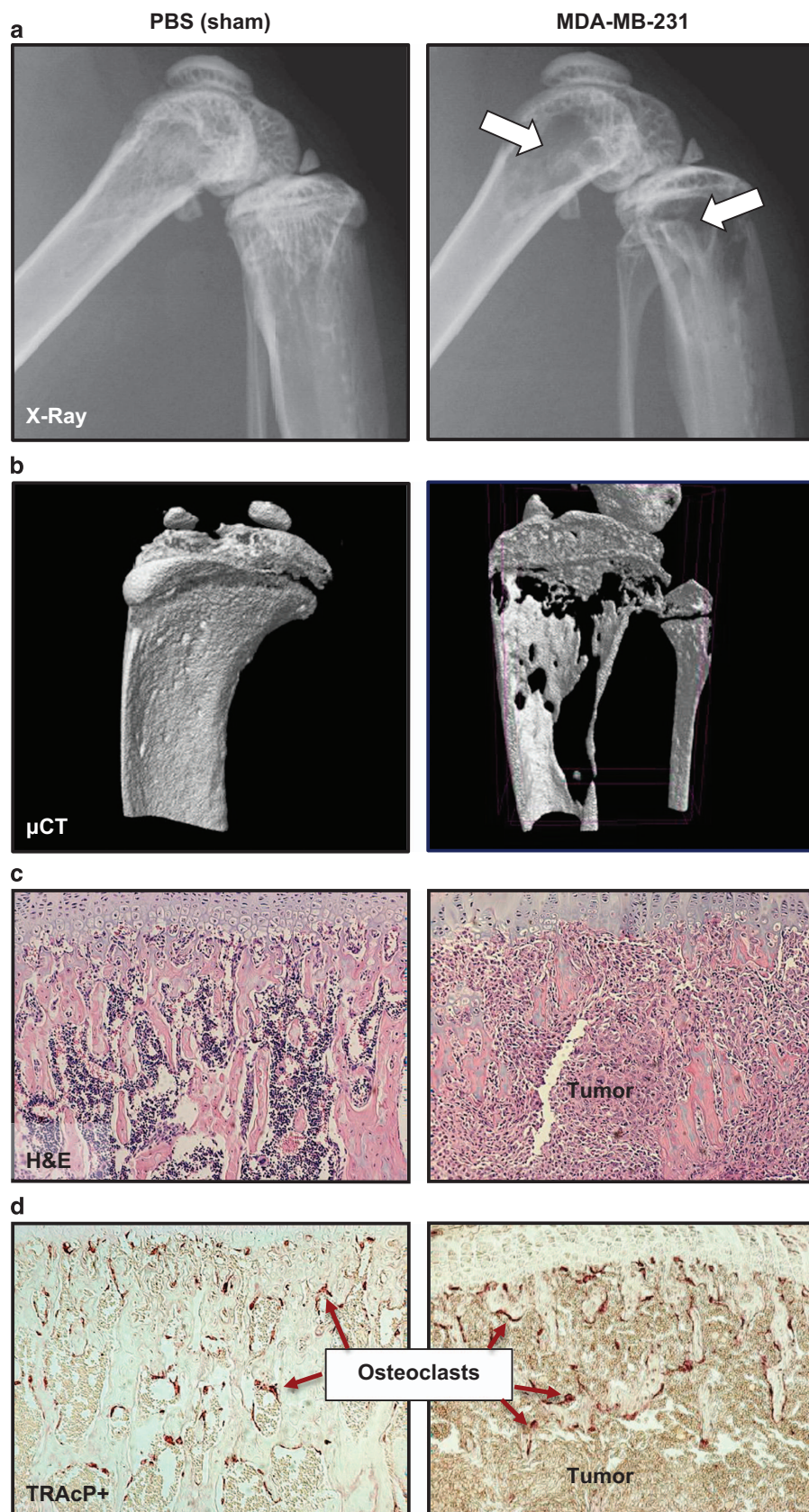


**Figure 6** The assessment of tumor progression in bone can be carried out by (a) quantitation of osteolytic lesion area by X-Ray, (b) measurement of bone volume fraction (BV/TV) by bone high-resolution microcomputed tomography ( $\mu$ CT), (c) histological assessment of tumor area using hematoxylin/eosin (H&E) staining of long bones and vertebrae and (d) quantitation of tartrate-resistant acid phosphatase (TRAcP) + osteoclasts.

**Table 3** Preparation of breast cancer tumor cells for inoculation in mice

Inoculation route	Cell number	Volume (PBS)	Syringe/needle
Intra-cardiac	100 000	100 $\mu$ l	0.5–1 cc insulin/27–29G, 0.5 inch
Intra-arterial (tail)	100 000	100 $\mu$ l	0.5–1 cc insulin/27–29G, 0.5 inch
Orthotopic	100 000–5 00 000	10–20 $\mu$ l	0.1 cc Hamilton/25–27G, 0.5 inch
Intra-tibial	10 000–2 50 000	10–20 $\mu$ l	0.1 cc Hamilton/25–27G, 0.5 inch

**Table 4** Principal end points used to characterize the development of bone metastases in mice

Type	Frequency
<i>In vivo analyses</i>	
Activity levels and hind limb mobility	Daily
Respiratory distress	Daily
Symptoms of cachexia	Daily
X-ray analysis of osteolytic lesions	Weekly or bi-monthly
Bioluminescence imaging (BLI; if applicable)	Weekly or bi-monthly
Type	Endpoint
<i>Post-mortem analyses</i>	
Gross dissection	Inspection for visceral metastases in lung, liver, adrenals and brain tissue
Bone microcomputed tomography ( $\mu$ CT)	Trabecular bone volume/total volume (BV/TV) of the proximal tibia, distal femur and lumbar vertebrae
Histomorphometric analysis of bone	Tartrate-resistant acid phosphatase (TRAcP) staining of bone Osteoclast number/bone surface (OcN/BS) Osteoclast surface/bone surface (OcS/BS) Osteoclast number at the bone–tumor interface
Tumor characterization	Hematoxylin/eosin (H&E) staining of bone for BV/TV and osteoblast number/bone surface (ObN/BS) H&E staining of forelimbs, hind limbs and spine for total tumor area in bone Immunohistochemical staining for proteins of interest (e.g., cytokeratin, phospho-smads)
Serum factors	H&E staining of visceral organs for quantitation of soft tissue metastases Biomarkers, if applicable (e.g., bone turnover markers, hormones, inflammatory factors, growth factors, tumor-derived factors)

osteolytic factors stimulate osteoclastic bone resorption and the development of bone lesions, which are quantifiable by X-ray. The most substantial bone destruction tends to occur in the metaphyses of the distal femur and proximal tibia, likely due to the high vascularization and metabolic activity characteristic of these trabecular bone compartments.<sup>42</sup>

Estrogen receptor (ER) + MCF-7 cells and triple negative MDA-MB-231 cells are two of the most commonly studied human breast cancer cell lines.<sup>40</sup> Although ER + primary tumors have a high propensity to metastasize to bone in patients,<sup>43</sup> ER + MCF-7 cells are utilized less frequently in models of breast cancer bone metastasis, as tumor-take can be limited using the intra-cardiac inoculation route, and MCF-7 cells require a longer time to develop osteolytic and osteoblastic lesions.<sup>44,45</sup> In contrast, ER – MDA-MB-231 cells readily metastasize to bone and develop osteolytic lesions as early as 2–3 weeks post inoculation.<sup>39</sup> In defense of the use of an ER – cell line, it should also be noted that there is a large discordance between the ER status of primary tumors and the ER status of the bone metastatic tumors in patients.<sup>43</sup>

The intra-tibial inoculation method is ideal for modeling the final stages of breast cancer bone metastasis and for studying direct interactions between tumor cells and the bone micro-environment without concerns about differential tumor-take from animal to animal. Murine-derived 4T1 cell proliferation in the tibia and subsequent development of osteolytic lesions can

occur with the injection of as few as 10 000 murine-derived cells. At higher cellular concentrations (50 000–200 000 cells), our laboratories have observed 4T1 cell metastasis to contralateral tibiae, femurs, forelimbs and the lungs, often limiting the duration and utility of the model. As with all techniques presented here, it is recommended that investigators thoroughly characterize their cell line and inoculation route of choice by conducting dose–response studies in order to establish the optimal protocols prior to embarking on large animal trials.

Inoculation of cancer cells into the tail vein is a well-established bone metastasis model for multiple myeloma.<sup>46,47</sup> Our laboratories and others have found that the injection of breast cancer cells into the tail vein results almost exclusively in lung metastases, with limited tumor-take in bone.<sup>22,48</sup> When skeletal metastases are desired, we therefore recommend utilization of the tail artery as the tumor inoculation route for breast cancer models.<sup>22,48–52</sup>

In addition to specific limitations related to model choice discussed above, standard methodologies used by bone metastasis researchers to assess bone destruction and tumor burden have their own limitations. Osteolytic lesion area and tumor burden area in bone are typically assessed by measurement of X-Ray scan or by serial histological sectioning, respectively, and are thus merely two-dimensional approximations of three-dimensional tumors. Improvement in imaging has enhanced sensitivity of detection and yields more accurate

quantification of metastases. Typically, BLI using codon-optimized luciferase-labeled cells yields higher detection than fluorescent imaging using GFP-labeled cells.<sup>53</sup> Small animal imaging of bone has forged ahead with the development of high-resolution *in vivo*  $\mu$ CT scanners<sup>54</sup> in combination with BLI.<sup>55</sup> However, the bone metastasis research community has been slower to adopt such methodologies. One reason for this is that cumulative radiation exposure from CT scanners has been found to enhance metastases<sup>56</sup> and thus could confound cancer metastasis models if radiation exposure is not monitored judiciously.

Despite their limitations and caveats, the established murine models of breast cancer bone metastases have proven to be excellent tools for the study of bone and cancer cross talk and for the evaluation of potential therapeutics that prevent cancer progression and disrupt the cycle of bone destruction driven by metastasis.

### Multimedia

The following article documents and visually demonstrates intra-cardiac and intra-tibial inoculation of cancer cells in mice and also demonstrates representative experimental end points of bone metastasis: <http://www.jove.com/video/4260>.

### Conflict of Interest

The authors declare no conflict of interest.

### Acknowledgements

We thank Alyssa Merkel and Kristin Kwakwa for capturing the photographs in **Figures 2 and 5** and Johnny Ribeiro and Khalid Mohammad for their technical input on the orthotopic and intra-tibial models, respectively. This work was supported by the Department of Defense Breast Cancer Research Program BC134025 (LEW) and by grants from INSERM (OP), the Comité Départemental de la Loire de la Ligue Contre le Cancer (OP), the Fondation ARC (OP), NIAMS AR43498 (GMP), The Netherlands Organization for Scientific Research NWO, VENI-Grant, 916.131.10 (JTB), the Department of Veterans Affairs 1101BX001957 (JAS) and NCI 1R01CA163499 (JAS). Supported by the IBMS-ECTS Young Investigators.

### References

- Coleman RE. Skeletal complications of malignancy. *Cancer* 1997; **80**: 1588–1594.
- Mundy GR. Metastasis to bone: causes, consequences and therapeutic opportunities. *Nat Rev Cancer* 2002; **2**: 584–593.
- Thompson DD, Simmons HA, Pirie CM, Ke HZ. FDA Guidelines and animal models for osteoporosis. *Bone* 1995; **17**: S125–S133.
- Ottewill PD, Wang N, Brown HK, Reeves KJ, Fowles CA, Croucher PJ *et al*. Zoledronic acid has differential antitumor activity in the pre- and postmenopausal bone microenvironment *in vivo*. *Clin Cancer Res* 2014; **20**: 2922–2932.
- Ottewill PD, Wang N, Brown HK, Fowles CA, Croucher PJ, Eaton CL *et al*. OPG-Fc inhibits ovariectomy-induced growth of disseminated breast cancer cells in bone. *Int J Cancer* 2015; **137**: 968–977.
- Lee JH, Kim B, Jin WJ, Kim JW, Kim HH, Ha H *et al*. Trolox inhibits osteolytic bone metastasis of breast cancer through both PGE2-dependent and independent mechanisms. *Biochem Pharmacol* 2014; **91**: 51–60.
- Werbeck JL, Thudi NK, Martin CK, Premanandan C, Yu L, Ostrowski MC *et al*. Tumor microenvironment regulates metastasis and metastasis genes of mouse MMTV-PyMT mammary cancer cells *in vivo*. *Vet Pathol* 2014; **51**: 868–881.
- Pécheur I, Peyruchaud O, Serre CM, Guglielmi J, Voland C, Bourre F *et al*. Integrin  $\alpha(v)\beta3$  expression confers on tumor cells a greater propensity to metastasize to bone. *FASEB J* 2002; **16**: 1266–1268.
- Ottewill PD, Deux B, Mönkkönen H, Cross S, Coleman RE, Clezardin P *et al*. Differential effect of doxorubicin and zoledronic acid on intraosseous versus extraosseous breast tumor growth *in vivo*. *Clin Cancer Res* 2008; **14**: 4658–4666.
- Kang Y, Siegel PM, Shu W, Drobnjak M, Kakonen SM, Cordon-Cardo C *et al*. A multigenic program mediating breast cancer metastasis to bone. *Cancer Cell* 2003; **3**: 537–549.
- Wetterwald A, van der Pluijm G, Que I, Sijmons B, Buijs J, Karperien M *et al*. Optical imaging of cancer metastasis to bone marrow: a mouse model of minimal residual disease. *Am J Pathol* 2002; **160**: 1143–1153.
- Nutter F, Holen I, Brown HK, Cross SS, Evans CA, Walker M *et al*. Different molecular profiles are associated with breast cancer cell homing compared with colonisation of bone: evidence using a novel bone-seeking cell line. *Endocr Relat Cancer* 2014; **21**: 327–341.
- Nasrazadani A, Van Den Berg CL. c-Jun N-terminal kinase 2 regulates multiple receptor tyrosine kinase pathways in mouse mammary tumor growth and metastasis. *Genes Cancer* 2011; **2**: 31–45.
- Fathers KE, Bell ES, Rajadurai CV, Cory S, Zhao H, Mourskaia A *et al*. Crk adaptor proteins act as key signaling integrators for breast tumorigenesis. *Breast Cancer Res* 2012; **14**: R74.
- Ottewill PD, Woodward JK, Lefley DV, Evans CA, Coleman RE, Holen I. Anticancer mechanisms of doxorubicin and zoledronic acid in breast cancer tumor growth in bone. *Mol Cancer Ther* 2009; **8**: 2821–2832.
- Aslakson CJ, Miller FR. Selective events in the metastatic process defined by analysis of the sequential dissemination of subpopulations of a mouse mammary tumor. *Cancer Res* 1992; **52**: 1399–1405.
- Abdelaziz DM, Stone LS, Komarova SV. Osteolysis and pain due to experimental bone metastases are improved by treatment with rapamycin. *Breast Cancer Res Treat* 2014; **143**: 227–237.
- Lelekakis M, Moseley JM, Martin TJ, Hards D, Williams E, Ho P *et al*. A novel orthotopic model of breast cancer metastasis to bone. *Clin Exp Metastasis* 1999; **17**: 163–170.
- Withana NP, Blum G, Sameni M, Slaney C, Anbalagan A, Olive MB *et al*. Cathepsin B inhibition limits bone metastasis in breast cancer. *Cancer Res* 2012; **72**: 1199–1209.
- Buijs JT, Matula KM, Cheung H, Kruihof-de Julio M, van der Mark MH, Snoeks TJ *et al*. Spontaneous bone metastases in a preclinical orthotopic model of invasive lobular carcinoma; the effect of pharmacological targeting TGF $\beta$  receptor I kinase. *J Pathol* 2015; **235**: 745–759.
- Iorns E, Drews-Elger K, Ward TM, Dean S, Clarke J, Berry D *et al*. A new mouse model for the study of human breast cancer metastasis. *PLoS ONE* 2012; **7**: e47995.
- Kuperwasser C, Dessain S, Bierbaum BE, Garnet D, Sperandio K, Gauvin GP *et al*. A mouse model of human breast cancer metastasis to human bone. *Cancer Res* 2005; **65**: 6130–6138.
- Holen I, Nutter F, Wilkinson JM, Evans CA, Avgoustou P, Ottewill PD. Human breast cancer bone metastasis *in vitro* and *in vivo*: a novel 3D model system for studies of tumour cell-bone cell interactions. *Clin Exp Metastasis* 2015; **32**: 689–702.
- Suva LJ, Washam C, Nicholas RW, Griffin RJ. Bone metastasis: mechanisms and therapeutic opportunities. *Nat Rev Endocrinol* 2011; **7**: 208–218.
- Engel LW, Young NA, Tralka TS, Lippman ME, O'Brien SJ, Joyce MJ. Establishment and characterization of three new continuous cell lines derived from human breast carcinomas. *Cancer Res* 1978; **38**: 3352–3364.
- Engel LW, Young NA. Human breast carcinoma cells in continuous culture: a review. *Cancer Res* 1978; **38**: 4327–4339.
- Soule HD, Vazquez J, Long A, Albert S, Brennan M. A human cell line from a pleural effusion derived from a breast carcinoma. *J Natl Cancer Inst* 1973; **51**: 1409–1416.
- Levenson AS, Jordan VC. MCF-7: the first hormone-responsive breast cancer cell line. *Cancer Res* 1997; **57**: 3071–3078.
- Yi B, Williams PJ, Niewolna M, Wang Y, Yoneda T. Tumor-derived platelet-derived growth factor-BB plays a critical role in osteosclerotic bone metastasis in an animal model of human breast cancer. *Cancer Res* 2002; **62**: 917–923.
- Thomas RJ, Guise TA, Yin JJ, Elliott J, Horwood NJ, Martin TJ *et al*. Breast cancer cells interact with osteoblasts to support osteoclast formation. *Endocrinology* 1999; **140**: 4451–4458.
- Canon J, Bryant R, Roudier M, Branstetter DG, Dougall WC. RANKL inhibition combined with tamoxifen treatment increases anti-tumor efficacy and prevent tumor-induced bone destruction in an estrogen receptor-positive breast cancer bone metastasis model. *Breast Cancer Res Treat* 2012; **135**: 771–780.
- Fearon KC, Glass DJ, Guttridge DC. Cancer cachexia: mediators, signaling, and metabolic pathways. *Cell Metab* 2012; **16**: 153–166.
- Waning DL, Mohammad KS, Reiken SR, Wenjun X, Anderssen DC, John S *et al*. TGF $\beta$  mediates muscle weakness associated with bone metastases. *Nat Med* 2015; **21**: 1262–1271.
- Rucci N, Capulli M, Ventura L, Angelucci A, Peruzzi B, Tillgren V *et al*. Proline/arginine-rich end leucine-rich repeat protein N-terminus is a novel osteoclast antagonist that counteracts bone loss. *J Bone Miner Res* 2013; **28**: 1912–1924.
- Ellenbroek SI, van Rheeën J. Imaging hallmarks of cancer in living mice. *Nat Rev Cancer* 2014; **14**: 406–418.
- Guise TA. Molecular mechanisms of osteolytic bone metastases. *Cancer* 2000; **88**: 2892–2898.
- Wright LE, Frye JB, Lukefahr AL, Timmermann BN, Mohammad KS, Guise TA *et al*. Curcuminoids block TGF- $\beta$  signaling in human breast cancer cells and limit osteolysis in a murine model of breast cancer bone metastasis. *J Nat Prod* 2013; **76**: 316–321.
- Arguello F, Baggs RB, Frantz CN. A murine model of experimental metastasis to bone and bone marrow. *Cancer Res* 1988; **48**: 6876–6881.
- Guise TA, Yin JJ, Taylor SD, Kumagai Y, Dallas M, Boyce BF *et al*. Evidence for a causal role of parathyroid hormone-related protein in the pathogenesis of human breast cancer-mediated osteolysis. *J Clin Invest* 1996; **98**: 1544–1549.



40. Yoneda T, Sasaki A, Dunstan C, Williams PJ, Bauss F, De Clerck YA *et al*. Inhibition of osteolytic bone metastasis of breast cancer by combined treatment with the bisphosphonate ibandronate and tissue inhibitor of the matrix metalloproteinase-2. *J Clin Invest* 1997; **99**: 2509–2517.
41. Johnson LC, Johnson RW, Munoz SA, Mundy GR, Peterson TE, Sterling JA. Longitudinal live animal micro-CT allows for quantitative analysis of tumor-induced bone destruction. *Bone* 2011; **48**: 141–151.
42. Rosol TJ, Tannehill-Gregg SH, Corn S, Schneider A, McCauley LK. Animal models of bone metastasis. *Cancer Treat Res* 2004; **118**: 47–81.
43. Coleman RE, Rubens RD. The clinical course of bone metastases from breast cancer. *Br J Cancer* 1987; **55**: 61–66.
44. Rucci N, Ricevuto E, Ficorella C, Longo M, Perez M, Di Giacinto C *et al*. In vivo bone metastases, osteoclastogenic ability, and phenotypic characterization of human breast cancer cells. *Bone* 2004; **34**: 697–709.
45. Lu X, Wang Q, Hu G, Van Poznak C, Fleisher M, Reiss M *et al*. ADAMTS1 and MMP1 proteolytically engage EGF-like ligands in an osteolytic signaling cascade for bone metastasis. *Genes Dev* 2009; **23**: 1882–1894.
46. Dallas SL, Garrett IR, Oyajobi BO, Dallas MR, Boyce BF, Bauss F *et al*. Ibandronate reduces osteolytic lesions but not tumor burden in a murine model of myeloma bone disease. *Blood* 1999; **93**: 1697–1706.
47. Mitsiades CS, Mitsiades NS, Bronson RT, Chauhan D, Munshi N, Treon SP *et al*. Fluorescence imaging of multiple myeloma cells in a clinically relevant SCID/NOD in vivo model: biologic and clinical implications. *Cancer Res* 2003; **63**: 6689–6696.
48. Yang S, Zhang JJ, Huang XY. Mouse models for tumor metastasis. *Methods Mol Biol* 2012; **928**: 221–228.
49. van der Horst G, van der Pluijm G. Preclinical models that illuminate the bone metastasis cascade. In: Joerger M, Gnant M (eds). *Prevention of Bone Metastases*. Springer-Verlag: Berlin, Heidelberg, Germany, 2012, p. 1–24.
50. Buijs JT, Henriquez NV, van Overveld PG, van der Horst G, Que I, Schwaninger R *et al*. Bone morphogenetic protein 7 in the development and treatment of bone metastases from breast cancer. *Cancer Res* 2007; **67**: 8742–8751.
51. Bachelier R, Confavreux CB, Peyruchaud O, Croset M, Goehrig D, van der Pluijm G *et al*. Combination of anti-angiogenic therapies reduces osteolysis and tumor burden in experimental breast cancer bone metastasis. *Int J Cancer* 2014; **135**: 1319–1329.
52. Croset M, Goehrig D, Frackowiak A, Bonnelye E, Ansieau S, Puisieux A *et al*. TWIST1 expression in breast cancer cells facilitates bone metastasis formation. *J Bone Miner Res* 2014; **29**: 1886–1899.
53. Peyruchaud O, Winding B, Pécheur I, Serre CM, Delmas P, Clézardin P. Early detection of bone metastases in a murine model using fluorescent human breast cancer cells: application to the use of the bisphosphonate zoledronic acid in the treatment of osteolytic lesions. *J Bone Miner Res* 2001; **16**: 2027–2034.
54. Bouxsein ML, Boyd SK, Christiansen BA, Guldberg RE, Jepsen KJ, Müller R. Guidelines for assessment of bone microstructure in rodents using micro-computed tomography. *J Bone Miner Res* 2010; **25**: 1468–1486.
55. Lim E, Modi K, Christensen A, Meganck J, Oldfield S, Zhang N. Monitoring tumor metastases and osteolytic lesions with bioluminescence and micro CT imaging. *J Vis Exp* 2011; **50**: 2775.
56. Cowey S, Szafran A, Kappes J, Zinn KR, Siegal GP, Desmond RA *et al*. Breast cancer metastasis to bone: evaluation of bioluminescent imaging and microSPECT/CT for detecting bone metastasis in immunodeficient mice. *Clin Exp Metastasis* 2007; **24**: 389–401.

Supplementary Information accompanies the paper on the BoneKEy website (<http://www.nature.com/bonekey>)

**Bisphosphonates prevent osteolysis and muscle weakness in aromatase inhibitor-treated mice with breast cancer bone metastases**

**Laura E. Wright<sup>1</sup>, Ahmed A. Harhash<sup>1</sup>, David L. Waning<sup>1</sup>, Khalid S. Mohammad<sup>1</sup>, Andrew R. Marks<sup>2</sup>, Theresa A. Guise<sup>1</sup>**

<sup>1</sup>*Department of Medicine, Division of Endocrinology, Indiana University, Indianapolis, IN, USA*

<sup>2</sup>*Department of Physiology, Columbia University, New York, NY, USA*

Aromatase inhibitor (AI) therapy for breast cancer causes muscle weakness, bone loss, and joint pain in 50% of patients. Moreover, a state of increased osteoclastic bone resorption has been shown to prime the bone microenvironment to accelerate metastatic growth at this site. We hypothesized that AI-induced bone loss could increase breast cancer progression in bone and exacerbate muscle weakness associated with bone metastases.

Four-week female athymic nude mice underwent OVX or sham surgery and were treated with vehicle or AI (letrozole; 10µg/day) +bisphosphonate (zoledronic acid, ZA; 0.1µg 3x/week; n=20/group). At week three, trabecular bone volume was reduced by 67% in OVX-AI mice ( $p<0.0001$ ) and increased by 304% in OVX-AI-ZA mice ( $p<0.0001$ ) relative to sham-vehicle. Mice were then inoculated with 100,000 MDA-MB-231 human breast cancer cells into the left cardiac ventricle and followed for cancer progression in bone. Since MDA-MB-231 cells are ER-negative, effects of estrogen deprivation on the tumor can be attributed to changes in the microenvironment. Five weeks after inoculation, osteolytic lesion area by X-ray was increased in OVX-AI mice (14.8 vs. 7.1mm<sup>2</sup>,  $p<0.05$ ) and reduced in OVX-AI-ZA mice (3.1 vs. 7.1mm<sup>2</sup>  $p<0.05$ ) relative to sham-vehicle. Tumor burden in bone was increased in OVX-AI mice relative to sham-vehicle (11.6 vs. 6.2mm<sup>2</sup>,  $p<0.05$ ) and relative to OVX-AI-ZA mice (11.6 vs. 6.6mm<sup>2</sup>,  $p<0.05$ ). Finally, muscle-specific force of the extensor digitorum longus was reduced in OVX-AI mice (399 vs. 451kN/m<sup>2</sup>,  $p<0.05$ ), and unchanged in OVX-AI-ZA mice relative to sham-vehicle tumor bearing mice (436 vs. 451kN/m<sup>2</sup>,  $p=ns$ ).

In summary, AI treatment induced bone loss and skeletal muscle weakness in mice, recapitulating effects observed in cancer patients. Prevention of AI-induced osteoclastic bone resorption attenuated the development of breast cancer bone metastases and improved muscle function in mice. These findings highlight the bone microenvironment as a powerful modulator of tumor growth locally and muscle function systemically. Further studies are necessary to determine the relative contribution of estrogen deficiency, bone loss, and direct AI toxicities to impaired muscle function in this model.



# INDIANA UNIVERSITY

DEPARTMENT OF MEDICINE  
School of Medicine

November 23, 2015

Laura Wright, PhD  
1902 N Talbott St Apt 6  
Indianapolis, Indiana 46202

Dear Dr. Wright:

We are delighted to offer you a position as a full-time faculty member in the Division of Endocrinology and Metabolism, Department of Medicine at the Indiana University School of Medicine. We would like to outline the Divisional and Departmental commitments regarding your appointment as Assistant Research Professor of Medicine. Upon your acceptance of this offer, we will continue the appointment process with the Dean's office. This will result in a separate letter from the Dean's office confirming the academic appointment.

This is an initial 1 year appointment in the Scientist track, with reappointment depending on your performance. Your appointment will be effective January 1, 2016. Faculty in the scientist track are required for promotion to excel in research, as described in the IU Faculty Academic Handbook and Promotion and Tenure Guidance Document. These and other resources are available from the Office of Faculty and Professional Development website: <http://faculty.medicine.iu.edu/>. Because of your plans to submit extramural funding applications, you are authorized to use the title Assistant Research Professor. Promotion in this track is dependent on your success in garnering grant support, publications, and establishing an independent research program.

The following are key elements contained in this offer.

**Research:** We wish to maximize your success as a researcher. Your primary mentor will be Dr. Theresa Guise. Please see the IU Research Gateway web portal <http://www.medicine.iu.edu/research/> for information about research development, grants and contracts, and research compliance. You are expected to apply for internal funding to augment your research support and gain a track record of successful applications. Your duties will consist of conducting experimental research projects related to the effects of cancer and cancer treatment on muscle and bone using in vivo models. You will also conduct pre-clinical therapeutic trials in these mouse models. In addition, you will be expected to work in a more independent manner and submit grant proposals for internal and extramural funds, as well as help Dr. Guise with the submission of her grant proposals. You will also be expected to write scientific manuscripts and review articles. It is anticipated that this will allow you to develop the skills necessary for becoming a fully independent investigator. Your salary is currently funded 100% by grant DOD-W81XWH-14-1-0358 and that funding is expected to continue through 9/29/17. One of your goals will be to transfer this support to additional research grants and contracts, which can earn you a research bonus.

You will be provided laboratory bench space and an office in the R3 building as part of Dr. Theresa Guise's lab. You will also have access to common equipment and shared support staff for your clerical needs. It is the expectation that you will comply with all appropriate regulations that govern your research (e.g., those of the Institutional Review Board (IRB), Animal use committee (IACUC), and Institutional Biosafety Committee) and that you will be fiscally responsible for all of your research accounts. For further information about our expectations of research faculty please refer to the *Department Policy on Startup and Bridge Funding and the Responsible Conduct of Research*.

**Teaching:** Excellence is expected in the quality of education provided in the Department. As part of that goal for high quality teaching, all faculty in the department are expected to complete a minimum of two units of educational development annually.

**Administration:** You will be expected to participate in all initial and continuing educational activities related to compliance and regulatory issues related to research, and to submit required reports and documentation in a timely fashion.

**Your total compensation will be as follows:**

1. Your salary will come from one source: Indiana University,

You will continue to be eligible for fringe benefits including the University's retirement and life and health insurance programs. Further details of the IU benefits can be obtained by going to the following website <http://www.indiana.edu/~uhhs/benefits/>.

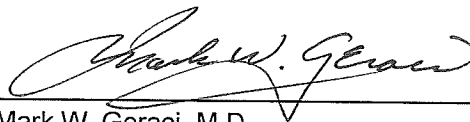
In addition, this offer is contingent on the University's verification of credentials and other information required by state law and IU policies, including the completion of a pre-employment physical which includes a drug screen and criminal history check.

We hope that you find these terms acceptable and that they reflect your understanding of our commitments from our previous discussions. We are very much looking forward to your joining us at the Indiana University School of Medicine in this new capacity. Please sign at the bottom of this letter and return a copy at your earliest convenience.

Sincerely,



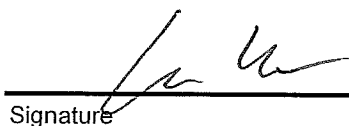
Michael J. Econs, M.D.  
Glenn W. Irwin, Jr., Professor in Endocrinology  
and Metabolism  
Professor of Medicine  
Division Chief, Endocrinology and Metabolism



Mark W. Geraci, M.D.  
John B. Hickam Professor of Medicine  
Chair, Department of Medicine

**ACCEPTANCE:**

I accept and acknowledge the terms and conditions of this appointment as set forth above.



Signature

LAURA WUBITT

Printed Name

11/25/15

Date

**Expectation for Appointment of Faculty in the Scientist Track  
(including Research Professor Appointments)**

The Department recognizes the valuable role that individuals in the research track provide to our overall research mission. In the past, we have honored requests by faculty to appoint individuals to this track who have contributed to their program and are supported on their grants.

Most if not all of our scientist track faculty are hired under these circumstances. What has not been explicitly arranged is the long term commitment to the individual being hired.

The long term funding (salary, research supplies, etc.) of individuals recruited in the scientist track will be the responsibility of the faculty member advocating for the hire. This will be incorporated into the offer letter and MOU and shared with the new appointee.

The faculty member sponsoring these recruitments will be responsible for performing the annual review of the individual and reporting to their division chief and vice chair for research the availability of funding in the coming year. This will provide time to plan for either termination if the individual can no longer be supported, or negotiation of a leave of absence.

Individuals in the scientist track will in general not be eligible for bridge funding, except as approved as part of the advocate faculty's own bridge request.

Individuals in the scientist track who have demonstrated their scientific independence (having obtained extramural funding supporting themselves independently of their original advocate and who have achieved promotion to associate or senior scientist) will be eligible to apply for bridge funding.

December 28, 2015

Laura Wright  
Indiana University

Dear Dr. Wright:

We are pleased to inform you that you have been chosen to receive a young investigator award to attend the AIMM-ASBMR John Haddad Young Investigators Meeting being held March 27-31, 2016 in Snowmass, Colorado, USA. Please respond to Jessica Baumgartner at [jbaumgartner@asbmr.org](mailto:jbaumgartner@asbmr.org) to confirm your acceptance of this award by **January 11, 2016, at 9 a.m. EST. If no reply has been received by then**, the award offer will be withdrawn and offered to another candidate.

As the recipient of an ASBMR John Haddad Young Investigator Award, you will receive \$1,600 for travel and other expenses and will present your research during a 15-20 minute interactive presentation with an additional 10 minutes for a detailed discussion. Please be prepared for interruptions in the form of constructive comments and questions during and after your presentation by senior investigators and other participants to the meeting. The president of AIMM will be contacting you with further details.

You are expected to pay the registration fee in advance and make your own arrangements for travel and accommodations. **As a condition of accepting this award, you are also expected to attend the entire meeting.** Your award will be presented to you as a component of the meeting.

We are delighted to welcome you as a John Haddad Young Investigator. Congratulations on your selection. For more information or if you have further questions please contact Christopher Kovacs, M.D., AIMM President, at [ckovacs@mun.ca](mailto:ckovacs@mun.ca).

We look forward to seeing you in Snowmass.



Douglas P. Kiel, M.D., M.P.H.  
*ASBMR President*



Christopher Kovacs, M.D.  
*AIMM President*

cc: Ann L. Elderkin, P.A., *ASBMR Executive Director*





# INDIANA UNIVERSITY

MELVIN AND BREN SIMON  
CANCER CENTER

## IUSCC New Member Checklist

March 7, 2016

Dear Laura,

Congratulations on your provisional membership with the Indiana University Melvin and Bren Simon Cancer Center (IUSCC)! As noted on the [Website](#), membership has many benefits, including use of shared facilities at discounted rates, access to ITRAC services, and even eligibility for exclusive pilot funding mechanisms.

As a member, expectations are that you will make meaningful contributions to the research, education, patient care, and community outreach activities of the cancer center, as demonstrated by: submission as PI or co-PI on a cancer-relevant grant, presentation of data at internal or external scientific meetings, publication as contributing author on peer-reviewed articles/book chapters, collaborative efforts via grants, publications or active membership in an IUSCC working group, regularly attend cancer seminars and IUSCC Grand Rounds, serve on various cancer center committees when called upon, recognize the support of the IU Simon Cancer Center on publications, when appropriate, attend regular program meetings, present at cancer center sponsored seminars and Grand Rounds and support the educational and philanthropic mission of the cancer center through private and public offerings.

To help you learn more about the mission of IUSCC, its research programs and resources available to members, we have put together a list (see second page) of people within the cancer center that you must meet with before your provisional membership can be approved.

Research Program Leader: *Please schedule a meeting with one of the Tumor Microenvironment and Metastasis research program leaders – either [Dr. Murray Korc](#) or [Dr. Theresa Guise](#) -- based on provisional approval to discuss how your research fits in with the program as well as the ongoing research of others within the program for future potential collaborations*

Program Leader Initials \_\_\_\_\_

Associate Director of Behavioral Research: *Please schedule a meeting with the AD of Behavioral and Population Sciences ([Victoria Champion](#)) based on your research expertise to discuss mentoring (do you have a committee in place yet or not) and expectations/responsibilities of membership.*

AD Behavioral and Population Sciences Initials \_\_\_\_\_

Translational Research Coordinator: *Please schedule a meeting with Crystal Munson for more information regarding ITRAC services including connections to collaborators, identification of internal and external funding mechanisms as well as information on IUSCC Working Groups*

Research Coordinator Initials \_\_\_\_\_

**Once you have met with each of the people above and had them initial this form, please e-mail a scanned copy to Elizabeth Parsons ([eparsons@iupui.edu](mailto:eparsons@iupui.edu)).**



INDIANA UNIVERSITY

MELVIN AND BREN SIMON  
CANCER CENTER

## Contact Information

### Research Program Leaders

#### *Breast Cancer:*

Kathy Miller  
Hari Nakshatri

#### *Cancer Prevention and Control:*

David Haggstrom  
Jiali Han

#### *Experimental and Developmental Therapeutics:*

John Turchi  
Bert O'Neil

#### *Hematopoiesis, Hematologic Malignancies, and Immunology:*

Hal Broxmeyer  
David Roodman  
Reuben Kapur

#### *Tumor Microenvironment and Metastasis:*

Theresa Guise  
Murray Korc

### Associate Director of Basic Science

Mark Kelley

### Associate Director of Clinical Research and Adult CTO Administrator

Sherif Farag  
Kerry Bridges

### Associate Director of Behavioral and Population Science

Victoria Champion

### Translational Research Coordinator

Crystal Munson



# LAURA E. WRIGHT

## *Curriculum Vitae*

Assistant Research Professor  
Indiana University School of Medicine  
Department of Medicine, Division of Endocrinology  
980 West Walnut Street  
Walther Hall R3, Room #C126  
Indianapolis, IN 46202

---

### EDUCATION

- Executive Certificate in the Business of Life Sciences, Kelley School of Business, Indiana University, Bloomington IN – 2015
- Ph.D., Physiological Sciences, University of Arizona, Tucson, AZ – 2012
- M.S., Physiological Sciences, University of Arizona, Tucson, AZ – 2007
- B.S., Human Biology, Biola University, La Mirada, CA – 2005

### OBJECTIVE

My long-term objective is to become an independent musculoskeletal investigator at a top-tiered academic institution where I am able to make meaningful contributions not only in research, but also in leadership, mentorship, and administrative roles.

### PROFILE

Multidisciplinary training, a strong commitment to research, and exceptional mentorship uniquely equip me to make a significant impact in the fields of endocrinology, oncology, and musculoskeletal disease. During my doctoral studies, I conducted basic and translational research focused on endocrine regulation of bone during ovarian senescence using chemical and surgical models of menopause. After firmly establishing an interest in endocrinology and metabolic bone disease, I obtained a National Institutes of Health (NIH) Research and Service Award (NRSA) to fund my pre-doctoral training. During this period, I worked to elucidate the bone-protective effects of a natural product-derived drug compound in models of osteoporosis and breast cancer bone metastasis. These pre-doctoral efforts resulted in five first author peer-reviewed publications. Cancer therapy-induced musculoskeletal complications emerged as a primary research interest; I therefore accepted a postdoctoral fellowship in the laboratory of Dr. Theresa Guise at Indiana University, a preeminent multidisciplinary research group that specializes in the study of solid tumor metastasis to bone. During my time at Indiana University, I have been promoted to Assistant Research Professor and published three first author peer-reviewed manuscripts, including primary research findings detailing the cellular mechanisms of radiation-induced bone loss and its impact on the tumor microenvironment. Importantly, I obtained three years of funding from the Department of Defense Breast Cancer Research Program, which supports my current investigative work focusing on the molecular mechanisms of musculoskeletal toxicities associated with anti-estrogen therapy in breast cancer patients.

### POSITIONS

2016 – present	Assistant Research Professor, Department of Medicine, Division of Endocrinology, Indiana University School of Medicine, Indianapolis, IN
2012 – 2015	Postdoctoral Research Fellow, Department of Medicine, Division of Endocrinology, Indiana University School of Medicine, Indianapolis, IN
2006 – 2012	Graduate Research Associate, Department of Medicine, Endocrinology Section, University of Arizona, Tucson, AZ
2005 – 2006	Graduate Research Assistant, McKnight Brain Institute, Neural Systems, Memory and Aging (NSMA), Department of Psychology, University of Arizona, Tucson, AZ
2005 – 2011	Graduate Teaching Assistant, Department of Physiology, University of Arizona, Tucson, AZ

## EXPERIENCE AND PROFESSIONAL MEMBERSHIPS

2016 – present Member, Indiana University Simon Cancer Center (IUSCC)  
2016 – present Member, Cancer and Bone Society (CABS)  
2015 – present Mentor, National Institutes of Health (NIH) Bridges to Baccalaureate Program, IUPUI, Indianapolis, IN  
2013 – present Member, American Medical Writers Association, Indiana Chapter  
2007 – present Member, The American Society for Bone and Mineral Research  
2009 – 2010 Member, Graduate Student Library Advisory Council Committee, University of Arizona  
2008 – 2009 Member, Recruitment & Admission Committee, University of Arizona, Graduate Interdisciplinary Program in Physiological Sciences

## SEMINARS

08/08/16 Indiana University Simon Cancer Center (IUSCC) Tumor Microenvironment and Metastasis annual retreat, invited seminar, Indianapolis, IN  
05/15/16 European Calcified Tissue Society (ECTS)/Cancer and Bone Society (CABS), Cancer and Bone Pre-Clinical Day, invited seminar, Rome, Italy  
03/29/16 Advance in Mineral Metabolism (AIMM) John Haddad Young Investigators Meeting, Snowmass, CO (*anticipated*)  
08/03/15 Orthopedic Research Society (ORS) Sun Valley Workshop on Musculoskeletal Biology, Featured Young Investigator, Sun Valley, ID  
11/1/13 Indiana University, Tumor Biology Microenvironment Program Seminar Series, Indianapolis, IN  
08/14/12 The National Institutes of Allergy and Infectious Diseases (NIAID) Medical Countermeasures Against Radiological Threats (MCART) site visit to Indiana University, invited seminar, Indianapolis, IN  
12/12/11 Indiana University, Tumor Biology Microenvironment Program Seminar Series, Indianapolis, IN  
12/07/11 Veterans Affairs Medical Center/University of California-San Francisco, Bone Imaging Core, Endocrine Research Unit, San Francisco, CA  
07/31/11 The American Society of Pharmacognosy Annual Meeting, Mechanism of Action Series, San Diego, CA  
03/07, 11/08, 11/10 Physiological Sciences Student Forum Series Speaker, Arizona Health Sciences Center, University of Arizona, Tucson, AZ  
11/04/10 Arizona Physiological Society, Featured Graduate Student Free Communication Lecturer, Midwestern University, Glendale, AZ

## TEACHING EXPERIENCE

2009 University of Arizona Undergraduate Department of Physiology, Graduate Teaching Assistant, PSIO 480 “Human Physiology,” Discussion Section Lecturer  
2005 – 2007 University of Arizona Undergraduate Department of Physiology, Graduate Teaching Assistant, PSIO 201 and PSIO 202 “Human Anatomy and Physiology,” Laboratory Instructor  
2007 Cortiva Institute, Tucson, AZ, ANP 223 “Anatomy and Physiology IV CORE,” Lecturer

## HONORS AND AWARDS

2016 John G. Haddad Young Investigator Award sponsored by Advances in Mineral Metabolism (AIMM) and the American Society for Bone and Mineral Research (ASBMR)  
2015 Harold M. Frost Young Investigator Award sponsored by the American Society for Bone and Mineral Research (ASBMR)  
2015 National Institutes of Health (NIH) Clinical Loan Repayment Program (LRP) through the National Cancer Institute (NCI)  
2014 Department of Defense (DoD) – Breast Cancer Research Program Postdoctoral Fellowship Award (BC134025)

## HONORS AND AWARDS (*continued*)

- 2012 Department of Defense (DoD) – Prostate Cancer Research Program Postdoctoral Fellowship Award (PC101890)
- 2013 Endocrine Fellows Foundation (EFF)/ASBMR Fellows Forum on Metabolic Bone Diseases award recipient, Baltimore, MD
- 2013 ASBMR President's Poster Competition award recipient, Baltimore, MD
- 2011 National Institutes of Health (NIH) National Graduate Student Research Conference (NGSRC) award recipient, Bethesda, MD
- 2011 University of California-San Francisco (UCSF), Postdoctoral Bootcamp award recipient
- 2011 Women in Science and Engineering (WISE) Stipend Award Recipient, University of Arizona, Tucson, AZ
- 2009 North American Research Conference on Complementary & Integrative Medicine Trainee Travel Award recipient, Minneapolis, MN
- 2009 American Society of Pharmacognosy Student Travel Award Recipient, Honolulu, HI
- 2008 Ruth L. Kirschstein National Research Service Award (NRSA) for Individual Predoctoral Fellowship Training (F31, NIH/NCCAM)
- 2008 Trainee Award Recipient for the Endocrine Society Annual Meeting, Basic Sciences
- 2008 Herb Society of America Inc. Research Award Recipient
- 2008 1<sup>st</sup> Place Award Recipient—Best Abstract, Natural Supplements: An Evidence-Based Update Conference, Scripps Institute, San Diego, CA
- 2008, 2010 Herbert E. Carter Travel Award recipient, Graduate Interdisciplinary Programs, University of Arizona, Tucson, AZ

## RESEARCH HIGHLIGHTS

### Peer-Reviewed Publications

1. **Wright LE**, Harhash AA, Kozlow WM, Waning DL, Regan JN, She Y, John SK, Murthy S, Niewolna M, Marks AR, Mohammad KS, Guise TA. Aromatase inhibitor-induced bone loss increases the progression of estrogen receptor-negative breast cancer in bone and exacerbates muscle weakness in vivo. *Oncotarget*. 2016 (under review).
2. **Wright LE**, Ottewell PD, Rucci N, Peyruchaud O, Pagnotti GM, Chiechi A, Buijs JT, Sterling JA. Murine models of breast cancer bone metastases. *Bonekey Rep*. 2016, doi:10.1038/bonekey.2016.31.
3. Waning DL, Mohammad KS, Reiken SR, Wenjun X, Anderssen DC, John S, Chiechi A, **Wright LE**, Umanskaya A, Niewolna M, Trivedi T, Charkhzarrin S, Khatiwada P, Wronska A, Haynes A, Benassi MS, Witzmann FA, Zhen G, Wang X, Cao Z, Roodman GD, Marks AR, Guise TA. TGF $\beta$  mediates muscle weakness associated with bone metastases. *Nature Med*. 2015, 21(11):1262-71.
4. **Wright LE**, Buijs JT, Kim HS, Coats LE, Scheidler AM, John SK, She Y, Murthy SM, Ma N, Chin-Sinex HJ, Bellido TM, Bateman TA, Mendonca MS, Mohammad KS, Guise TA. Single-limb irradiation induces local and systemic bone loss in a murine model. *J Bone Miner Res*. 2015, 30(7):1268-79.
5. **Wright LE**, Guise TA. The role of PTHrP in skeletal metastases and hypercalcemia of malignancy. *Clin Rev Bone Miner Metab*. 2014, 12(3):119-29.
6. **Wright LE**, Guise TA. The microenvironment matters: estrogen deficiency fuels cancer bone metastases. *Clin Cancer Res*. 2014, 20(11):2817-9.
7. **Wright LE**, Frye JB, Gorti B, Timmermann BN, Funk JL. Bioactivity of turmeric-derived curcuminoids and related metabolites in breast cancer. *Current Pharma Design*. 2013, 19(34):6218-25.
8. **Wright LE**, Frye JB, Timmermann BN, Mohammad KS, Guise TA, Funk JL. Curcuminoids block TGF- $\beta$  signaling in human breast cancer cells and limit osteolysis in a murine model of breast cancer bone metastasis. *J Nat Prod*. 2013, 76(3):316-21.
9. Frye JB, Lukefahr AL, **Wright LE**, Marion SL, Hoyer PB, Funk JL. Modeling perimenopause in Sprague-Dawley rats by chemical manipulation of the transition to ovarian failure. *Comp Med*. 2012, 62(3):193-202.

### Peer-Reviewed Publications (*continued*)

10. Lukefahr AL, Frye JB, **Wright LE**, Marion SL, Hoyer PB, Funk JL. Decreased BMD in rats rendered follicle deplete by an ovotoxic chemical correlates with changes in follicle-stimulating hormone and inhibin A. *Calcif Tissue Int*. 2012, 90(3):239-49.
11. **Wright LE**, Frye JB, Lukefahr AL, Marion SL, Hoyer PB, Besselsen DG, Funk JL. 4-vinylcyclohexene diepoxide (VCD) inhibits mammary epithelial differentiation and induces fibroadenoma formation in female Sprague Dawley rats. *Reprod Toxicol*. 2011, 32(1):26-32.
12. **Wright LE**, Frye JB, Timmermann BN, Funk JL. Protection of trabecular bone in ovariectomized rats by turmeric is dependent on extract composition. *J Agric and Food Chem*. 2010, 58(17):9498-504.
13. **Wright LE**, Christian PJ, Rivera Z, Van Alstine WG, Funk JL, Bouxsein ML, Hoyer PB. Comparison of skeletal effects of ovariectomy versus chemically-induced ovarian failure in mice. *J Bone Miner Res*. 2008, 23(8):1296-303.

### Abstracts (Presented):

1. **Wright LE**, Waning DL, Harhash AA, Mohammad KS, Marks AR, Guise TA. Aromatase inhibitor-induced bone loss causes muscle weakness and increased progression of ER-negative breast cancer in bone in a murine model. American Society for Bone and Mineral Research Annual Meeting, Seattle, WA, October 2015.
2. **Wright LE**, Harhash AA, Waning DL, Chiechi A, Mohammad KS, Marks AR, Guise TA. Letrozole and ovariectomy cause bone loss, muscle weakness and increased breast cancer bone metastases in mice. American Society for Bone and Mineral Research Annual Meeting, Houston, TX, September 2014.
3. **Wright LE**, Harhash AA, Waning DL, Chiechi A, Mohammad KS, Marks AR, Guise TA. Ovariectomy combined with aromatase inhibitor treatment cause bone loss, muscle weakness and increased breast cancer metastases in mice. International Bone & Mineral Society's 13<sup>th</sup> International Conference on Cancer-Induced Bone Disease, Miami, FL, November 2013.
4. **Wright LE**, Joseph D, Harhash A, Waning D, John S, Mohammad KS, Marks AR, Guise TA. Effects of sex steroid deprivation on skeletal muscle function and ryanodine receptor (RyR1) modulation. American Society for Bone and Mineral Research Annual Meeting, Baltimore, MD, October 2013.
5. **Wright LE**, Buijs JT, John S, Peng Z, Harhash A, Waning D, Mohammad KS, Mendonca M, Chua HL, Wolfe H, Marks A, Orschell C, Guise TA. Ionizing radiation induced both direct and systemic bone loss in murine models. International Bone & Mineral Society's 12<sup>th</sup> International Conference on Cancer-Induced Bone Disease, Lyon, France, November 2012.
6. **Wright LE**, Guise TA, Mohammad KS, Funk JL. Curcuminoids decrease osteolytic breast cancer bone metastases. The Endocrine Society Annual Meeting, Boston, MA, June 2011.
7. **Wright LE**, Lukefahr AL, Frye JB, Hoyer PB, Besselsen DG, Funk JL. 4-Vinylcyclohexene Diepoxide (VCD)-induced fibroadenomas: a novel rat model of mammary tumorigenesis. The Endocrine Society Annual Meeting, San Diego, CA, June 2010.
8. **Wright LE**, Beischel Frye J, Timmermann BN, Funk JL. Curcuminoid-containing turmeric protects bone mass and microarchitecture in ovariectomized rats. American Society for Bone and Mineral Research Annual Meeting, Denver, CO, September 2009.
9. **Wright LE**, Timmermann BN, Funk JL. Differential effects of medicinal Zingiberaceae on the prevention of bone loss. American Society of Pharmacognosy Annual Meeting, Honolulu, HI, June 2009.
10. **Wright LE**, Beischel Frye J, Timmermann BN, Funk JL. Effects of medicinal Zingiberaceae on bone loss in musculoskeletal disease. North American Research Conference on Complementary & Integrative Medicine, Minneapolis, MN, May 2009.
11. **Wright LE**, Beischel Frye J, Timmermann BN, Funk JL. Medicinal Zingiberaceae in the prevention of menopausal bone loss. *Planta Medica*. 74:1174, 2008.
12. **Wright LE**, Christian PJ, Rivera Z, Funk JL, Bouxsein ML, Hoyer PB. Skeletal deterioration in an ovary-intact mouse model of menopause. The Endocrine Society Annual Meeting, San Francisco, CA, June 2008.

## RESEARCH SUPPORT

### Ongoing Research Support

- ♦ BC134025 Wright (PI) 9/2014 – 9/2017  
Department of Defense (DoD) – Breast Cancer Research Program  
*Musculoskeletal complications and bone metastases in breast cancer patients undergoing estrogen deprivation therapy*  
The objective of this grant is to evaluate the effects of aromatase inhibitor therapy on the musculoskeletal system by determining how estrogen depletion impairs muscle function and whether estrogen deprivation-induced bone loss can prime the bone microenvironment in ways that increase the progression of breast cancer bone metastases.

### Completed Research Support

- ♦ IU Health Strategic Research Initiative in Oncology Wright & Waning (co-PI's) 11/2013 – 10/2014  
Melvin and Bren Simon Cancer Center, Bio-Plex Core Pilot Project Grant  
*Systemic factors responsible for cancer- and cancer therapy-induced ryanodine receptor 1 remodeling and muscle weakness*  
The goal of this project was to identify systemic factors and signaling molecules responsible for maladaptive biochemical modifications to a critical calcium channel in skeletal muscle (RyR1), which leads to muscle weakness during cancer therapy-induced bone loss.
- ♦ PC101890 Wright (PI) 6/2012 – 5/2014  
Department of Defense (DoD) – Prostate Cancer Research Program  
*Mechanisms of radiation-induced bone loss and effects on prostate cancer bone metastases*  
The main objective of this study was to elucidate the mechanisms of radiation-induced bone loss and to determine how radiation exposure alters the bone microenvironment to increase the progression of prostate cancer bone metastases.
- ♦ F31 AT004875-04 Wright (PI) 9/2008 – 5/2012  
National Institutes of Health (NIH)  
National Center for Complementary and Alternative Medicine (NCCAM)  
Ruth L. Kirschstein National Research Service Award (NRSA)  
*Ginger extracts in the prevention of metabolic bone disease*  
This was an individual fellowship training grant supporting four years of doctoral training in physiological sciences. Specifically, this grant supported my dissertation research on the bone-sparing effects of natural product-derived compounds in translational models of osteoporosis and lytic breast cancer bone metastases.

## STATEMENT OF WORK

### **Task 1. Determine effects of the aromatase inhibitor (AI) letrozole and the selective estrogen receptor modulator (SERM) tamoxifen on skeletal muscle function *in vivo*. (Months 1-4)**

- a. Complete training in confocal microscopy, micro-dissection and muscle force measurement in the Marks Laboratory.
- b. Conduct *in vivo* study comparing effects of OVX alone with or without AI treatment (letrozole; 5mg/kg/d; i.p., for two months) or SERM treatment (tamoxifen; 50mg/kg/d; i.p., for two months) relative to E<sub>2</sub>-replete sham-operated animals with endpoints to include serum levels of 17 $\beta$ -estradiol and inflammatory cytokines by Bio-Plex assay, body composition by DXA, grip strength, *ex vivo* muscle specific force production and fatigability of the extensor digitorum longus (EDL) and soleus muscles.
- c. A subset of mice will be selected from each group on the day the study is terminated for the testing of RyR1 channel open probability using confocal microscopy planar lipid bilayer measurements in order to assess channel “leakiness.”
- d. Complete data analyses for changes in body composition by DXA and assay serum levels of inflammatory markers by Bio-Plex assay (baseline vs. final measurement).

\*Completion of this task will reveal 1) whether estrogen (E<sub>2</sub>) deprivation by use of the AI letrozole or the SERM tamoxifen, common adjuvant therapies for the management of breast cancer, lead to muscle weakness and 2) whether muscle dysfunction in this model is associated with systemic inflammation, low or undetectable levels of 17 $\beta$ -estradiol, and/or calcium mishandling in the skeletal myocytes.

*Animal usage:* 60 female C57Bl/6 mice ( $n = 15$  sham + vehicle;  $n = 15$  OVX + vehicle;  $n = 15$  OVX + AI;  $n = 15$  OVX + SERM).

*Collaborators/consultants:* Begin quarterly meetings with Donna Threlkeld, breast cancer patient advocate, and Kathy Miller, M.D., breast cancer oncologist.

### **Task 2. Evaluate biochemical changes in skeletal muscle resulting from estrogen (E<sub>2</sub>) deprivation therapy. (Months 5-6)**

- a. Using frozen muscle samples saved from Task 1, nitrosylation and oxidation of RyR1 as well as assessment of calstabin1 depletion from RyR1 will be evaluated by co-immunoprecipitation in tissues from E<sub>2</sub>-replete sham-operated mice, OVX mice, OVX + AI-treated mice and OVX + SERM-treated mice.

\*Completion of this task will reveal whether muscle dysfunction associated with estrogen deprivation treatment is associated with oxidation or nitrosylation of RyR1 and/or dissociation of calstabin1 from RyR1.

### **Task 3. Evaluate whether the degree of AI- and SERM-induced muscle weakness correlates with treatment-induced bone loss. (Month 7)**

- a. Using the DXA and  $\mu$ CT scans acquired during task 1, changes in bone mineral density (BMD; whole body, proximal tibia, distal femur and spine), trabecular bone microarchitectural properties (BV/TV, Tb.N. Tb.Sp, Tb.Th, Conn-D, SMI) and cortical bone properties (BA/TA, CortThick, medullary area) will be quantified at baseline and at the final endpoint in E<sub>2</sub>-replete sham-operated mice, OVX mice, OVX + AI-treated mice and OVX + SERM-treated mice. Regression analyses and ANOVA will be utilized to assess the relationship between bone loss and muscle weakness in our model. Representative  $\mu$ CT images will be reconstructed and saved for future presentations and publication.

\*Completion of this task will reveal whether the degree of bone loss in OVX, AI and/or SERM treated mice correlates with muscle weakness, thus justifying further study of a potentially direct link between bone loss and muscle weakness (to be explored in Task 4).

**Task 4. Determine whether prevention of osteoclastic bone resorption can ameliorate muscle weakness associated with E<sub>2</sub> deprivation *in vivo*. (Months 8-11)**

- a. Effects of the bisphosphonate zoledronic acid (ZA; 0.5 mg/kg/d), an anti-bone resorptive therapeutic, will be evaluated in AI-treated OVX mice, and grip strength, muscle specific force and muscle fatigability will be assessed after two months of treatment.
- b. Using DXA and  $\mu$ CT scans acquired at baseline and at the final time-point, changes in bone mineral density (BMD; whole body, proximal tibia and spinal), trabecular bone microarchitectural properties (BV/TV, Tb.N, Tb.Sp, Tb.Th, Conn-D, SMI) and cortical bone properties (BA/TA, CortThick, medullary area) will be quantified. Regression analyses will be utilized to assess the relationship between bone protection and muscle weakness. Representative  $\mu$ CT images will be reconstructed and saved for future presentations and publication.
- c. RyR1-calstabin1 stability will be assessed by co-immunoprecipitation in frozen skeletal muscle samples from treated mice.

\*Completion of this task will elucidate whether prevention of bone loss can ameliorate muscle dysfunction in the context of estrogen deprivation treatment.

*Animal usage:* 60 female C57Bl/6 mice ( $n = 15$  sham + vehicle,  $n = 15$  OVX + vehicle,  $n = 15$  OVX + AI + vehicle,  $n = 15$  OVX + AI + ZA).

**Task 5. Test the direct effects of E<sub>2</sub> deprivation therapies letrozole (AI) and tamoxifen (SERM) and the anti-resorptive therapy bisphosphonate (zoledronic acid) on skeletal muscle *in vitro*. (Months 12-17)**

- a. Using an *in vitro* muscle culture system, a dose-response of aromatase inhibitor (letrozole; 0.001-10 $\mu$ g/mL), selective estrogen receptor modulator (SERM; tamoxifen, 0.001-10 $\mu$ g/mL), and bisphosphonate (zoledronic acid; 0.001-10 $\mu$ g/mL) will be performed on differentiated C2C12 myotube cultures. Potential molecular endpoints of interest include:
  1. oxidation of RyR1 and SERCA1
  2. nitrosylation of RyR1 and SERCA1
  3. relative SERCA1 expression levels
  4. muscle cell proliferation and death by MTT and LDH assays, respectively
  5. ubiquitin ligase expression
  6. phosphorylated and un-phosphorylated myosin heavy chain expression
  7. phosphorylated and un-phosphorylated myosin light chain expression
  8. changes muscle fiber morphology

\*Completion of this task will reveal a molecular mechanism for anti-E<sub>2</sub> therapy-induced muscle weakness.

**Task 6. Determine the impact of estrogen deprivation therapy (AI and SERM) on the accumulation of bone marrow adipose tissue (MAT), and whether bisphosphonate treatment (zoledronic acid) can prevent MAT accumulation *in vivo*. (Months 18-20)**

- a. The right tibia will be collected from mice harvested at the completion of Tasks 1 and 4. Bones will be scanned by micro-computed tomography (microCT) and total bone marrow cavity volume will be measured.
- b. Bones will be decalcified, stained with osmium tetroxide, which is lipid-specific and radio-dense, re-scanned by microCT, and MAT volume will be calculated and expressed as % of total marrow cavity.

\*Completion of this task will reveal whether estrogen deprivation therapies are associated with maladaptive accumulation of MAT and whether protection of bone prevents this change to the bone microenvironment.

*Animal usage:* The right tibia will be collected from non-tumor bearing C57bl/6 mice in Tasks 1 and 4. The ordering of additional animals is not required for this Task.

**Task 7. Prepare manuscript containing novel findings from Tasks 1-6. (Months 21-22)**

\*Completion of this task will result in a peer-reviewed publication in a high-impact breast cancer journal.

**Task 8. Determine whether the E<sub>2</sub> deprivation therapies letrozole (AI) or tamoxifen (SERM) accelerate the progression of breast cancer bone metastases *in vivo*. (Months 23-28)**

- a. Conduct *in vivo* study comparing effects of OVX alone with or without AI treatment (letrozole; 5mg/kg/d; i.p., for two months) or SERM treatment (tamoxifen; 50mg/kg/d; i.p., for two months) relative to E<sub>2</sub>-replete sham-operated animals on bone metastases in athymic nude mice inoculated with MDA-MB-231 cells. After tumor cell inoculation, animals will be followed prospectively for six weeks for the development of bone metastases. Endpoints will include body composition by DXA, osteolytic lesion area by X-ray, changes in bone by  $\mu$ CT, serum levels of 17 $\beta$ -estradiol and inflammatory cytokines by Bio-Plex assay and grip strength.
- b. Analyze bone tissue sections by histomorphometry for tumor burden, osteoclast#/mm bone-tumor interface, osteoclast#/mm<sup>2</sup> and osteoblast #/mm<sup>2</sup>.

\*Completion of this task will reveal whether bone loss resulting from E<sub>2</sub> deprivation increases honing of breast cancer to bone and/or accelerates the progression of bone metastases.

*Animal usage:* 60 female athymic nude mice ( $n = 15$  sham + vehicle;  $n = 15$  OVX + vehicle;  $n = 15$  OVX + AI;  $n = 15$  OVX + SERM).

**Task 9. Determine whether prevention of E<sub>2</sub> deprivation-induced bone loss can reduce the progression of breast cancer bone metastases *in vivo*. (Months 29-34)**

- a. Using the same *in vivo* model of breast cancer bone metastases described in Task 8, OVX mice treated with AI (letrozole; 5mg/kg/d; i.p., for two months) will be treated with the bisphosphonate zoledronic acid (ZA; 0.5 mg/kg/d), and monitored for changes in bone. After two months, mice will be inoculated with MDA-MB-231 cells and followed for six weeks for the development of bone metastases. Endpoints will include body composition by DXA, osteolytic lesion area by X-ray, changes in bone by  $\mu$ CT, serum levels of 17 $\beta$ -estradiol and inflammatory cytokines by Bio-Plex assay and grip strength.
- b. Analyze bone tissue sections by histomorphometry for tumor burden, osteoclast#/mm bone-tumor interface, osteoclast#/mm<sup>2</sup> and osteoblast #/mm<sup>2</sup>.

\*Completion of this task will reveal whether bisphosphonates, which prevent OVX and E<sub>2</sub> deprivation-induced bone loss, can prevent bone metastases or slow their progression in mice treated with the AI letrozole.

*Animal usage:* 60 female athymic nude mice ( $n = 15$  sham + vehicle,  $n = 15$  OVX + vehicle,  $n = 15$  OVX + AI + vehicle,  $n = 15$  OVX + AI + ZA).

**Task 10. Prepare manuscript containing novel findings from Tasks 8-9. (Month 35-36)**

\*Completion of this task will result in a peer-reviewed publication in a high-impact breast cancer journal.

**Site of performance:**

Indiana University, School of Medicine, Department of Medicine, Division of Endocrinology  
Walther Hall R3, Room C122; 980 West Walnut Street, Indianapolis, IN 46202